Drought monitoring system for Austrian agriculture AgroDroughtAustria

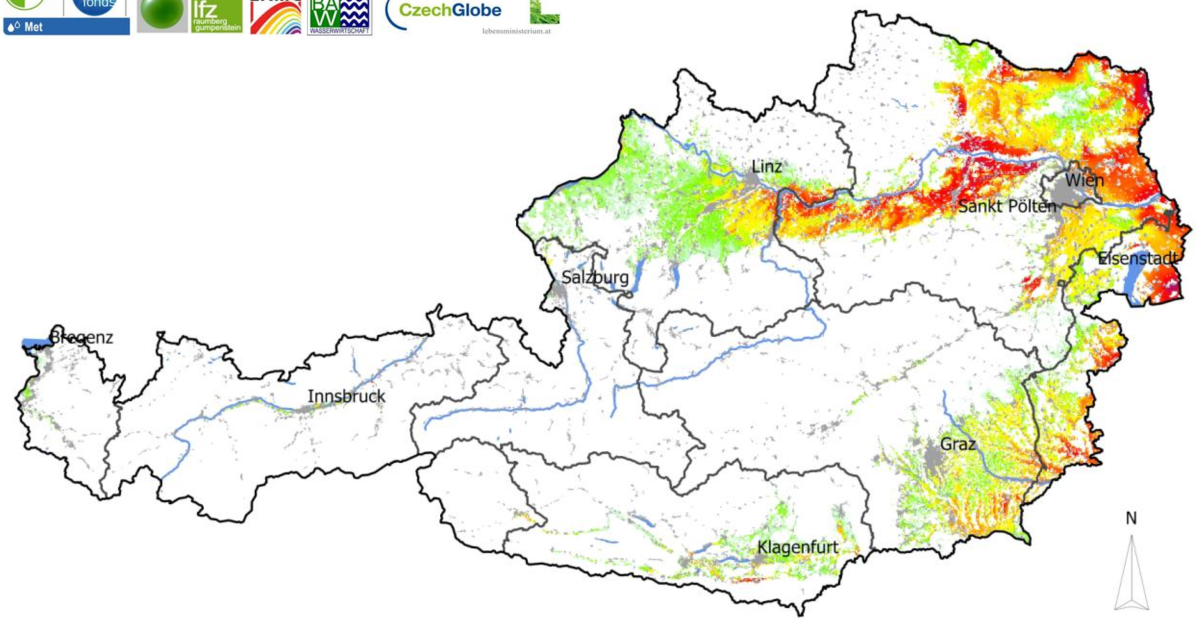

Final Project Report
Supported by Austrian Climate and Energy Fund (ACRP)

Institut für Meteorologie (BOKU-Met)
Department Wasser – Atmosphäre – Umwelt
Universität für Bodenkultur

May 2016

ISSN 1994-4179 (Print)
ISSN 1994-4187 (Online)

BOKU-Met Report 25

Diese Publikation sollte folgendermaßen zitiert werden:

Eitzinger, J., Daneu, V., Bodner, G., Kubu, G., Loiskandl, W., Macaigne, P., Thaler, S., Schaumberger, A., Wittmann, C., Weidle, F., Kann, A., Murer, E., Krammer, C., Trnka, M., Hayes M. (2016): Drought monitoring system for Austrian agriculture – AgroDroughtAustria (Final Scientific Report of project "AgroDroughtAustria" of the Austrian Climate Change Research Program).
BOKU-Met Report **25**, ISSN 1994-4179. ISSN 1994-4187 (on-line) – https://meteo.boku.ac.at/report/

Impressum:

Medieninhaber und Herausgeber:

Universität für Bodenkultur, Department für Wasser – Atmosphäre – Umwelt
Institut für Meteorologie, Peter-Jordan-Straße 82, 1190 Wien, Österreich

URL: http://met.boku.ac.at/

Universität für Bodenkultur Wien
University of Natural Resources and Applied Life Sciences, Vienna

Department für Wasser-Atmosphäre-Umwelt
Institut für Meteorologie
Peter-Jordan Str. 82
A-1190 Wien

„Drought monitoring system for Austrian agriculture – AgroDroughtAustria"

Supported by Austrian Climate and Energy Fund (ACRP)

Final Project Report

A.o. Prof. Dipl.Ing. Dr. Josef EITZINGER (Project lead)

Project team:

Josef Eitzinger[1], Vojko Daneu[1], Gernot Bodner[1], Gerhard Kubu[1], Willibald Loiskandl[1], Peggy Macaigne[1], Sabina Thaler[1], Andreas Schaumberger[2], Christoph Wittmann[3], Florian Weidle[3], Alexander Kann[3], Erwin Murer[4], Carmen Krammer[4], Mirek Trnka[5], Michael Hayes[6]

(1) Univ. of Natural Resources and Life Sciences (BOKU), Vienna, Austria
(2) Lehr- und Forschungszentrum für Landwirtschaft Raumberg-Gumpenstein (LFZRG)
(3) Central Institute for Meteorology and Geodynamics (ZAMG),
(4) Bundesamt für Wasserwirtschaft (BAW), Petzenkirchen,
(5) Global Change Research Centre AS CR v.v.i, CZ,
(6) National Drought Mitigation Center (NDMC), USA

May 2016

Content

1 Introduction 3
2 WP 1 – Data base on crop specific drought and heat vulnerability and impacts under Austrian conditions 4
2.1 Overview 4
2.2 Soil moisture and meteorological data base 5
2.3 Crop data base 5
3 WP 2 - Adaptation, calibration and validation of drought and drought impacts indicators for arable crops and grassland 7
3.1 Overview 7
3.2 Soil water balance model SOILCLIM 7
3.3 Crop phenology model 10
3.4 Crop drought and heat stress impact analysis and indicators 11
4 WP 3 – Development of drought-specific forecasting products 27
4.1 Overview 27
4.2 Available analysis and forecast data sets for ADA 28
4.3 On the uncertainty of drought related forecast parameters 36
5 WP 4 – Geographic Information System (GIS) for monitoring and forecasting crop specific drought and heat stress parameters 50
5.1 Overview 50
5.2 System development and structure 51
5.3 The ADA Web-Interface 72
6 WP 5 – ADA System test 80
7 Conclusions and recommendations 81
8 Literature 84

1 Introduction

There is an emerging consensus amongst a wide range of national to local environmental and resource policy makers and stakeholders that climate change has been clearly demonstrated. These findings, recently summarized by Richardson *et al.* (2009), indicate that many key climate indicators are already moving beyond the patterns of natural variability within which contemporary society and economies have been able to develop and thrive. These indicators also include extreme climatic events and it is clear that with unabated emissions, many current negative climate trends will likely accelerate, leading to an increasing risk of abrupt or irreversible climatic shifts. For instance, recent climatic trends already had implications for the estimated return-period of heat-waves and drought as seen on examples of 2003 (Ciais et al., 2005), 2010 and 2012 summers in European regions (European Environment Agency, 2013).

Drought is defined in general as an extended period of deficient rainfall relative to the statistical multi-year average for a region (Wilhite and Glantz, 1987). Additionally, drought related problems are enhanced by climate change through an increased variability of temperature and rainfalls and the increased occurrence of extreme climatic events (Olesen and Bindi, 2002). It impacts different spheres of the society by reducing or supressing crop growth and yield, hydrological resources and related economic benefits. In this respect different drought terms are distinguished depending on their impacts and lead times, e.g. meteorological, agricultural, hydrological and socio-economic drought. Drought not only does affect arid or semi-arid areas, but also temperate or more humid climate regions. It is thus recognized as a major risk in agriculture and is of critical importance in large parts of Europe and particularly in Austria at various spatial and time scales (APCC, 2013; Trnka *et al.*, 2009; Trnka *et al.*, 2011).

Although most regions of Austria are humid or semi-humid, main important crop production regions are frequently and with an increasing trend over the past decades affected by agro-meteorological droughts (often combined with heat stress), where water deficit and/or heat effects leads to significant yield decrease of various crops. Crop model studies show that these conditions will accelerate under future climate scenarios in Central Europe including Austrian crop production regions (Thaler et al., 2012; Eitzinger et al., 2013; Semenov and Shewry, 2011). Studies in adjacent regions of Czech Republic just north of the key Austrian agricultural region (Marchfeld) showed that drought (i) negatively affects yield of all crops; (ii) this effect (drought damages) grows exponentially with the increasing drought intensity; and (iii) the negative effect of drought increased when 1870-1910 and 1961-2007 are compared.

In Austria severe agricultural drought damages were reported in the past decade, especially in the years 2003, 2006, 2010, 2012, 2013 and 2015 crops were affected negatively by drought and heat in different crop production regions. For example, the Austrian Hail Insurance reported increasing trend of crop damage due to weather extremes over the past decade, were drought plays an important role due to large regions affected. In 2012, the agricultural damages due to weather extremes, reported by Austrian Hail Insurance, reached a new record of 120 million Euros mainly due to drought, which strongly affected Eastern Austria (with a regional precipitation deficit of up to 60% and a 300% increase of the number of heat days over the growing season (www.hagel.at)). Based on a lack of an operational drought monitoring and forecasting system specifically designed for the needs of agriculture in Austria the main project goal was the development of such a tool supporting management and mitigation of drought/heat impacts on crops.

Given the considerable uncertainties around projections of climate impacts on agriculture at local and regional scales, there is an evident and urgent need for reliable science-based early warning systems providing timely and understandable information for decision-makers and stakeholders (Reidsma et al., 2010). In our project, we addressed these challenges for agriculture in Austria, by designing and developing a crop specific drought monitoring system for Austria through the achievement of the following objectives:

1) Establish a set of calibrated indicators and methods on crop specific drought and heat vulnerability and impacts based on field experiment data and crop model application.
2) Assess crop drought and heat stress at high spatial resolution by using improved spatial precipitation and temperature input (INCA data).
3) Establish a near-time (up to 10 days) forecasting method for drought occurrence
4) Adapt and validate methods for crop drought and heat stress detection and yield impact implemented in a GIS-based monitoring system with high spatial resolution (500x500m) for main vulnerable arable crops in Austria.
5) Test crop specific drought monitoring system for operational use including stakeholder involvement.

2 WP 1 – Data base on crop specific drought and heat vulnerability and impacts under Austrian conditions

2.1 Overview

In this Work Package the data base was established which was necessary for evaluation of the models and algorithms to be used in the drought monitoring system. The data base was used also for spatial validation and test of the drought monitoring system during the project time period. The data were gathered from field experiments, statistical reports and other sources of available data. The site and crop specific data include:

• Data on soil conditions of test sites, times series of weather data, soil water content and soil water deficit under various selected crops.
• Crop and management data, describing drought effects on crops and crop stress status (i.e. biomass development, yield and yield reduction).
• Simulated times series of growth and development of the selected crops for development and calibration of a simple crop phenology model by dynamic crop model application.

2.2 Soil moisture and meteorological data base

For validation of soil moisture model 25 measurement sites were selected. At these sites soil moisture was measured in different soil depths. In order to proof their representativeness for Austrian climates a classification of the available stations was made taking into account the land use and climatic conditions. The stations sea levels vary from 150 to 2010m. From the total of 58 measurement plots, 17 are located on grassland, 36 on arable land and 4 in forest. Taking into account the climatic water balance of regions, one site is situated in the region with negative and 7 with mostly negative water balance. 6 sites are located in regions until 250 mm, 5 until 500 mm, 4 until 1000 mm and 2 until 1500 mm positive water balance.

Data sources
The data were delivered by Institute of Land and Water Management in Petzenkirchen (BAW), Technical University (TU) Vienna, Austrian Agency for Health and Food Safety (AGES) Vienna, Joanneum Research in Graz, L.F.Z. Raumberg - Gumpenstein and Hydrological Services in Styria, Salzburg, Tirol, Vorarlberg, Burgenland and Lower Austria and Institute of Meteorology, BOKU. For each station the data base structure is organised as general station information, land use with crop rotation and yield, soil information with soil type, horizons and soil physical and chemical characteristics as well the soil moisture measured in different depths and weather data.

Data base structure
The data of each site are saved in separate EXCEL files, where the worksheet structure is as follows:
Metadata: General information about the station, soil moisture station and weather station, where one was available in situ.
Crop: information about crop type, crop rotation, begin and end of the crop growth, crop yield.
Soil: Information about soil profile, soil horizon and laboratory analysis of soil parameters.
Water content: Daily soil moisture data of different depths
Weather: Daily weather data: air temperature, air humidity, global radiation, wind velocity, precipitation.

2.3 Crop data base

The objective of WP1 includes a data base of representative crop yields of the major crops in Austria for the past ten years. Crop and grassland yield statistics of more than 40 sites were collected including additional weather data from the sites.
During this first period agronomic and yield data were collected from the Chambers of agriculture for several cultivated regions of Austria (Table 1). Analysis was then performed to identify crop yield sensitivity to dry and wet years, pre-crop and cover crop and tillage. Several drought indices have been selected and were tested using this data base in WP2.

Data for the analysis of crop response to climatic stresses comprise yield and management data from farmers' fields and meteorological data for the respective sites. The yield data were obtained from detailed data collections made by the Chamber of

Agriculture of Lower Austria within their district level Farmer's Working Groups ("Ackerbau Arbeitskreise"). The data contain all relevant management information and the respective crop yields for individual farmer's fields. Table 1 gives an overview of key information available and the factors evaluated within the current project.

Table 1: Farmers' field data base from Chamber of Agriculture Lower Austria. Parameters included in the evaluations with the current project are marked in bold.

Parameter	Unit / Factor levels	Note
Year	2002-2014	Start date: Horn: 2001; Mistelbach and Krems: 2003-2014; Hollabrunn: 2006
Site	Baden, Hollabrunn, Horn, Krems, Mistelbach, Wiener Neustadt	
Pre-crop	Type (Winter cereal, spring cereal, maize, sunflower, rapeseed, legume, sugar beet, others)	
Cover crop	Type (bare soil, legume, brassica, mixture, others)	
Tillage	Type (plough, no plough)	Information collected since 2010 only
Seeding date	Day of year (early, normal, late)	Early=lower quartile; normal=median; late=upper quartile
Yield	t ha^{-1} (Crops: Maize, spring barley, winter wheat, sugar beet)	

The total dataset of the four crops evaluated in more detail in this study contained 16.717 entries covering six sites and between nine (Hollabrunn) and 14 (Horn) years. All yield data were previously checked for plausibility by applying biologically reasonable upper and lower thresholds to exclude outliers from wrong declaration or input errors. For maize the yield data were standardized to 25 % moisture content of grain.

The data do not provide geo-referenced information. Thus the evaluation does not allow an explicit consideration of the influence of soil type on individual yields and provides only information of the average relation between yield and climatic factors for the region under consideration. Still an indirect effect of soil type was obtained by further subdividing the dataset into high and low yielding fields in each individual year using the lower quartile and upper quartile as boundaries for grouping.

3 WP 2 - Adaptation, calibration and validation of drought and drought impacts indicators for arable crops and grassland

3.1 Overview

Models and algorithms for detecting agricultural drought, soil water deficit and drought effects on crops were evaluated, adapted and calibrated based on the data base established in the WP 1. These included the model SOILCLIM, and a set of algorithms for drought impacts on crops.

The evaluated algorithms describe:
• Soil and crop water deficit on a daily basis and site specific
• Measurable drought and heat effects on the selected crops (i.e. phenology, biomass development, leaf area, yield depression)
• Indicators of heat and drought stress status

3.2 Soil water balance model SOILCLIM

For the most of the first year the evaluation of the SoilClim model, which was implemented in the ADA drought monitoring system, relied on the use of data collected by CzechGlobe and BOKU Wien. Figure 1 to Figure 3 show part of the results achieved by the SoilClim model. It is apparent that at sites with high-quality measurement of soil moisture where soil moisture is measured at number of replicates and at multiple depths (Hirschstetten and Gumpenstein) the performance of the SoilClim model is very good and the model correctly depicted both timing and duration of all episodes of low soil moisture content (Figure 1 and Figure 2). There is some concern that the SoilClim model might suffer from too few soil layers that causes latter onset of the drought signal in some cases (Figure 2). This issue will be explored further in the coming months.

Figure 3 shows comparison of SoilClim method with the observations and two other means of soil moisture monitoring i.e. process based crop model (DSSAT 4.0.2.0) and remote sensing based method based on the ASCAT instrument. It is apparent that the agreement of the SoilClim with the observation is lower than in (Figure 1 and Figure 2) but nevertheless the SoilClim method is superior of other two in most of the seasons. At the moment the mean bias of the estimates by SoilClim at the tested sites is between 3-8% and relative root mean square error varies between 15 and 20%. However we are convinced that the ongoing improvements of the SoilClim model utilizing results of over 50 observations sites from the ADA database will improve the performance of the model.

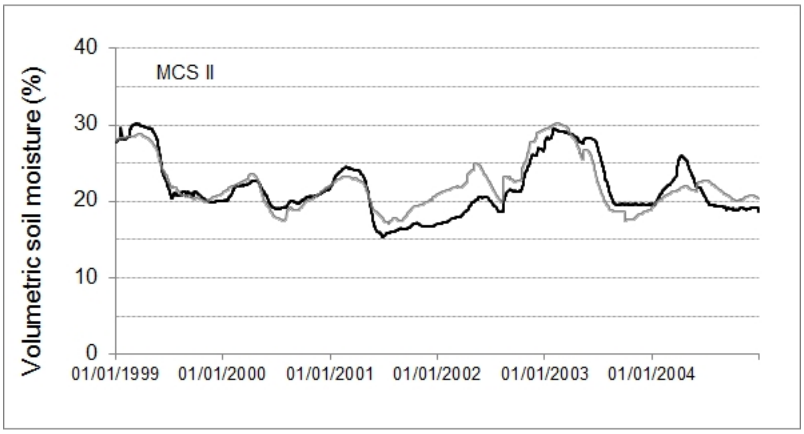

Figure 1: Initial evaluation of the SoilClim model at the Hirschstetten site (lower layer 40-100 cm).

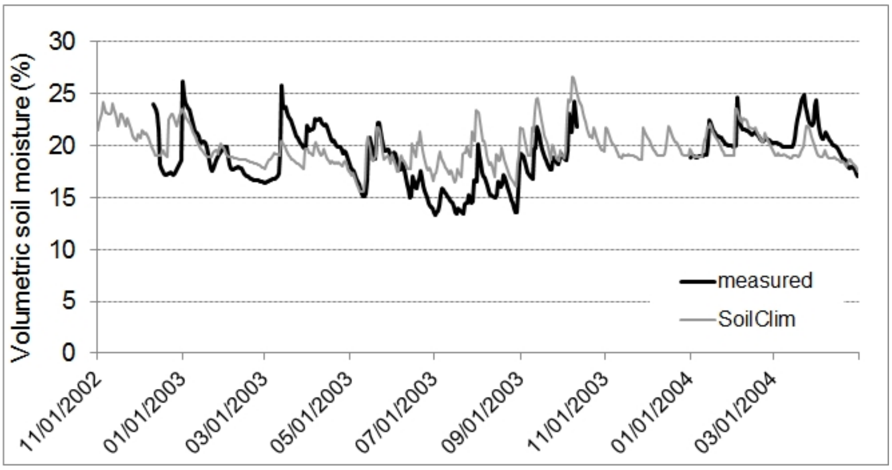

Figure 2: Evaluation of the SoilClim model at the Gumpenstein site for the top layer (0-40 cm).

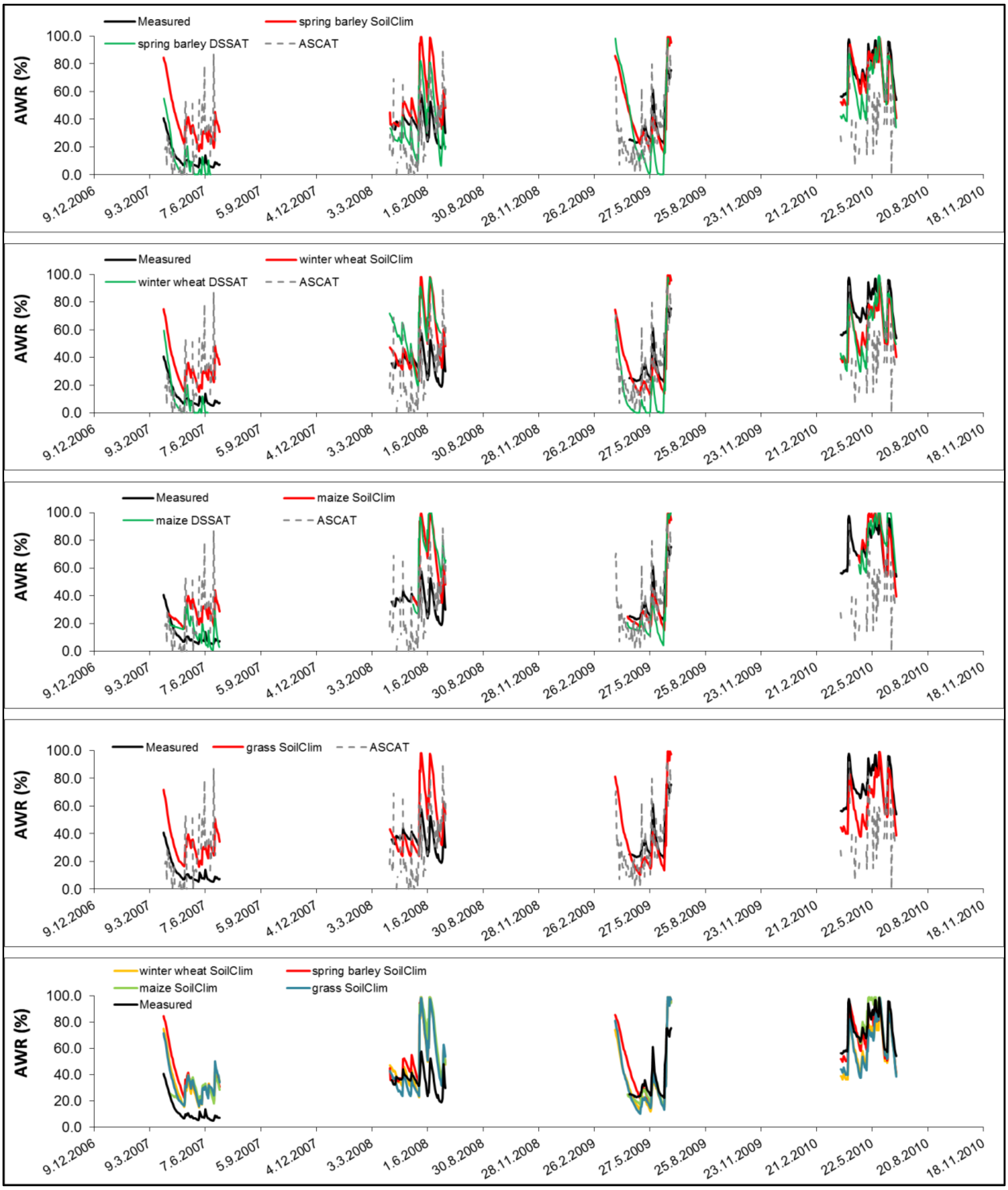

Figure 3: Results of SoilClim evaluation at Gross-Enzersdorf station. The SoilClim, crop model DSSAT 4.5 and ASCAT based estimate of relative saturation of the soil profile are compared with the measurements under the grass cover. Four different canopies of SoilClim are depicted at the lowest figure and compared with the observation.

3.3 Crop phenology model

As basis for the crop specific determination of crop water use and soil water depletion a phenology model, calculating the crop phenology related crop water use parameter K_c was calibrated and implemented into the modeling system in context to the soil water balance model SOILCLIM. K_c is the crop coefficient defined for a given crop and growth stage for calculating actual crop evapotranspiration (=crop water use) from grass reference evapotranspiration (Allen et al., 1998) and is usually determined experimentally. Each agronomic crop has a set of specific crop coefficients which can be used to predict water use rates at different growth stages.

Four main crop growth stages can be defined: initial, crop development, mid season, and late season (Figure 3). For Austria the four crop growth stages as well as the Kc factor were defined for grassland, winter wheat, spring barley, spring maize and sugar beet. As experimental data were not available, calibrated crop growth models were used to determine the crop specific temperature sums required for reaching main development stages and related Kc factors. The DSSAT v4.02 model was used for maize, winter wheat and spring barley. The simulations were run from 1992-2012, weather station Groß-Enzersdorf, soil Chernozem, rain-fed, fertilization according ÖPUL guideline. On 1st March for winter wheat and spring barley as well as on 1st April for maize started the first stage A (Figure 4). The Kc factor and temperature sum for sugar beet were simulated with the crop model Daisy. For grassland the approach of the GRAM model is used, which is already available from the partner LFZR and BOKU.

Crop Coefficient Model for ADA

Reference Evapotranspiration (ET0) for December, January and February is a constant value of **0.2 mm**.

Start of Growing Season (SGS): **First day of 5 consecutive days with daily mean temperatures above 5°C**

Start of Growing Season for Maize (SGS-M): **First day of 5 consecutive days with daily mean temperatures above 10°C**

Base temperature for calculation of degree day temperature sum (BT): **5 °C**

Base temperature for calculation of degree day temperature sum for Maize (BT-M): **8 °C**

Culture	Initial (Evaporation)			Crop Development		Mid-Season		Late Season		End of Growing		
	Entry of A		Entry of B		Entry of C		Entry of D		Entry of E		Entry of F	
	Kc	Time	Kc	Time	Kc	Time	Kc	Time	Kc	Time	Kc	Time
Grassland (3-cut)	Will be done by LFZ Raumberg-Gumpenstein (according to Schaumberger, 2011)											
Winter Wheat	0.4	01.03.	0.4	SGS	1.2	350	1.2	692	0.5	+14 days	0.5	30.11.
Spring Barley	0.4	01.03.	0.4	SGS	1.2	502	1.2	568	0.5	+14 days	0.5	30.11.
Spring Maize	0.4	01.04.	0.4	SGS-M	1.2	249	1.2	1238	0.5	+14 days	0.5	30.11.
Sugar Beet	0.4	01.03.	0.4	300	1.2	2400					1.1	31.12.

Phenology model

(to be used for evapotranspiration calculation and stress indicators)

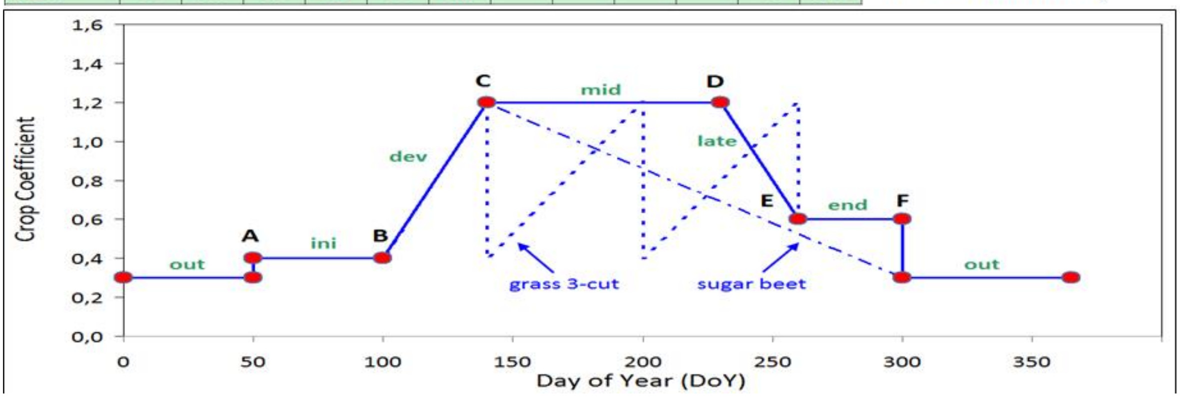

Figure 4: Crop growth stages and Kc factor for grassland, winter wheat, spring barley, maize and sugar beet as calibrated for Austrian conditions.

3.4 *Crop drought and heat stress impact analysis and indicators*

Meteorological information was obtained from local weather stations of ZAMG. From the basic weather data at daily time step, we derived several indices to capture stress periods (Table 2). Some of the indices were obtained by including calculations from other working packages of the ADA project.

Table 2: Meteorological indices used to study crop yield – climate relations.

Indicator	Description
Short term indicators	
Precipitation (P)	Amount (yearly, monthly, critical periods), distribution (in- vs. off-season)
Reference evapotranspiration (ET_0)	Penman Monteith (global radiation, relative humidity, minimum, maximum temperature, wind speed); amount (yearly, monthly, critical periods) and distribution (in- and off-season)
P-to-ET_0	Rainfall deficit
Temperature (T)	Heat days and cumulative temperature above 27°C and 32°C; Heat degree hours (Bristow and Abrecht, 1991)
Combined heat and drought index	Calculated within ADA from heat degree days and soil moisture depletion
Long term indicators	
Palmer Drought Severity Index	Monthly deviation of water supply from 30 year average (Input: precipitation, temperature, soil water storage capacity; Palmer, 1965)
Crop Moisture Index	Weekly deviation of water supply from 30 year average (Input: precipitation, temperature, soil water storage capacity; Palmer, 1968)

<u>Drought and heat indicators were tested according to the following steps:</u>
-Selection of relevant meteorological and crop yield data for the selected crops for representative agricultural regions of Austria,
-Calculation and adoption of drought and heat indicators, and
-Comparison of the impact of drought stress versus the impact of heat stress on crop yields in the region.

Meteorological data were further evaluated to identify the key differences in climatic site conditions. Yield data were analyzed for significant differences in crop yield among sites and years as well as distinct yield stability between single crops constituting the dominant species of the prevailing crop rotations at the investigated sites. Furthermore, we analyzed the influence of selected management measures indicated in Table 2 (cover cropping, tillage) on crop yield. Site and year effects on crop yield were determined by a general linear model ANOVA using PROC GLM in SAS. Pairwise comparisons were done using PROC TTEST. For all comparisons we used a Welch test as this procedure allows a robust comparison accounting for inhomogeneous variances which are frequent in datasets not obtained from designed experiments and thus involving mostly unbalanced observations.

A main interest in this WP of ADA was to determine relations among meteorological input parameters (Table 2) and yield data in order to establish the empirical basis for drought and heats stress impact modeling. For this purpose we performed stepwise regressions between yield data and climatic indices using the SAS procedure

PROC REG with the MAXR selection method for all available environments constituted by year x site combinations.

Figure 5 shows the average meteorological characteristics of the different sites for the indicators given in Table 1 (see main body report). Hollabrunn and Mistelbach have lowest average rainfall, differing significantly from Baden, Horn and Wiener Neustadt, while Krems is in between. Rainfall distribution shows highest in-season rainfall for Krems with significant distinction from Baden and Mistelbach. Thus in terms of rainfall, Mistelbach can be considered the site with less favorable conditions due to low annual mean rainfall and comparatively high contribution of off-season rainfalls.

Reference evapotranspiration (ET_0) as a proxy for crop water demand was clearly lowest in Horn, intermediate in Krems and Wiener Neustadt and at a similarly high level in the other locations. Distribution of ET_0 shows less variability with Baden having slightly lower cumulative ET_0 in-season compared to Horn.

Heat indicators significantly differ among sites for the number of heat days > 27°C with Horn having less heat days, while the other sites showing similar values. Heat degree hours showed the same pattern as heat days, still not being statistically significant in the differences among the sites.

Long-term indicators (PDSI and CMI) showing drought events via comparison of actual (monthly, weekly) metrological data to average site characteristics (30 year means) did not provide significant differences for both types of indicators.

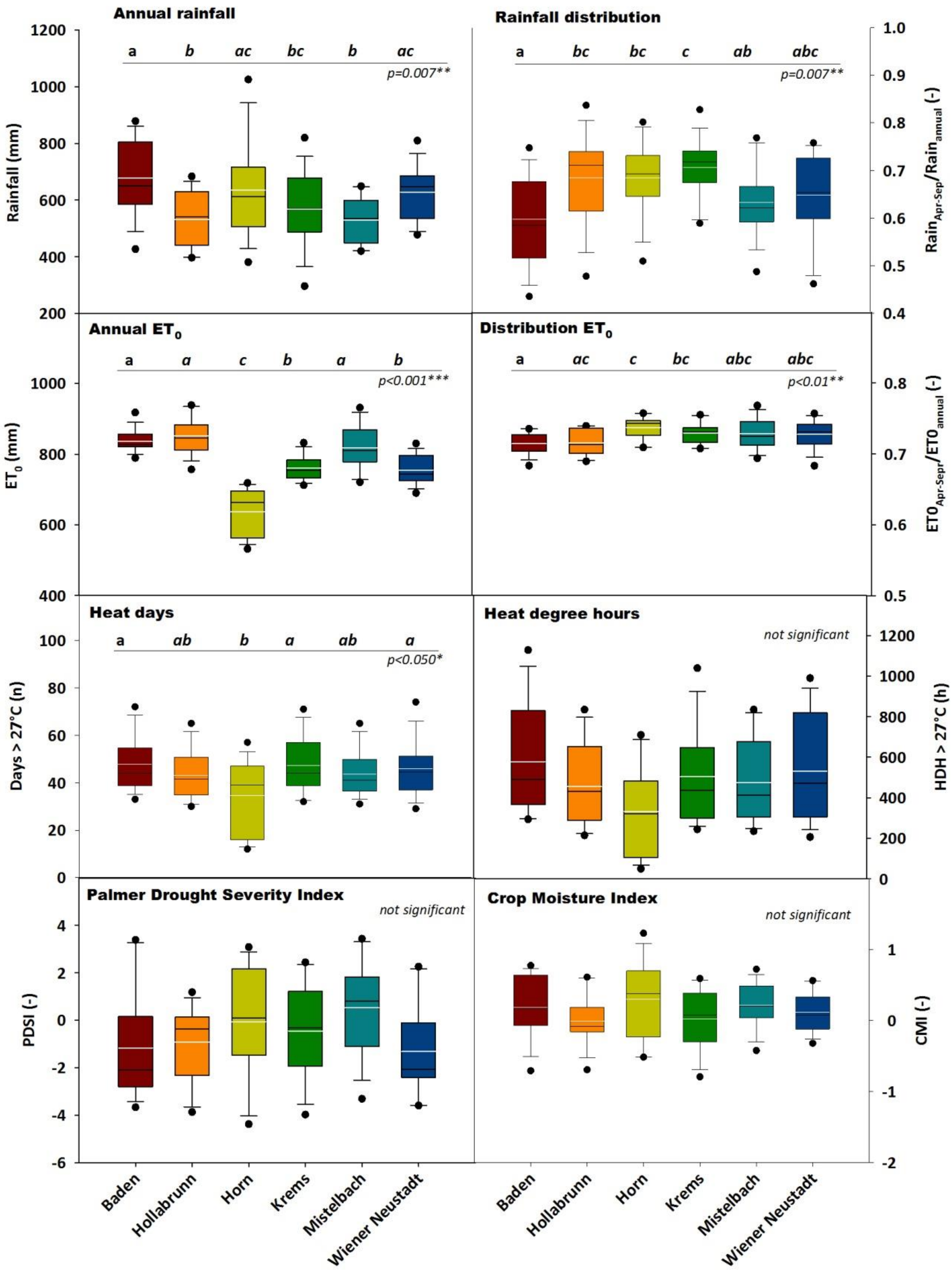

Figure 5: Meteorological characteristics of the sites investigated and used for distinguishing climatic stress regimes. Sites with the same letters do not differ significantly at *p*<0.05.

The meteorological characterization of the sites reveals that rainfall is the main distinctive indicator among sites. When using an aridity index relating annual precipitation to ET_0 (UNEP, 1992) Hollabrunn and Mistelbach are the driest sites (0.62 and 0.65) followed by Krems (0.75), Baden (0.80), Wiener Neustadt (0.83) and Horn as the most humid site with P/ET_0 being 0.99.

Yield and yield stability
Figure 6 shows the percentage of crops grown currently on arable land in Lower Austria. Winter wheat is by far the dominant crop, followed by grain maize, spring barley and sugar beet. Therefore further detailed analyzes on yield focuses on these four dominant species in Lower Austrian crop production which in total cover 49.3 % of total arable land.

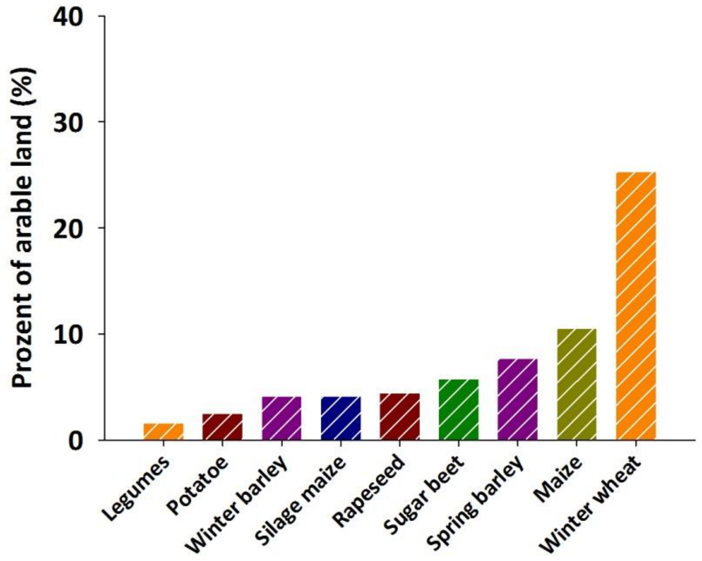

Figure 6: Dominant crops grown on arable land in Lower Austria in 2014 (Source: Grüner Bericht 2015, www.gruenerbericht.at/)

Overall the contribution of year to yield variability of the four dominant crops is high compared to the effect of site (i.e. differences among districts). The respective coefficients of variation are given in Table 3.

Table 3: Coefficients of variation (%) of crop yield due to the influence of site and year.

Crop	Site	Year
Maize	7.1	15.4
Sugar beet	2.5	11.7
Spring barley	2.4	14.9
Winter wheat	3.0	13.8

Maize shows the highest coefficient of variation for both site and year indicating a slightly higher sensitivity to environmental influences compared to the other crops. Particularly for the year effect sugar beet reveals to be the most stable crop.

Figure 7 shows the detailed pattern of the influences of site and year on crop yield respectively registered on farmers' fields.

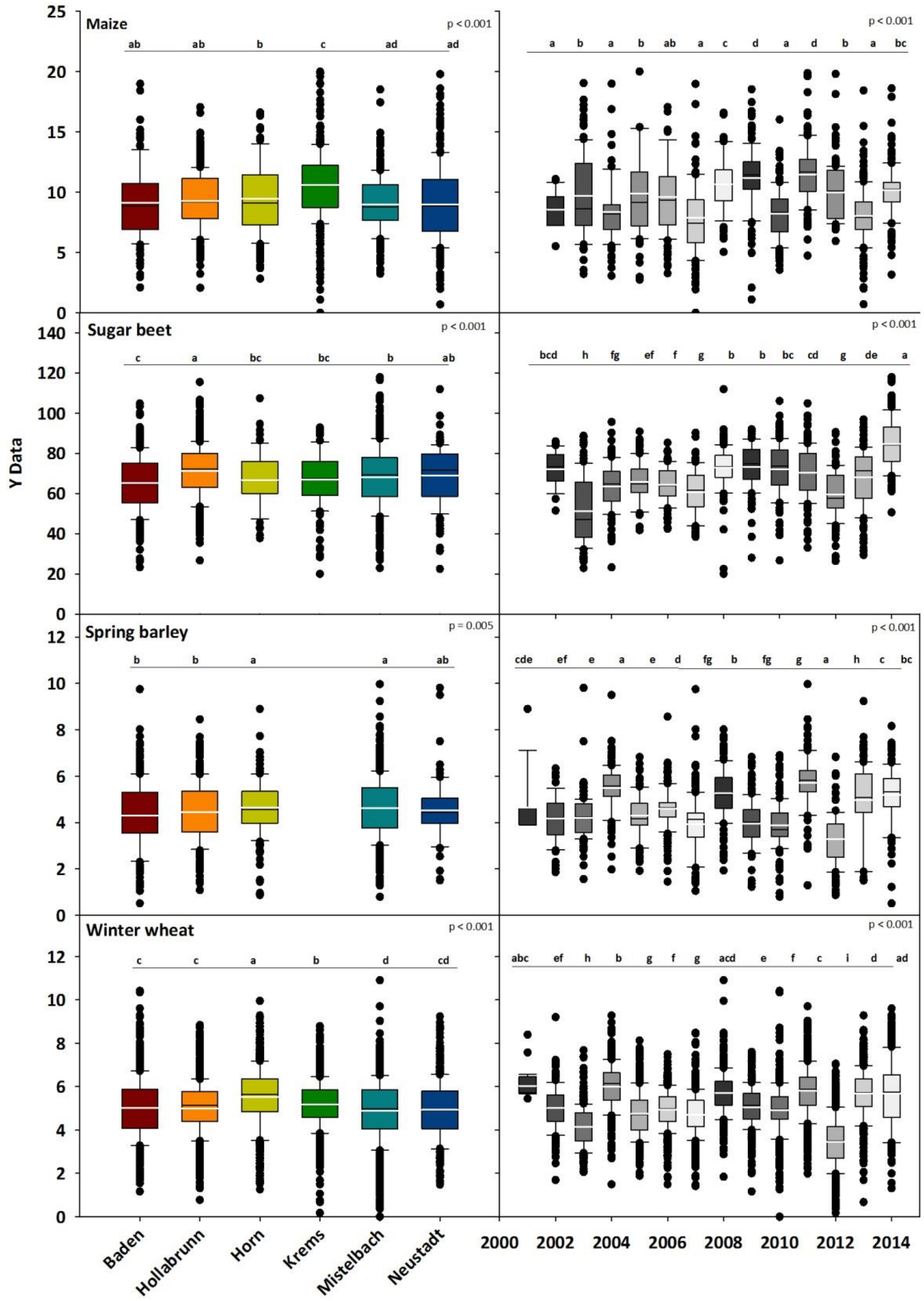

Figure 7: Yield of maize, sugar beet, spring barley and winter wheat as influenced by site (district) and year. Box plots comprise the single yields from the individual farmer's fields for the respective sites (comprising all years; left side) and years (comprising all sites; right side). Box plots with the same letter do not show significant differences of the mean (white line) at $p < 0.05$.

The high number of observations allows a very sensitive statistical extraction of distinctive factors in crop yield. Although the statistical results reveal a significant site effect, the large variability indicated by the box plots suggests strong effects of other factors such as year, soil conditions and different management measures. For maize differences between the average yield at the highest yielding site (Horn) and the lowest yielding site (Mistelbach) are most evident (19 %), while for the other crops differences between the highest and lowest yielding sites are between 5.1 % (spring barley) and 6.9 % (winter wheat) only.

The effect of climatically favorable and adverse years on different crops is similar, although there is a slightly high similarity in yield response between crops with similar seasonality (i.e. maize and sugar beet; spring barley and winter wheat) as between these two groups (within group R^2 0.89 vs. between group R^2 0.83). For maize the most favorable years were 2009 and 2012, while 2007 and 2013 were highly adverse years. Sugar beet had an outstanding yield performance in 2014 while 2003 was clearly the lowest yielding year. Spring barley had highest yields in 2004 and 2011 and lowest in 2012. For winter wheat there were several years with similarly high yields, while 2012 constituted the lowest yielding year like also found for spring barley.

We also assessed yield stability of a wider range of crops for Mistelbach which represents the driest site included in our analysis. This was done by calculating the coefficient of variation (CV) for each individual year and comparing the mean CVs. We thereby assume that a crop with high yield stability is characterized by (i) low CV in individual years because of low sensitivity towards different soil conditions of individual fields and (ii) and low mean CV over years indicating that the response level towards individual fields is stable over years with different meteorological conditions.

Figure 8 shows the result which indicates that sugar beet and sunflower are yield-stable crops, while both spring and winter barley are sensitive towards differences in environmental growing conditions.

Figure 9 compares the yield sensitivity of different crops shown in Figure 8 in relation to a standardized average yield level (actual yield at each environment/mean yield of the crop). All crops have higher yield variability in years with adverse growing conditions as expressed by a below average relative yield, while more favorable growing conditions reduce the coefficient of variation. Also the response (slope) is similar except for spring barley. Maize and spring barley have the highest average coefficient of variation among the four crops compared, with maize showing a stronger response to growing conditions. Sugar beet is at the lower end of yield variability over all yield levels.

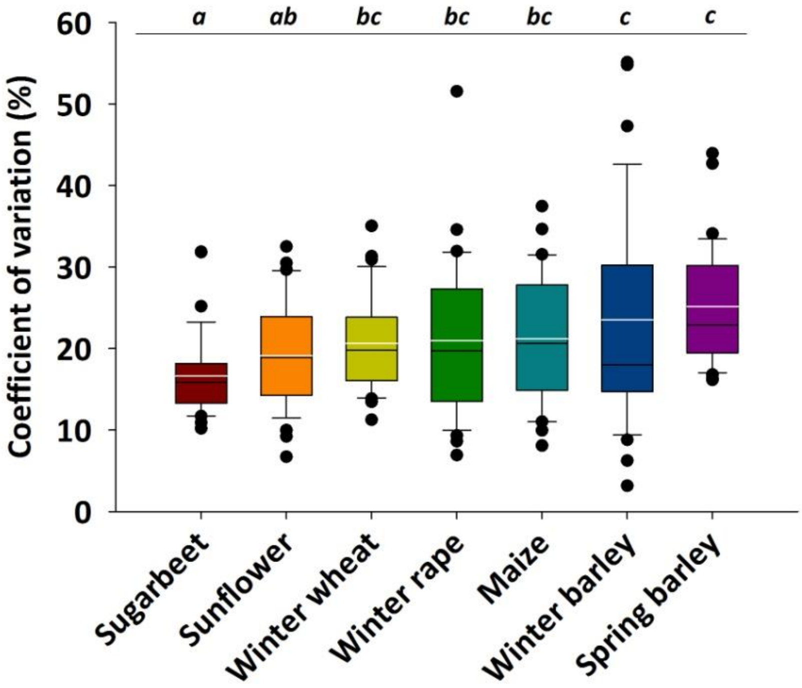

Figure 8: Yield stability as expressed by coefficient of variation (CV) for different crops at the district of Mistelbach. A high CV shows strong response of a crop species to different environmental conditions. Box plots with the same letter do not show significant differences of the mean (white line) at $p < 0.05$.

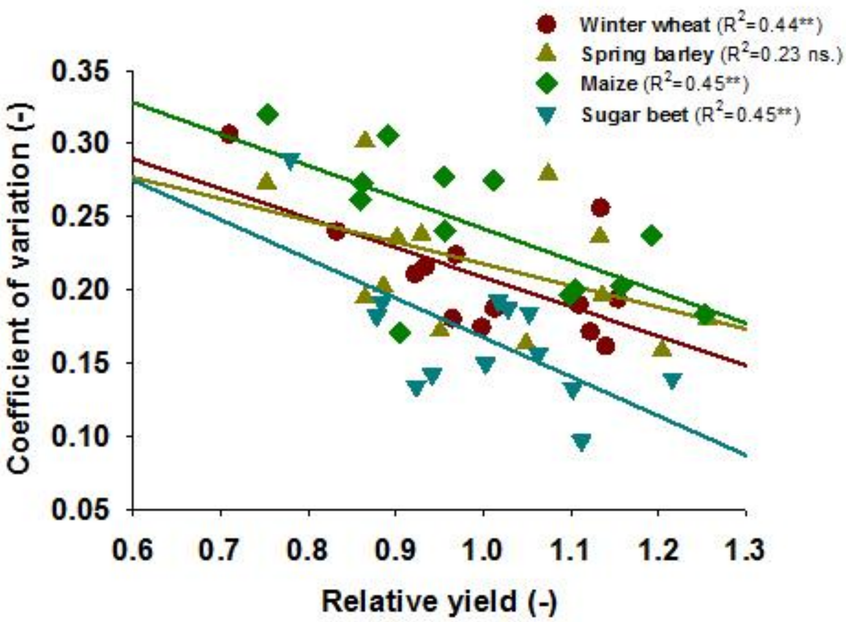

Figure 9: Yield stability as expressed by coefficient of variation (CV) in relation to the relative yield level. Relative yield values higher one express favorable growing conditions, while values lower one show more adverse conditions.

Yield – climate relations

The relation between yield and climatic indicators was calculated using all site x year combinations representing different environments with distinct climatic settings. Figure 10 shows the relation with highest R^2 between the tested indicators and yield when including all environments. Table 4 gives the values of the slope parameters and R^2 of the linear regressions for each individual site.

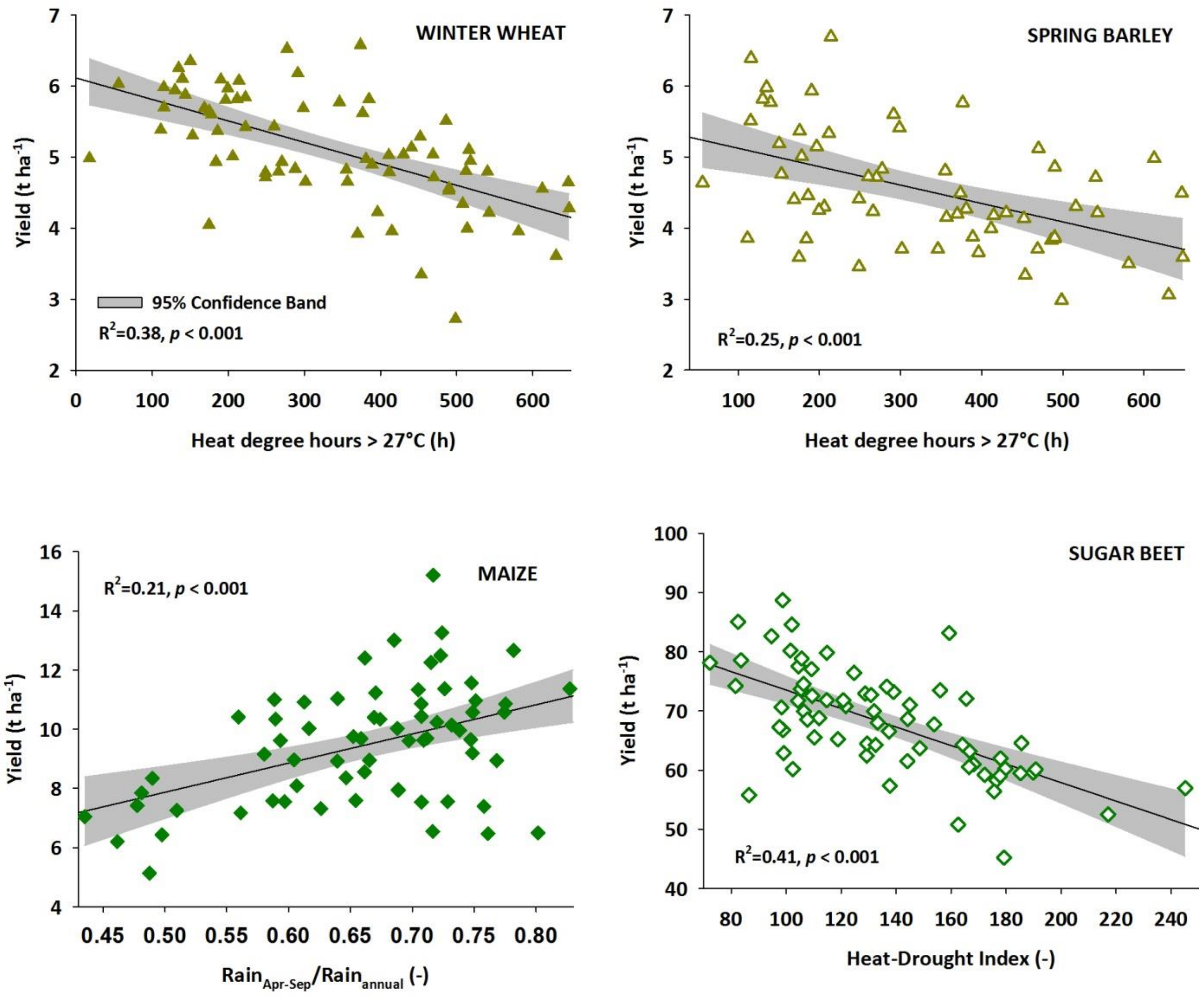

Figure 10: Relation between climatic indicators and yield with highest R2 for different indicators tested.

Table 4: Regression relations between yield and the climatic indicators shown in Figure 6 for each individual site (ns. indicates those cases where the linear regression model was not significant at $p < 0.05$).

Crop	Site	R2	Slope	p-value
Winter wheat	Baden	0.57	$-3.6*10^{-3}$	0.0028
	Hollabrunn	0.49	$-4.4*10^{-3}$	0.0366
	Horn	0.02	$-0.9*10^{-3}$	ns.
	Krems	0.61	$-3.5*10^{-3}$	0.0027
	Mistelbach	0.44	$-4.2*10^{-3}$	0.0188
	Wiener Neustadt	0.65	$-2.7*10^{-3}$	0.0009
Spring barley	Baden	0.21	$-1.9*10^{-3}$	ns.
	Hollabrunn	0.69	$-5.0*10^{-3}$	0.0057
	Horn	0.08	$-1.9*10^{-3}$	ns.
	Krems	No data		
	Mistelbach	0.30	$-3.4*10^{-3}$	ns.
	Wiener Neustadt	0.27	$-2.4*10^{-3}$	ns.
Maize	Baden	0.41	11.44	0.0169
	Hollabrunn	0.17	7.38	ns.
	Horn	0.07	8.78	ns.
	Krems	0.09	5.42	ns.
	Mistelbach	0.27	11.47	ns.
	Wiener Neustadt	0.30	13.91	0.051
Sugar beet	Baden	0.52	-0.14	0.0054
	Hollabrunn	0.57	-0.20	0.0185
	Horn	0.04	-0.06	ns.
	Krems	0.69	-0.15	0.0008
	Mistelbach	0.43	-0.24	0.0194
	Wiener Neustadt	0.55	-0.18	0.0037

For both species of small grain cereals (winter wheat, spring barley) heat stress as expressed by heat degree hours (HDH) with a threshold of > 27°C was the strongest predictor of yield. The relation is more evident for winter wheat compared to spring barley, particularly when comparing single locations. In case of spring barley, the yield effect of HDH is significant for Hollabrunn only, while for winter wheat it is significant for all locations except Horn. The steepest slope, i.e. the strongest yield reduction due to heat stress, occurs in Hollabrunn and Mistelbach for winter wheat and in Hollabrunn for spring barley. Still the differences between the slope parameter values among locations are not significant, sustaining the common mechanism underlying heat induced yield losses.

The long season crops (maize, sugar beet) are more affected by water availability. For maize the strongest relation to yield was found for rainfall distribution with a high amount of in-season rainfalls favoring high yields. When analyzing separately the single locations, the relation is significant only for Baden and Wiener Neustadt. These two locations show the strongest response of maize yield to high in-season rainfall with a similar slope as in Mistelbach where the regression model is not significant however. In case of sugar beet a combined drought and heat stress indicator was revealed as best yield predictor with comparatively high average R^2. As expected, Horn is again an exception where no significant relation to this indicator was found when analyzing the sites separately. For the other single locations, rather high R^2 values between 0.43 and 0.69 were obtained and differences in the slope of the regression were not significant, demonstrating a stable predictive relation between the stress indicator used and the predicted yield level at farmers' fields.

We also tested the yield-climate relations for the mean of all high (75% quantile) and low (25 % quantile) yielding sites in the different environments (site x year combinations). This indirectly subdivides the available yield data between more and less stress prone soils profiles within an environment respectively. There was no fundamental change in the indicators with highest predictive strength: in all cases of both lower and higher yielding sites the same indices performed best compared to the ones determined for the mean yield level. The higher yielding sites however consistently showed a weaker response compared to the average (winter wheat R^2 =0.29; spring barley R^2 =0.10; maize R^2 =0.11; sugar beet R^2 =0.27). Differences in R^2 between the mean yield level of all sites and the lower yielding sites were only minor (winter wheat R^2=0.32; spring barley R^2=0.22; maize R^2=0.23, sugar beet R^2=0.44). This demonstrates that yield is strongly dependent on weather conditions that are only slightly buffered by soil storage capacity in case of sites with higher physical soil quality.

Management effects on yield performance

Beside the general yield analysis which was the focus of the present ADA subproject, we also studied the effect of some selected management measured in terms of their yield influences. Here we report the influence of cover cropping and tillage type as these are relevant management decisions with expected influence on environmental stress impact on crop yields, particularly via changes in soil water availability.

Figure 11 shows the influence of cover crops vs. bare soil for the respective main crops.

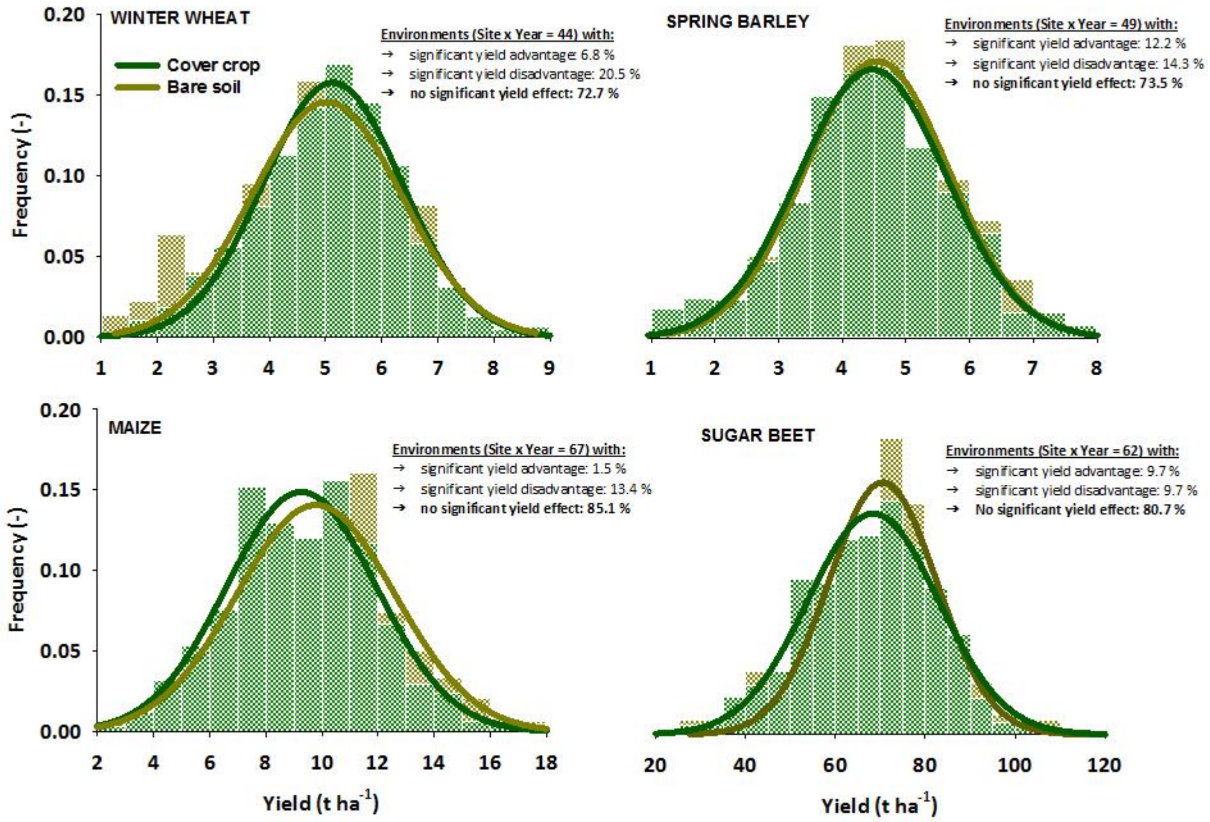

Figure 11: Yield distribution with and without preceding cover crops. The percentage of sites with and without significant yield effect is given in the text for each main crop.

For all four crops the yield effect of a preceding cover crop is minor. In winter wheat the sample size with a preceding cover crop is very small and thus the resulting dataset is strongly unbalanced as most farmers do not practice cover cropping before a winter crop in the rotations. Therefore comparison has to be taken with care for this crop. For spring barley and sugar beet the percentage of environments (site x year) with significant yield advantages and disadvantages is balanced, while for maize there are more environments with significant yield disadvantage following a cover crop compared to sites with yield advantage. However in all cases the predominant number of environments does not show any significant influence of cover cropping on yield.

Figure 12 gives the same type of graph for conventional tillage with plough and reduced tillage without plough, i.e. including all types of tillage systems from chisel based minimum tillage to no-tillage which however is very rare in the region. We also compared the yield effect at different yield levels of the two tillage systems via joint regression.

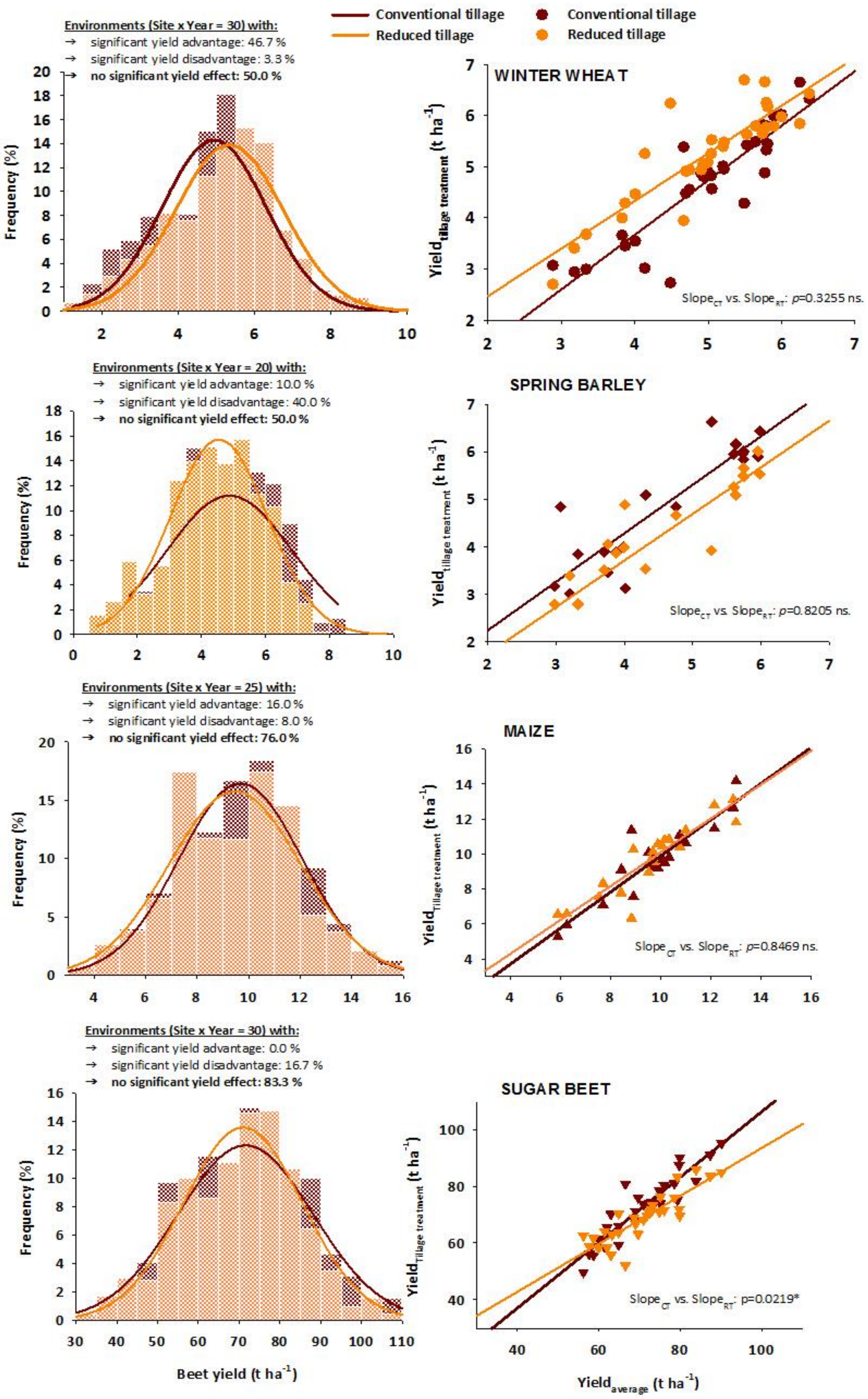

Figure 12: Yield distribution with and without ploughing. The percentage of sites with significant yield effect of tillage system is given in the text for each crop (left). Joint regression of tillage systems with slope comparison (right).

Tillage was registered in the data set since the year 2010, thus the number of environments available for analysis was less. Short season cereals showed a stronger response to tillage over all yield levels while for long season crops (maize, sugar beet) most environments did not show a significant yield difference in response to the tillage system. Interestingly winter wheat had consistently higher yields in response to reduced tillage, while spring barely showed consistently lower yields.

The long season crops had only minor response to primary tillage which is generally practiced between late summer and autumn of the previous year. In both cases there is a tendency of yield advantages in years with lower yield (stress years), while under favorable conditions ploughing provides a yield advantage. This trend however is significant only for sugar beet where a positive effect of more intensive soil loosening for beet growth under non-stress conditions can be expected.

<u>Summary</u>

We investigated the influence of climatic site characteristics on yield of main crops achieved under practical farming conditions in Eastern Austria. Such analysis is of high relevance to understand the vulnerability of crop production to climate change and to provide an empirical background of yield-abiotic stress relations that can be used in model based assessment of climate change vulnerability and potential adaptive measures.

Eastern Austria is a transition region between semi-arid continental climates, characterized by frequent water limitation and pronounced temperature fluctuations between cold winters and hot summers, and sub-humid climates with more temperate temperature regimes. In such a region both assumptions related to climate change impact on crop production might occur: on the one hand increasing temperatures could prolong vegetation periods, allow earlier sowing and an extension of the growing season; on the other hand frequency of abiotic stress situations can increase both in terms of drought as well as heat stress which are already now relevant yield limiting factors.

Concerning the amount of rainfall during the investigated period at the six sites, 56 % of the years had higher annual rainfall compared to the long term (1981-2010) average. Rainfall distribution in the region is generally favorable with most precipitation falling in the vegetation period (April-September). Climate change simulations demonstrated that a major change in rainfall pattern will be a shift of from in-season to off-season (October-March) precipitation (Strauss et al., 2013). In average the investigated period showed lower than average winter rainfall in 59 % of years while summer rainfall was lower than average in only 49 % of years. Thus in the short time period the predicted change in rainfall pattern could not be observed. In 29 % of the cases dry years had both below average winter as well as summer rainfalls.

The rainfall pattern in years with highest stress incidence on yield of the analyzed crops (2003: sugar beet; 2007: maize; 2012: winter wheat and spring barley) is shown in Figure 13. It is evident that the periods with low rainfall coincide with critical growing stages, i.e. tillering in cereals (April), flowering in maize (July) and row closure in sugar beet (July/August –shift of the assimilate sink from leaves to beet). In these periods the respective years are generally below the long term average. Still these years are not always the years with minimum rainfall for the entire period considered in our analysis. This indicates that the yield-climate response is complex, generally involving several variables and possibly acting on a shorter time scale during the critical growing stages than the monthly means considered here.

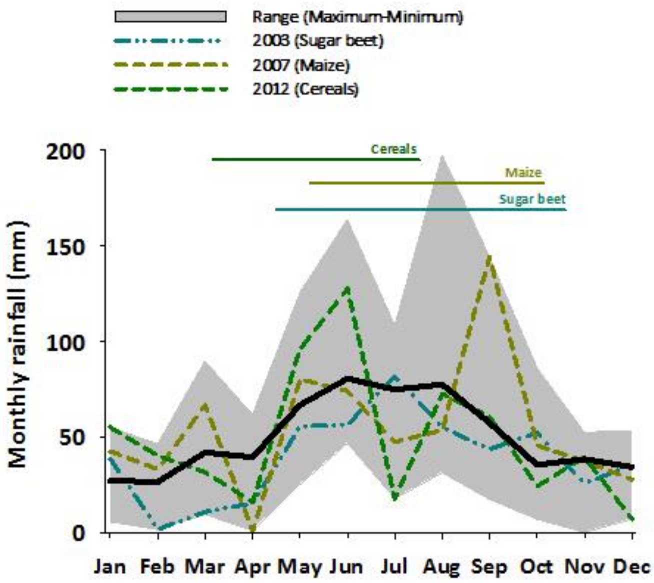

Figure 13: Rainfall distribution in years with lowest yields in cereals (spring barley, winter wheat), maize and sugar beet, range of monthly rainfall between minimum and maximum and long term (1981-2010) average.

As demonstrated by different studies for European climates, heat is a highly relevant stress factor that might even be more critical compared to water stress for yield formation (e.g. Semenov and Shewry, 2011). Also from our data a dominant impact of heat as a driving factor for yield variability in cereals is suggested. The year 2012 had lowest yields in both winter and spring cereals. This year was characterized by the highest number of heat days > 27°C of the entire period analyzed. When including all yield data of the available year x site combinations, it could be demonstrated that also beyond the extreme year of 2012 there is an average significant negative trend of yield reduction with heat hours. This relation is strongest for winter wheat which can be possible explained by the lower water stress sensitivity of a winter compared to a spring cereal (deeper root system, higher water use efficiency) particularly in case of early season drought. It is likely that the highly sensitive flowering stage has been negatively affected by heat in 2012 resulting in a significant yield reduction (Barnabás et al., 2008).

For maize and sugar beet water availability seems to be more relevant compared to cereals. For these crops the most sensitive stages for yield formation can coincide with the onset of early summer drought (July to first half of August). In this period the evaporative demand of the atmosphere is already high and short dry spells can quickly induce water stress in crops. Their resistance against environmental stresses is more dependent on the soil buffering capacity of such stress periods which is a function of site (soil profile depth, soil texture), precedent meteorological (amount of winter rainfall) and crop specific factors (rooting depth, osmotic adjustment, xylem vulnerability; *cf.* Bodner et al., 2015). Sugar beet and sunflower (which was not further analyzed due to its minor importance in the region and therefore less available entries in the data set) are the crops with lowest sensitivity to adverse environmental conditions. Sugar beet is generally grown on deep soils (site factor) and has a high capacity of making use of available water resources due to its deep root system and osmotic adjustment (Bloch et al., 2006; Vastarelli et al., 2013). Sunflower has been found to have particularly resistant xylem elements enabling sustained water extractions from dry soil (Sperry et al., 1998). We found the best predictive relation for sugar beet yield using a combined drought and heat stress index. Drought severity in this index is obtained from a model calculating the average soil water storage depletion. The heat factor might be related to several influences such as the evaporative demand determining the duration until stored soil water reserves are depleted or also to increased respiration losses. Thus for sugar beet it seems to be of particular importance to address water stress via a soil storage related indicator in order to capture its capacity to make use of stored water resources.

Maize was most sensitive to rainfall distribution. Generally maize is well known to respond with high yield losses in case of water stress during flowering leading to disturbed pollination and subsequently low grain set on the cob (Herrero and Johnson, 1981). Maize is grown on more variable sites compared to sugar beet. This can be inferred from the yield data when comparing e.g. the yield differences between the lower quartile and at upper quartile: this is 32.0 % for sugar beet and 41.7 % for maize. For maize best relation between yield and climatic indicators was found for rainfall distribution. This indicates that maize is highly dependent on in-season water supply and has lower potential to buffer stress events via stored soil water resources compared to sugar beet. However, when analyzing sites separately, only for Baden and Wiener Neustadt the relation to rainfall distribution was significant. This might be related to the regional importance of shallow soils (Pararendzina, Lithosol) with low storage capacity and thus stronger yield dependence on in-season rainfalls at these two sites. Furthermore yield limitation in maize can be responsive to short time scales of stress between anthesis and silking which might not be captured sufficiently well by our indicators with a monthly time interval.

Besides the general relation of yield to environmental/climatic stresses, we also studied the role of cover cropping and tillage as two management measures with particular relevance for agricultural water management. Cover cropping is frequently considered as incompatible with water limited sites as it is supposed to deplete soil water storage. Our data demonstrate that in most environments (years x sites) in Eastern Austria cover cropping is feasible and does not result in significant yield differences. Maize seems to be most sensitive to potential depletion effects: although in most cases no significant yield differences are detected, there are more cases of adverse yield effects than favorable ones. This is not the case in sugar beet and spring barley (winter wheat is not considered here due to the unbalanced data owing to rare cover cropping before winter crops).

Tillage strongly influences soil physical properties and is one of the key measures in relation to water management. It has been shown that reduced tillage results in yield advantages in dry environments, while in more humid climates often yields are lower compared to conventional plowing (Van den Putte et al., 2010). Thus the region investigated here can be considered a critical transition region with variable yield effects of reduced tillage systems. Our data suggest that in most cases (site x year) there are no significant yield effects of different tillage systems. Joint regression analysis demonstrated that for maize and sugar beet there is a trend towards favorable yield effects under dry conditions (i.e. in years with lower average yield level), while conventional tillage is superior particularly in sugar beet when environmental growing conditions are not limiting. Winter wheat and spring barley showed contrasting response to reduced tillage: while winter wheat had always higher yields under reduced tillage, the contrary was found for spring barley. This might be related to the more frequent occurrence of a cover crop in reduced tillage systems before spring barley as well as with slightly earlier seeding dates in case of ploughing where quicker drying of a looser soil in spring might allow more timely sowing operations.

Overall management operations can only partially mitigate environmental stresses due to adverse climatic factors. Still under more extreme climatic conditions under climate change it can be expected that management decisions might have stronger – either adverse (e.g. water depletion by cover crops) or favorable (e.g. water saving by reduced tillage) – impacts.

Based on the analysis of drought and heat impacts for the selected major crops in Austria (spring barley, maize, winter wheat and sugar beet) and grassland, and considering related uncertainties as described above, most simple indicators for drought and/or heat impact of crop yields were calibrated.

Table 5 shows the best performing indicators which were used for implementation in the ADA GIS system to calculate drought and heat stress related crop yield depletion.

Table 5: Calibrated and statistically significant crop yield impact functions as implemented in the GIS model.

Crop	Daily heat indicator	Daily drought indicator	Daily drought/Heat indicator		Actually implemented yield depression functions		
Grassland 2nd cut		WSI = DR * 100.0 / TAW			YD = 87.53 + (-.0055 *Σ WSI)	Σ 1.5. - cut date	R^2=0.23
Winter Wheat	Σ HDH > 27	WSI = DR * 100.0 / TAW	TM > 26: CSI = WSI * (TM -25.0) TM < 26: CSI=WSI		YD = 6.64 + (-.000084 *Σ CSI)	Σ 1.3. – harvest	R^2=0.27
Spring barley	Σ HDH > 27	WSI = DR * 100.0 / TAW	WSI > 33 & TM>30: CSI= ((TM-29)*WSI)-33		YD = 5.11 + (-.0002 *Σ CSI)	Σ 1.3. – harvest	R^2=0.20
Maize		WSI = DR * 100.0 / TAW	WSI > 33 & TM>30: CSI= ((TM-29)*WSI)-33		YD = 10.99 + (-.0005 *Σ CSI)	Σ 1.5. - harvest	R^2=0.20
Sugar beet		WSI = DR * 100.0 / TAW	TM > 26: CSI = WSI * (TM - 25.0) TM < 26: CSI=WSI		YD = 89.22 + (-.0008 *Σ CSI)	Σ 1.5. - harvest	R^2=0.41

WSI = water stress indicator [%]
DR = root zone depletion [mm]
TAW = available soil water content at available field capacity [mm]
CSI = combined water and heat stress indicator [-]
TM = maximum daily temperature [°C]
YD = Yield depression relative to not stressed conditions [%]
HDH: Heat Degree Hours [°C]

4 WP 3 – Development of drought-specific forecasting products

4.1 Overview

Reliable meteorological input data is one of the key factors to make useful monitoring and forecasting of drought occurrence. The Zentralanstalt für Meteorologie und Geodynamik (ZAMG) operates and has access to a variety of state of the art analysis and forecasting models that cover forecast ranges from several hours up to few months. These forecast models provide reliable weather forecasts which include drought relevant parameter such as near surface temperature and precipitation. In the framework of the ADA project, special tools have been developed to post-process the model output to drought specific parameters and provide the model data on a common grid and format for downstream applications of the project partners. Although all forecasting models are under continuous development they are affected by a certain degree of uncertainty. To assess these uncertainties probabilistic forecasts are available for all numerical weather prediction (NWP) models in this project. The uncertainties were quantified and evaluated by the use of ensemble forecasting systems. For the ensemble systems operated by ZAMG new methods were developed and tested targeted to improve the probabilistic forecasts especially for drought relevant parameters. A number of evaluations based on case studies as well as on long term verifications showed the usefulness of probabilistic forecasts as additional information to forecasts of drought occurrence from state of the art NWP models.

Work package 3 within the ADA project dealt with the preparation of drought relevant meteorological parameters, mainly temperature and precipitation, from state of the art numerical weather prediction (NWP) and nowcasting models. ZAMG as the Austrian national weather service can provide input for downstream applications from several weather forecasting models varying in horizontal resolution and forecast ranges. The operational model chain includes, among others, the analysis and nowcasting system INCA (Integrated Nowcasting through Comprehensive Analysis) with a horizontal resolution of 1km and the deterministic ALARO model with a horizontal resolution of 4.8km. Since ALARO fields are used as input for INCA both systems provide 'seamless' forecasts from the nowcasting range up to 3 days ahead. ZAMG has also access to forecasts from the European Centre for Medium-Range Weather Forecasts (ECMWF) which global NWP-model covers a forecast range of up to 10 days ahead with a horizontal resolution of 16km.

Since all nowcasting algorithms and NWP forecasts are affected by a certain degree of uncertainty, the importance of ensemble systems for numerical weather forecasts is constantly increasing. At ZAMG there are ensemble counterparts to all deterministic system operationally available. INCA is coupled with the Limited Area Model (LAM) EPS ALADIN-LAEF (Aire Limitée Adaptation dynamique Développement InterNational – LAM) to allow the quantification of uncertainty in the nowcasting range (Ensemble INCA). ALADIN-LAEF can be used to assess the uncertainty in the ALARO forecasts for predictions up to 3 days ahead. The ECMWF ensemble is the counterpart of the ECMWF global model to estimate the uncertainty in the forecasts up to 10 days. For longer lead times ECMWF provides the seasonal forecasting system with a forecast range up to 7 months ahead.

One aim of this work package was the further development of proper methods to quantify the uncertainties of the meteorological input for downstream applications. The tested methods were targeted to improve the forecasts especially for the drought relevant parameter precipitation and near surface temperature. The new methods as well as the existing systems were validated with a focus on drought specific parameter.

For all available models data flow was implemented to enable the use of the data in the GIS system. The model data were post-processed, interpolated to a common horizontal grid and provided to the project partners in the required format.

4.2 Available analysis and forecast data sets for ADA

ZAMG runs their own nowcasting and weather prediction models in an operational mode to provide weather analysis and forecast data up to 3 days ahead to users. In addition ZAMG has access to forecast data from ECMWF which runs global models targeted to provide forecast from medium range up to several months. Below the ZAMG analysis and nowcasting tool and the available NWP models are briefly introduced.

INCA analysis and nowcasting tool

The analysis and nowcasting system INCA (Haiden et al., 2011) algorithmically combines station observations, NWP model output and remote sensing data (radar, satellite) in order to provide meteorological analysis and nowcasting fields at high temporal (5 min) and spatial (1 km) resolution. INCA is used to calculate analyses and forecasts of a variety of parameters.

The INCA analysis and nowcasting system is being developed primarily as a means of providing improved numerical forecast products in the nowcasting range (up to +4 h) and very short range (up to about +12 h) even though it adds value to NWP forecasts up to +48 h through the effects of downscaling and bias correction. INCA algorithmically combines station observations and remote sensing data (radar, satellite) in order to provide meteorological analysis and nowcasting fields at high temporal (5min – 1h, depending on parameter) and spatial (1 km) resolution.

Data

NWP background

For the three-dimensional INCA analyses of temperature, humidity and wind, NWP forecast fields provide the first guess on which corrections based on observations are superimposed. Beginning with 1st of March 2011 a new operational ALADIN configuration named ALARO was set to operations at ZAMG, replacing the old 9.6 km version ALADIN-AUSTRIA. The new 4.8 km version is coupled to the IFS model and uses the ALARO physics package. However, the INCA analysis and nowcasting methods do not depend critically on the horizontal resolution of the NWP fields and could as well be based on other NWP models.

Surface observations

One crucial data source for the INCA system is the input from surface stations. ZAMG operates a network of approximately 260 automated stations (TAWES) across the country which provides data in high temporal resolution. In addition, a high number of data from other providers such as hydrological services, avalanche warning services etc. are used.

Radar data
The Austrian radar network is operated by the civil aviation administration (Austrocontrol). It consists of five radar stations and ZAMG operationally obtains 2-d radar data synthesized from these five locations, containing column maximum values in 14 intensity categories, at a time resolution of 5 minutes. Ground clutter has already been removed from the data.

Satellite data
The Meteosat 2nd Generation (MSG) satellite products used in INCA are ‘Cloud Type’ which consists of 17 categories, and the VIS image. Cloud type differentiates between three cloud levels (low, medium, high) as well as different degrees of opaqueness. It also diagnoses whether clouds are more likely convective or stratiform in character. The VIS image is used to downscale the infrared-based (and thus coarser resolution) cloud types during the day.

Elevation data
The 1-km topography used in INCA was obtained through bilinear interpolation from the global 30’’ elevation dataset provided by the US Geological Survey. The resolution of 30’’ of the original dataset corresponds to ~930 m in latitudinal, and ~630 m (at 48°N) in longitudinal direction.

INCA output fields used for ADA
The ADA project partners have been provided with INCA analyses for drought specific applications (see Table 6, Figure 14 and Figure 15). The features of the most important fields are described in the following.

Temperature
The three-dimensional analysis of temperature in the INCA system starts with the ALARO forecast as a first guess. This first guess is corrected based on differences between observation and forecast at surface station locations. Since the station observations are all made in the atmospheric surface layer it is important to take the daytime temperature surplus and the nighttime temperature deficit near the surface into account in the interpretation of these differences. Thus the model 2m-temperature forecast is conceptually and computationally separated into a ‘3-d’ or model-level part, and a 2-d surface-layer contribution.

$$T_{ALA} = TL_{ALA} + DT_{ALA} \tag{1}$$

Here, T_{ALA} is the standard model 2m-temperature output, and TL_{ALA} is the temperature at the lowest model level. The difference DT_{ALA} between the two temperatures is the temperature surplus (or deficit) in the surface layer. To construct the first guess, model forecasts of temperature on pressure levels are interpolated tri-linearly onto the 3-d INCA grid.

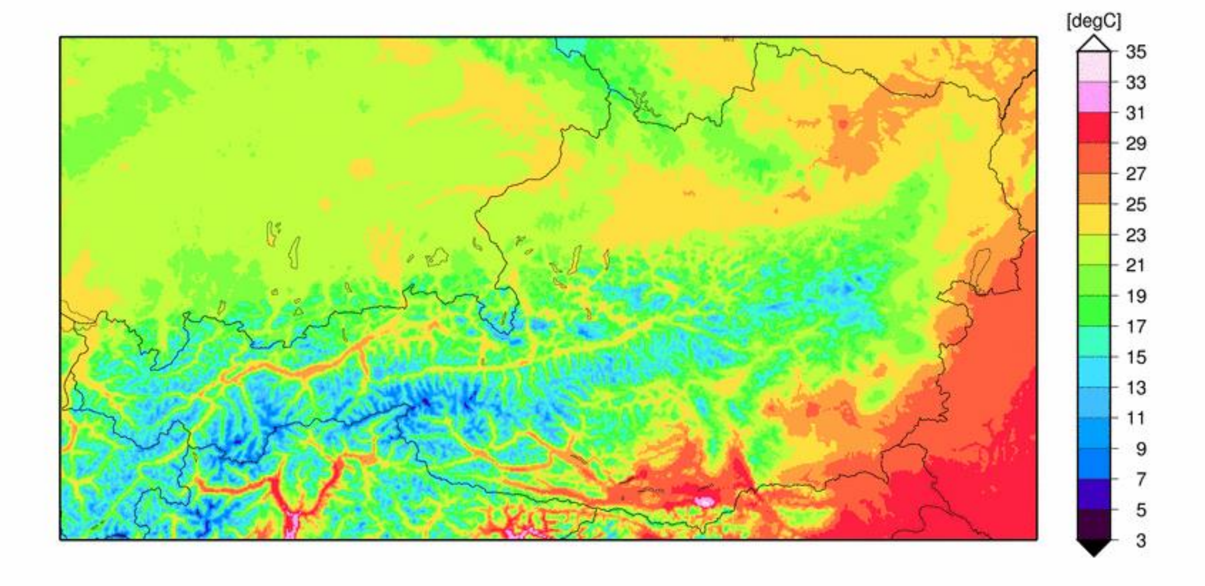

Figure 14: INCA temperature analysis for 20110711, 12 UTC for the Austrian domain.

Precipitation

The precipitation analysis is a combination of station data interpolation including elevation effects, and radar data. It is designed to combine the strengths of both observation types, the accuracy of the point measurements and the spatial structure of the radar field. The radar can detect precipitating cells that do not hit a station. Station interpolation can provide a precipitation analysis in areas not accessible to the radar beam. Naturally, the combination method has to deal with the weaknesses of both types of observation as well, namely the potentially unrepresentative locations, and low density, of stations, and the fundamental quantitative uncertainty of precipitation estimated by radar. The precipitation analyses are computed in 7 steps:

- Interpolation of station data: The irregular point values are interpolated onto the regular 1 km x 1 km INCA grid using inverse distance weighting (IDW).
- Climatological scaling of radar data: The radar data is bi-linearly interpolated onto the INCA grid. Since the radar field is strongly range-dependent and contains biases due to topographic shielding it must be scaled before use in the precipitation analysis.
- Re-scaling of radar data using the latest observations: The climatologically scaled radar field is re-scaled on the basis of a comparison at analysis time of station observations and radar values at the stations.
- The interpolated station and radar data are finally combined to one field that gives a better estimate of the precipitation distribution than each individual field.
- Parameterization of elevation effects (Haiden and Pistotnik, 2009).

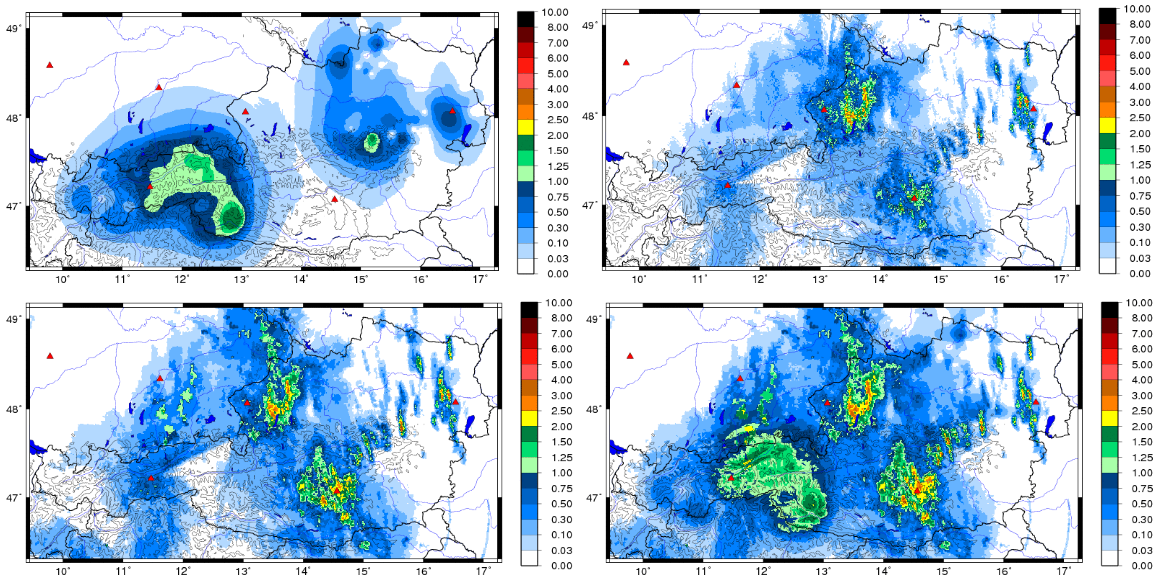

Figure 15: Example of a 15-min INCA precipitation analysis based on the combination of station and radar data. Upper left panel: pure station interpolation, upper right panel: uncorrected radar field (Max-CAPPI), bottom left panel: corrected radar field, bottom right panel: final INCA precipitation analysis.

Wind

The wind analysis is constructed by a first guess of the NWP model (ALARO), a 2D (10-m wind vector) and 3D (lowest model level wind vector) component. Within INCA a distinction is made between the model-level wind and the 10-m wind. To determine the differences between model-level wind and a 10-m wind observation, a factor, which translates a model level wind into a 10-m wind, has to be estimated. After multiplying the observed wind by this factor, differences of the u and v components between the model and the observations are computed and interpolated, using a modified inverse-distance weighting.

However, the inverse distance squared interpolation of observation corrections does not produce a mass consistent field. Therefore, an iterative relaxation algorithm is applied. A brief discussion of different methods for obtaining mass consistent wind fields is given by Wang et al. (2005).

The algorithm used here is similar to the method introduced by Sherman (1978), but takes into account the reduced volume of grid boxes intersecting the terrain in the divergence computation. Such kind of kinematic downscaling can simulate channeling and corner effects but cannot represent dynamical flow effects such as mountain waves, or vortices in the lee of steep topography (Wang et al. 2005), unless they are already present in the NWP field or in the observations. Additionally the generally higher wind speeds over lakes compared to the surrounding land, due to reduced roughness length is taken into account using boundary-layer similarity theory, as described in Haiden et al. (2011).

In Figure 16 an example for the resulting INCA 10-m wind analysis is shown in comparison to the first guess NWP (ALARO) 10-m wind field.

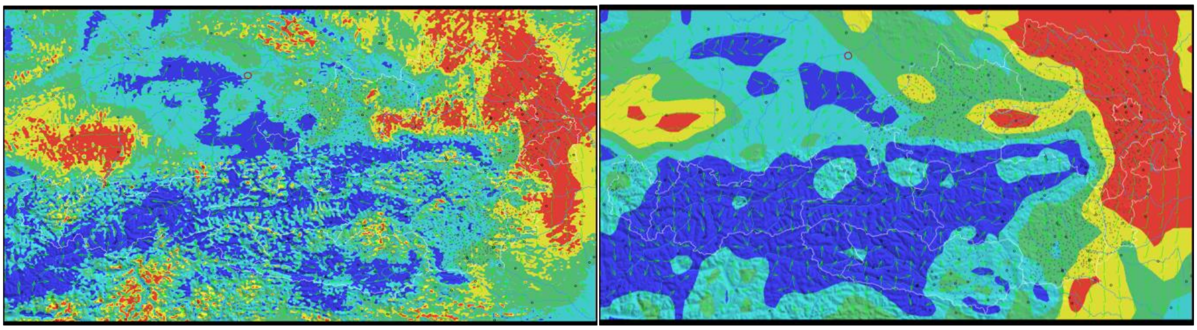

Figure 16: Example of a 10-m wind analysis provided by the INCA wind module for 20110308, 14 UTC (left). The right figure shows the corresponding first guess field taken from the ALARO 20110308 00 UTC model run +14 hours forecast.

Global radiation

The method consists of the following steps:

- Read global radiation observation data
- Correction of data based on offset in the previous night
- Read INCA cloudiness parameter (Kann et al. 2015)
- Read INCA precipitable water
- Read sunrise and sunset times of stations
- Compute solar vector (day, time)
- Compute shadow mask based on solar vector and INCA topography
- Correct shadow mask using station observations of sunshine duration, INCA cloudiness, and sunrise and sunset times
- Correct INCA cloudiness parameter to match station values of sunshine duration
- Compute 1st guess of global radiation, with gaseous absorption effects, topographic effects, and with cloud effects parameterized based on Sauberer and Dirmhirn (Barry 1992)
- Determine differences between global radiation observed at stations and 1st guess
- Interpolate differences (inverse distance squared), separately for non-shadow and shadow gridpoints, using stations in non-shadow and shadow locations, respectively

The method gives a reasonable estimate of the global radiation distribution. The biggest current weakness is that the global radiation station data are not corrected for micro-topographic and other local effects (e.g. reflection from nearby snow surfaces).

Table 6: Summary of the INCA analyses fields, provided to the project partners

Parameter	From year	Forecast (d)	Resolution
Minimum temperature (24 h) [°C d^{-1}]	2003	3 bzw. 10	1 km
Maximum temperature (24 h) [°C d^{-1}]	2003	3 bzw. 10	1 km
Mean temperature (24 h) [°C d^{-1}]	2003	3 bzw. 10	1 km
Daily mean temperature (12 h) [°C d^{-1}]	2003	3 bzw. 10	1 km
Global radiation [MJ m^{-2} d^{-1}]	2003	3 bzw. 10	1 km
Relative Humidity [% d^{-1}]	2003	3 bzw. 10	1 km
Wind [m s^{-1} d^{-1}]	2003	3 bzw. 10	1 km
Precipitation [mm d^{-1}]	2003	3 bzw. 10	1 km

<u>Numerical weather prediction models</u>
For the NWP models operationally available at ZAMG the parameters presented in Table 6 are calculated from standard model output and provided to the project partners. As it can be seen from Table 6, the update frequency for the parameters is 1 per day. Since NWP model output is available with higher temporal resolution, the data had to be aggregated to meet the need of the project partners. Finally all types of model data were interpolated to the INCA grid with 1 km resolution to facilitate the use by project partners. The NWP systems used within the ADA project are briefly described in the following.

ECMWF
The European Centre for Medium-range Weather Forecast runs a global numerical weather prediction model, the Integrated Forecasting System (IFS), operational both as a high resolution model and as ensemble system.

The high resolution forecasts run four times per day on a horizontal resolution of approximately 16 km with 137 levels in the vertical with a forecast range up to 10 days. The initial state is provided using a four-dimensional variational data assimilation (4D-Var) technique which uses observations from SYNOP stations as well as non-conventional data (e.g. satellite data). In 4D-Var, a cost function which measures the distance between a model trajectory and the information already available from background and observations is minimized over a given time window (Andersson and Thepaut, 2008). Model data are available at 3-hourly intervals up to a forecast range of +144h and at 6-hourly intervals for longer forecast ranges up to 10 days ahead.

The ECMWF ensemble system consists of 50 perturbed and one unperturbed members and runs on a horizontal resolution of approximately 32 km and 91 levels in the vertical. The forecast range of the ensemble is up to 15 days where the horizontal resolution is decreased after day 10 to 64 km. The initial perturbations are generated by a combination of singular vectors (Buizza and Palmer 1995) and ensemble data assimilation (EDA). The singular vector method calculates those perturbations at initial time that maximize during a 48h forecast (Barkmeijer et al. 1999), hence represent perturbation which will have a high impact in the future. Singular vectors are calculated separately for Northern and Southern Extratropics and the Tropics, and are finally combined. Those perturbations are updated by differences between EDA-members.

EDA is an ensemble of 4D-Var data assimilations with perturbed observations, model forecasts and sea surface temperature. In total 25 initial perturbations are calculated and are used for the first 25 ensemble member, while the same perturbations are used with reversed sign for the remaining 25 ensemble member. To account for model uncertainties, thus errors in the model parameterizations, two stochastic perturbation techniques are implemented. First, the tendencies in the physical parameterization schemes are perturbed randomly, and second, vorticity tendencies are perturbed stochastically to model the kinetic energy in the unresolved scales (stochastic backscatter, Palmer et al. 2009). The ensemble system also uses a dynamic three-dimensional circulation ocean model for two-way coupling every hour.

ALARO
ALARO is used as the operational limited area model (LAM) at ZAMG since March 2011. It runs 4 times per day on a horizontal resolution of 4.8 km and uses 60 levels in the vertical. The model is integrated up to 72 hours lead time. ALARO (the

configuration run at ZAMG is also named ALARO5-AUSTRIA) is coupled to the global IFS model. For ALARO, the initial state for the free atmosphere is provided by interpolation of the IFS model fields to the ALARO 4.8 km model grid. A surface assimilation system is implemented at ZAMG and supplied with SYNOP and high-density TAWES (Semi-automatic weather stations in Austria) data to produce the initial state for the surface fields using an optimum interpolation method. ALARO replaced ALADIN, which was run on a 9.6 km horizontal resolution and coupled to the French global model ARPEGE. ALARO is being developed within the international numerical weather prediction community ALADIN, a cooperation of 16 national weather services.

ALARO is a special further development of the ALADIN model for horizontal resolutions around 5km. The main differences between ALARO and its precursor ALADIN can be found in the model physics, whereas convection and turbulence should be named in the first place. Running numerical weather prediction models in horizontal scales of 5 km pose a special challenge for numerical model developer. At these scales convection is neither completely resolved by the model, which means that convective phenomena are covered by a sufficient number of grid points, nor the model grid is coarse enough the usage of classical convection parameterization schemes assuming that typical convective cells are usually smaller than a model box. For that reason horizontal scales around 5 km are also called the “grey zone” in the numerical weather prediction community. The parameterization of convection is realized through a scheme called 3MT (Gerard *et al.*, 2009), a prognostic convection scheme which was developed within the ALADIN community.

LAEF

ALADIN-LAEF is the operational limited area ensemble system at ZAMG since June 2011 and runs since July 2013 in its current setup. It consists of 16 perturbed member and one unperturbed control run. The horizontal resolution is 10.9 km with 45 levels in the vertical. The system runs two times per day at 00 and 12 UTC respectively, with a forecast range of up to 72h. All ALADIN-LAEF members are coupled to the global ECMWF ensemble where the perturbed members of LAEF are coupled to the first 16 ECMWF ensemble members.

For a skillful limited area ensemble system the appropriate perturbation of initial conditions is crucial to consider the uncertainties of the forecast in a reasonable way. In ALADIN-LAEF a unique setup is implemented to generate initial perturbations for the atmospheric fields as well as for the surface fields. The perturbed initial conditions in the atmosphere are created by the so called Breeding-Blending cycling (Wang et. al 2011, Wang et al. 2014). In this method ALADIN-LAEF breeding vectors (Toth and Kalnay, 1993) are combined with perturbations from the driving global ECMWF ensemble member using a digital filter. The idea of this method is that the initial conditions should contain perturbations on scales that can be resolved by ALADIN-LAEF (originating from breeding vectors) as well as large scale perturbations from ECMWF ensemble which is considered as the best global ensemble available.

The application of a digital filter assures a smooth transition between scales of ALADIN-LAEF breeding vectors and ECMWF ensemble perturbations. Surface perturbations for the initial conditions are generated by ensemble data assimilation. An Optimum Interpolation method is applied to assimilate 2 m temperature and 2 m relative humidity measurements from SYNOP stations and the high-density TAWES network to update the surface fields in the model. To account for observation errors the observations are randomly perturbed before the assimilation procedure. The combination of the perturbed observations with the use of a first guess from different ALADIN-LAEF members leads to different initial states of the uppermost surface layers in the model.

Besides the uncertainties in the initial and boundary conditions, uncertainties in the model itself exist, due to subscale processes that cannot be resolved by the model as well as to imperfect parameterizations. To consider these errors in the forecast a multi-physics approach is used in ALADIN-LAEF. Every member uses a slightly different model configuration which varies in settings for microphysical processes, parameterization of deep and shallow convection, radiation, turbulence, gusts, and screening level parameter.

ECMWF Seasonal forecasts

In the course of the project the usefulness of long term weather predictions with a forecast range of weeks to months arose. ZAMG has access to the output of the seasonal forecasting system of ECMWF, hence an interface for downstream applications was implemented and the forecast performance for the relevant drought specific parameter was evaluated.

Once per month ECMWF provides seasonal weather predictions with a forecast range of up to 7 months. Although the seasonal forecasting system bases on the same NWP model than the medium range forecasts there are consistent differences in the way of how to use the products of the seasonal systems. Seasonal forecasts cannot predict certain weather situations several months in advance but they can provide information about the climate to be expected on the long term, hence some months in the future. This is possible since some of the components that determine the general state of the atmosphere show long term variations which are to some extend predictable. The most important factors are the oceanic circulations and the related sea surface temperatures, thus a sophisticated ocean-atmosphere coupling is crucial for a reliable seasonal forecasting system. Due to the chaotic nature of the atmosphere seasonal forecasts can only provide a range of possible climates for the coming months.

ECMWF first implemented a seasonal forecasting system in 1997 based on a global ocean-atmosphere coupled model. With this system ECMWF was able to make a successful forecast of the major El-Nino event of 1997-1998. Since 1997 the seasonal forecasting system was constantly upgraded, with the current setup being implemented in 2011 (Molteni et al. 2011).

The seasonal forecasting system at ECMWF is an ensemble system that consists of 51 ensemble members that provide forecasts for the next 1 to 7 months. The forecasts run once per month on a horizontal resolution of approximately 80 km and 91 levels in the vertical. The initial state for the seasonal forecast ensemble members are downscaled from the operational ECMWF analysis which is on an original horizontal resolution of approximately 16 km. Perturbations are introduced by using a combination of the operational 5 member ocean analysis ensemble with perturbed SST and the use of stochastic physics.

In general all data fields required for the downstream applications of this project are available also for the seasonal forecasts and archived in MARS at ECMWF. However there are some limitations since some parameter, namely solar radiation, evaporation, and precipitation are archived in 24 hour intervals only while all other parameter can be retrieved in 6h intervals.

To make appropriate use of a seasonal ensemble forecasting system the model climate has to be available. This is necessary since all seasonal forecast models show a bias to the observed climate which has to be taken into account. Thus ECMWF provides a set of reforecasts for the past to allow the estimation of the average bias of the seasonal forecast. In addition the calculation of a model climate allows the generation of derived products like monthly mean anomalies for the forecasted period. From ECMWF seasonal forecasts monthly mean anomalies for temperature and precipitation are available in MARS.

A skillful seasonal forecast system can provide valuable information for drought monitoring and forecasting. If the risk for drought relevant climate scenarios are already known some months in advance necessary action can be taken by the stakeholder to reduce or even avoid negative impacts on the crop (e.g. by improved watering management). Hence ZAMG implemented the necessary conversion tools to provide seasonal forecasts in the appropriate formats to the project partners.

4.3 On the uncertainty of drought related forecast parameters

Numerical weather predictions and analyses are affected by a certain degree of uncertainty. A major part of the project was to quantify the uncertainties in the forecasts of the drought related parameters and to develop methods to further improve the quality of the existing ensemble systems.

<u>Uncertainty in analyses and nowcasts</u>

Uncertainty of INCA analyses and nowcasts
Cross-validation shows that the skill of the precipitation analysis, which combines radar data and surface station data including parameterized elevation dependence, exceeds that of the pure radar data, and is also significantly better than pure station interpolation, see Table 7.

Table 7: Cross-validation of the INCA 15-min precipitation analysis for different regions and different types of precipitation events.

Period /Type	Validation Area	Number of Analyses	Number of Stations	Relative MAE station interpolation	Relative MAE INCA analysis	Relative improvement
21.11.2008 00-12Z stratiform	Eastern Lower Austria (lowlands)	48	39	45.5%	42.3%	7%
21.11.2008 00-12Z stratiform	Salzburg (mountainous)	48	27	51.2%	46.3%	10%
28.07.2008 15-19Z convective	Salzburg (mountainous)	16	23	104.0%	55.6%	47%
03.06.2008 16-22Z convective	Tyrol (mountainous)	24	29	78.1%	64.6%	17%
04.06.2008 00-24Z strat+conv	Austria	96	260	101.5%	64.5%	36%

As can be seen from Table 7 the improvement of INCA compared to station interpolation is most pronounced in convective cases. In stratiform cases, the improvement is smaller because (a) the stations already capture a larger portion of the spatial variance of the precipitation field, and (b) spurious structures in the radar field caused by beam shielding and attenuation, bright band effects, etc. limit analysis quality.

Cross validation of the temperature analysis for a month typical of fall/winter stability conditions (Nov 2007) shows an MAE near 1 K, and an RMSE near 1.5 K. During the course of that month, the MAE averaged over all stations varied between 0.7 K (well-mixed conditions) and 1.9 K (inversion conditions, partly with Foehn effects). The difference of MAE between stations is even larger, ranging from values near 0.3 K in lowland areas with high station density, to values above 2 K in some deep alpine valleys (Table 8). The main reasons for large analysis errors are insufficient information about inversion heights and about patterns of Foehn-induced mixing in mountain areas.

Table 8: Cross-validation of the INCA 1-h temperature analysis for the whole month of Nov 2007, for stations in different topographic settings.

Station	Elevation (m)	Topographic setting	BIAS (K)	MAE (K)	RMSE (K)
11035 Vienna	198	Lowland	0.0	0.3	0.4
11053 Ried	431	Lowland	-0.4	0.7	0.9
11136 Krimml	1009	Alpine valley	0.3	1.8	2.4
11127 Obergurgl	1938	Alpine valley	0.8	2.0	2.6
11126 Patscherkofel	2247	Mountain top	0.4	1.0	1.3
11343 Sonnblick	3105	Mountain top	0.9	1.5	2.1

Averaged over all stations and seasons, the nowcast of temperature is significantly better than that of the NWP model during the first 6 hours of the forecast (Figure 17). Beyond +6 h there is a small but non-negligible benefit from the downscaling procedure. In the classical nowcasting range the INCA forecast by roughly one-half. The bias is reduced to very small values.

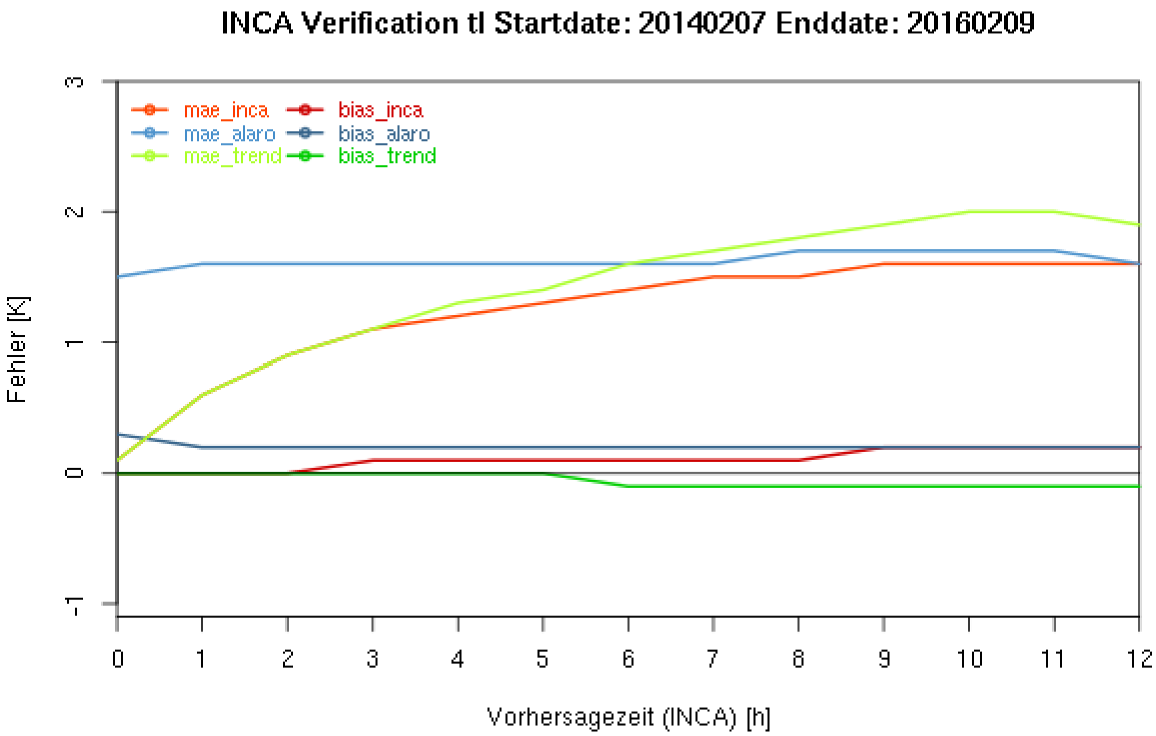

Figure 17: 2m temperature forecast error as a function of forecast time, averaged over all stations, for the 24 month period Feb 2014 – Feb 2016. Light and dark blue curves show MAE and BIAS of the reference forecast (ALARO model). Light and dark red curves show MAE and BIAS of the INCA forecast. Light and dark green curves show MAE and BIAS of the persistence forecast.

Verification of the global radiation nowcasts shows a similar result, with significant improvements relative to the NWP forecast in the nowcasting range. However, the benefit of the nowcasting vanishes at lead times of 5-6 hours (Figure 18).

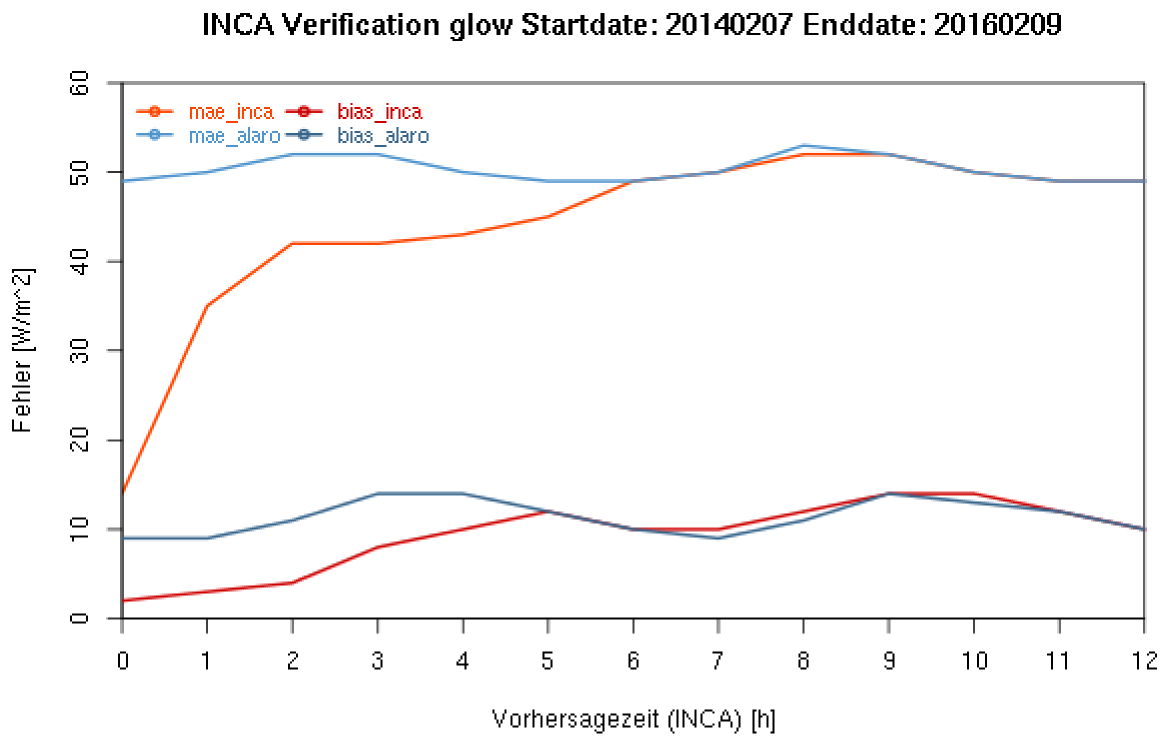

Figure 18: Global radiation forecast error as a function of forecast time, averaged over all stations, for the 24 month period Feb 2014 – Feb 2016. Light and dark blue curves show MAE and BIAS of the reference forecast (ALARO model). Light and dark red curves show MAE and BIAS of the INCA forecast.

Quantification of analysis/nowcasting uncertainties: Ensemble INCA
The Ensemble Nowcasting System (En-INCA) is developed at the Central Institute for Meteorology and Geodynamics (ZAMG, Suklitsch et al., 2015). It basically combines the high resolution deterministic nowcasting approach of INCA (Integrated Nowcasting through Comprehensive Analysis; Haiden et al., 2011) with the probability information provided by the ALADIN-LAEF ensemble system (Wang et al., 2011).

The INCA system, which is under constant development since a decade, is based on blending observations and NWP model fields. In the current version, the (deterministic) INCA uses the NWP model ALARO as background information. It also exploits remote sensing information (such as radar and satellite data) as well as high resolution time invariant information like topography and surface type. The INCA system provides frequently updated analyses and forecasts in the nowcasting range (up to about 6 hours ahead) for a domain covering Austria and its surroundings at a spatial resolution of 1 km by 1 km. It also further improves the pure NWP forecasts for up to +48 hours through statistical downscaling and error correction. The atmospheric fields processed with INCA include temperature, humidity (both with a vertical resolution of 200 m) and wind components (vertical resolution: 125 m). Surface and near surface fields provided by INCA contain wind speed and gusts, precipitation amount and type, total cloud cover and global radiation.

The second component of En-INCA is ALADIN-LAEF, the limited area ensemble forecasting system developed at ZAMG in cooperation with LACE members. LAEF provides the ensemble spread and through that probabilistic information for En-INCA. With En-INCA, the INCA blending algorithm is applied to all 17 members of the LAEF system. By doing that the best of both systems are combined: on the one hand the observation based nowcasting at very high resolution, on the other hand the probabilistic short range forecasting of a state-of-the-art LAM-EPS.

Validation of Ensemble INCA
Several verification scores have been calculated for a period of one month for En-INCA compared to ALADIN-LAEF. The observations used for verification are taken from surface point observations of TAWES (automatic weather stations in Austria).

The CRPS clearly shows the benefit of the En-INCA, especially during the first 6 hours, but also beyond the nowcasting range. The ensemble dispersion matches the dispersion of the distribution of verifying observations a bit better than ALADIN-LAEF, see Figure 19. Also the percentage of outliers is reduced.

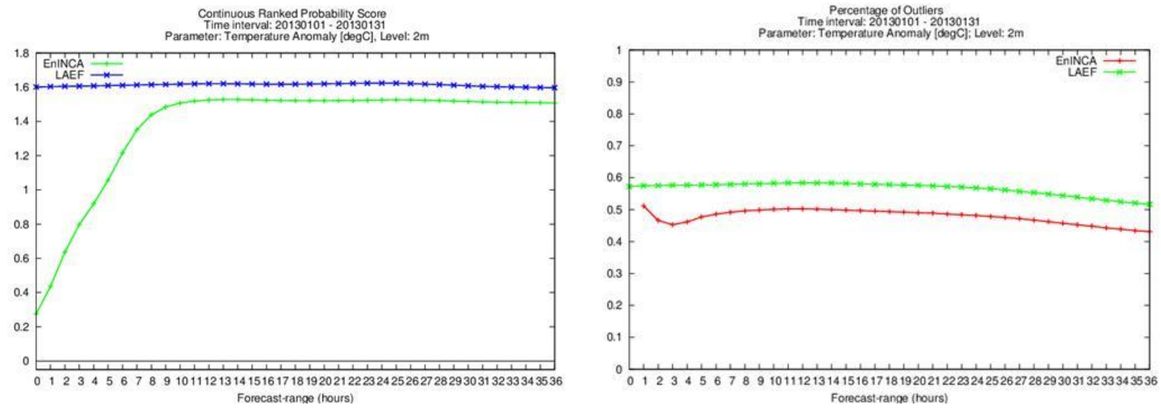

Figure 19: Verification results for a period of one month (January 2013) compared to LAEF for temperature. Left: CRPS (Continuous Ranked Probability Score); Right: percentage of outliers.

Uncertainties in the forecasts

Forecast uncertainties of the operational deterministic NWP model ALARO are assessed by the limited area EPS ALADIN-LAEF. The main uncertainties that exist in regional model forecasts, namely in the initial conditions of the model run, in the boundary conditions and in the model forecast itself, are considered by the methods introduced in chapter 4.2.

Most parameters relevant for downstream applications of the drought monitoring system are near surface parameters. Hence the impact of the model surface plays a key role for the quality of the forecasted parameter since near surface parameter like 2 m temperature/humidity are retrieved by interpolating the parameter between the lowest model level and the model surface. In ALADIN-LAEF uncertainties in the uppermost model surface layers are directly perturbed only in the initial conditions of the model but not during the forecast itself. These initial perturbations are retrieved by running the surface assimilation, where randomly perturbed measurements of 2 m temperature and 2 m relative humidity are assimilated using an Optimum Interpolation method to modify the temperature and humidity of the model surface. Such perturbation of surface fields in the initial conditions is quite common in operational limited area and global ensemble systems.

A new approach that was tested in the framework of WP3 is to stochastically perturb physic tendencies in the surface fields of ALADIN-LAEF during the integration. Therefore a so called Stochastically Perturbed Parameterization Tendencies (SPPT) scheme was adapted for model surface fields. The SPPT scheme was developed at ECMWF (Buizza et al. 1999, Palmer et al. 2009) and is in use to stochastically perturb tendencies of fields in the free atmosphere in the ECMWF-EPS. The idea of SPPT is to account for uncertainties in the forecast due to parameterizations in the model physics. The random number for the perturbation of the physic tendencies in the model is defined by a spectral random pattern generator that creates a field of random numbers over the whole integration domain that is smooth in space and time. The random number follows a Gaussian distribution with an average value of zero, to avoid the introduction of a systematic error, and the standard deviation σ.

Via tunable parameter the amplitude, structure and temporal change of the perturbation field is controllable. The following surface parameter can be disturbed during the ALADIN-LAEF forecast: surface temperature, liquid soil water content, frozen soil water content, snow albedo, snow reservoir water content, snow density and water intercepted by vegetation.

For all these variables, tendencies are calculated in the model to retrieve the corresponding values for the next model time step. These tendencies are perturbed according to the following formula:

$$\tilde{X} = (1 + r) * X, \qquad (2)$$

where $\tilde{X}$ represents the final perturbed tendency, while X is the original unperturbed tendency and r is the random number.

The amplitude and the variation of the random number in space and in time as well, are tunable and several settings have been tested to find an optimal setup for the SPPT scheme applied on surface fields.

Figure 20 shows an example for the distribution of the random number generated by the spectral pattern generator.

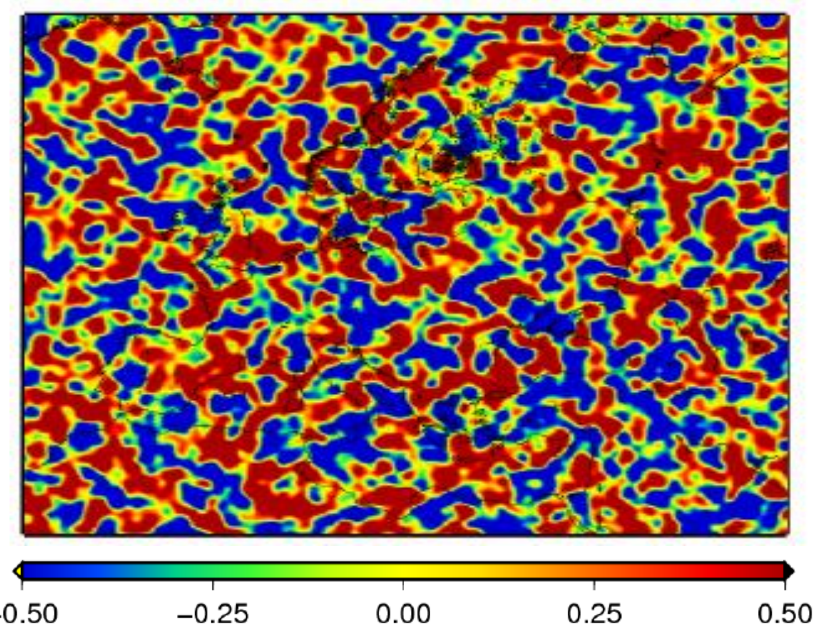

Figure 20: Example of distribution of random numbers used to perturb the model physics tendencies. The maximum amplitude of the random number was limited to be between -0.5 and +0.5 in this example.

To investigate the functionality and the possible impact of the perturbation of the surface fields during model integration a case study is presented where a basic version of ALADIN-LAEF is used. This version is a pure downscaling of the control run of the ECMWF-Ensemble on a resolution of 5km instead of the operational 11 km version of ALADIN-LAEF. In this setup all ALADIN-LAEF members were run with the same model configuration, using identical initial and boundary conditions. The only difference between the perturbed members are the random patterns used to disturb the tendencies of the surface fields during the ALADIN-LAEF integration.

Figure 21 shows the difference of surface temperature (upper panel) and for large scale precipitation (lower panel) between the control run with unperturbed surface and Member 1 with activated surface SPPT scheme for a 54h forecast. The case study shows that differences in surface temperature are in the order of several degrees and that the different surface fields also have a clear impact on the large scale precipitation (maximum differences about 40mm precipitation in 54h). These results emphasize the importance of an appropriate representation of uncertainties in the representation of physical processes in the model surface for parameter relevant for a skillful drought monitoring.

To assess the impact of surface SPPT in different configurations on the average forecast quality of a LAM-EPS two experiments have been set up. For a three month period in summer 2011 a basic version of ALADIN-LAEF was implemented with and without surface SPPT. As in the case study presented above, in the basic version of ALADIN-LAEF no Breeding-Blending cycle and no surface ensemble data assimilation was implemented. It was shown that the setup used in SPPT in the experiment lead to better results, although the improvement was rather small. Additional experiments with different tuning of SPPT, with the focus on different amplitudes and spatial correlations, were performed to find an optimum setup for ALADIN-LAEF. Due to computational limitations those experiments could only be run for one month, but it was found the forecasts are most sensitive to the choice of the perturbation amplitude and not so much to the spatial and time correlation. For the optimum setup, with standard deviation $\sigma = 0.25$ of the perturbation amplitude, the spread of the temperature forecasts was considerably increased accompanied by a small decrease of the error. The combination of increased spread and decreased error is beneficial for ALADIN-LAEF since for near surface parameter the operational version of ALADIN-LAEF has a too small spread compared to the mean error. For other parameters, e.g. precipitation, the results over the verification period were rather neutral for all tested SPPT-tunings.

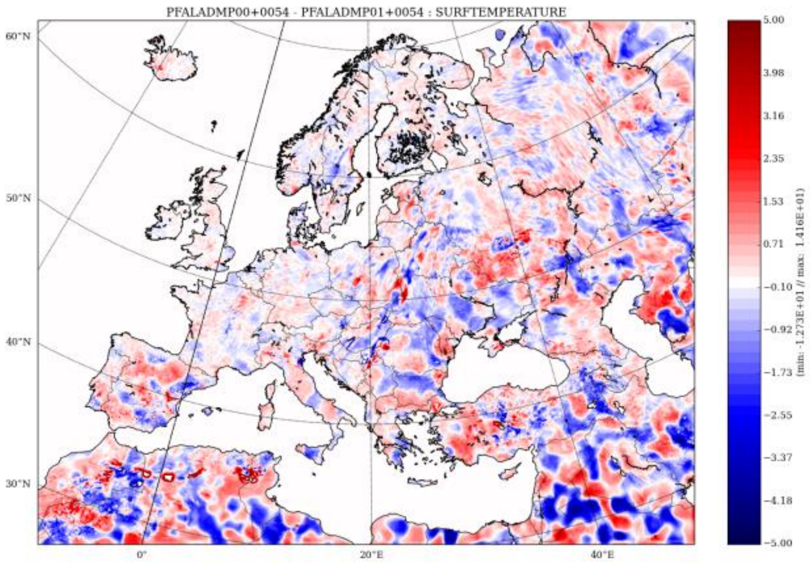

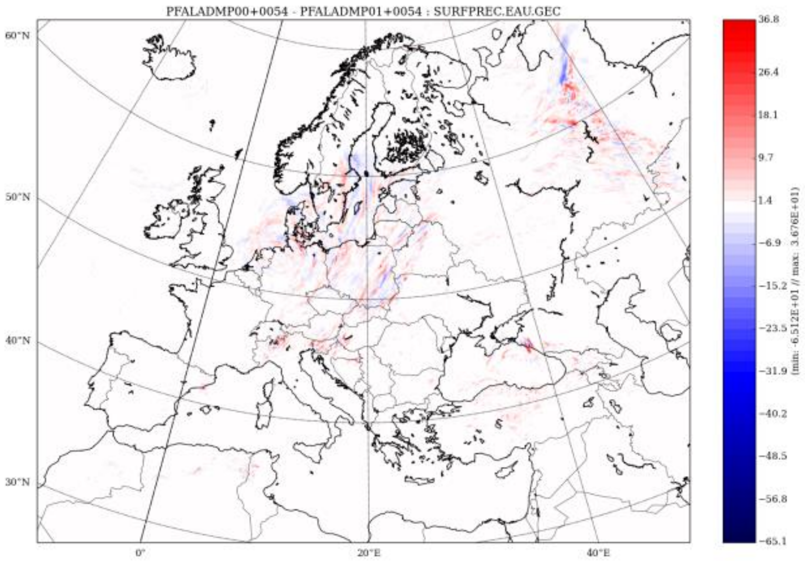

Figure 21: Difference between one member without SPPT and one member with SPPT after 54h forecast for surface temperature (top) and large scale precipitation (bottom).

Evaluation of forecast quality

The forecast quality of the drought relevant parameter was evaluated especially in the sense of the appropriate estimation of the uncertainty. The heat wave that occurred over Austria in July 2015 provided a good period for evaluation that could be used to investigate the performance of the involved forecast models and ensemble systems in an extreme weather period compared to the performance in “normal” weather conditions.

July 2015 was the warmest July in Austria in the last 248 years, the period where ZAMG measurements are available in Austria. The mean temperature in Austria was approximately 3 degrees warmer compared to the reference period from 1981-2010. In addition the precipitation in July 2015 reached only 25 to 50 % of the July average values in the north and north east parts of Austria, causing a major drought in some parts of Austria (Figure 22).

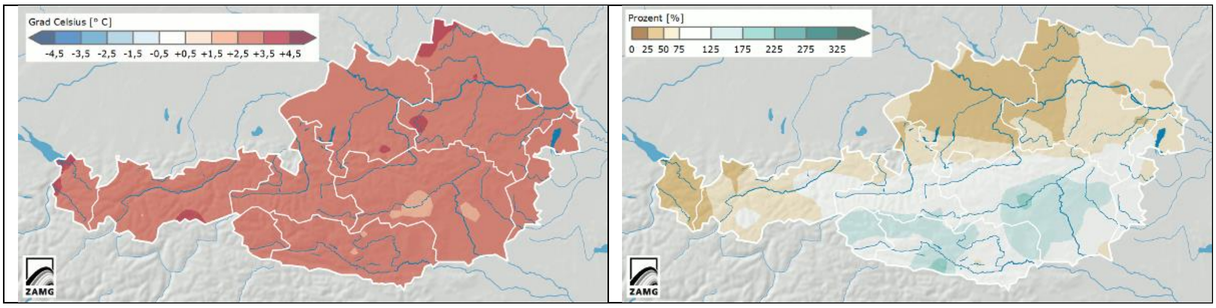

Figure 22: Observed temperature anomaly (upper panel) and precipitation for July 2015 with respect to long term mean (available at http://www.zamg.ac.at/cms/de/klima/klima-aktuell/monatsrueckblick/wetterrueckblick?monat=07&jahr=2015)

The ensemble systems ALADIN-LAEF and ECMWF-EPS were verified using a variety of the most common probabilistic verification scores, with the focus on 2m temperature and precipitation as these are the most important parameter for the downstream applications in this project. One of the most used scores to evaluate probabilistic forecast quality is the Continuous Ranked Probability Score (CRPS). The CRPS summarizes the overall forecast performance of an ensemble system by comparing the forecast distribution with the observed one, where both are represented by cumulative distribution functions:

$$CRPS = \frac{1}{N} * \sum_{n=1}^{N} \int_{-\infty}^{\infty} \left(P_n^f(X) - P_n^o(X)\right)^2 dx, \qquad (3)$$

where $P_n^f(X)$ is the forecasted probability for a certain event *n* and $P_n^o(X)$ the observation with value 1 or 0 when event occurred or not. CRPS is negative oriented with a value of 0 for perfect forecasts.

Both available ensemble forecasting systems, ALADIN-LAEF and ECMWF-EPS, have been verified against observations at 248 stations in Austria and the close surrounding. To investigate the performance of the two systems in drought relevant weather situations July 2015 was chosen as verification period. The results of this verification period were compared to the performance of the ensemble systems in July 2014 which was selected as reference month, since mean temperature and precipitation amounts were close to long term average values in July 2014.

It was shown that for 2 m temperature the forecast quality of both systems was worse in the hot period of 2015 compared to the reference period in 2014 (e.g. CRPS in Figure 23).

For ALADIN-LAEF the degradation is stronger than for ECMWF-EPS. Especially for forecast day 3 the ALADIN-LAEF forecasts suffer from a considerable overestimation of 2m temperature in July 2015, visible in a strong positive bias of 1.5K in the ensemble mean, which cannot be seen in July 2014. For precipitation the scores in July 2015 are generally better than in 2014. This is also visible in the CRPS for precipitation with lower values for both systems and a decrease in the diurnal cycle (Figure 23).

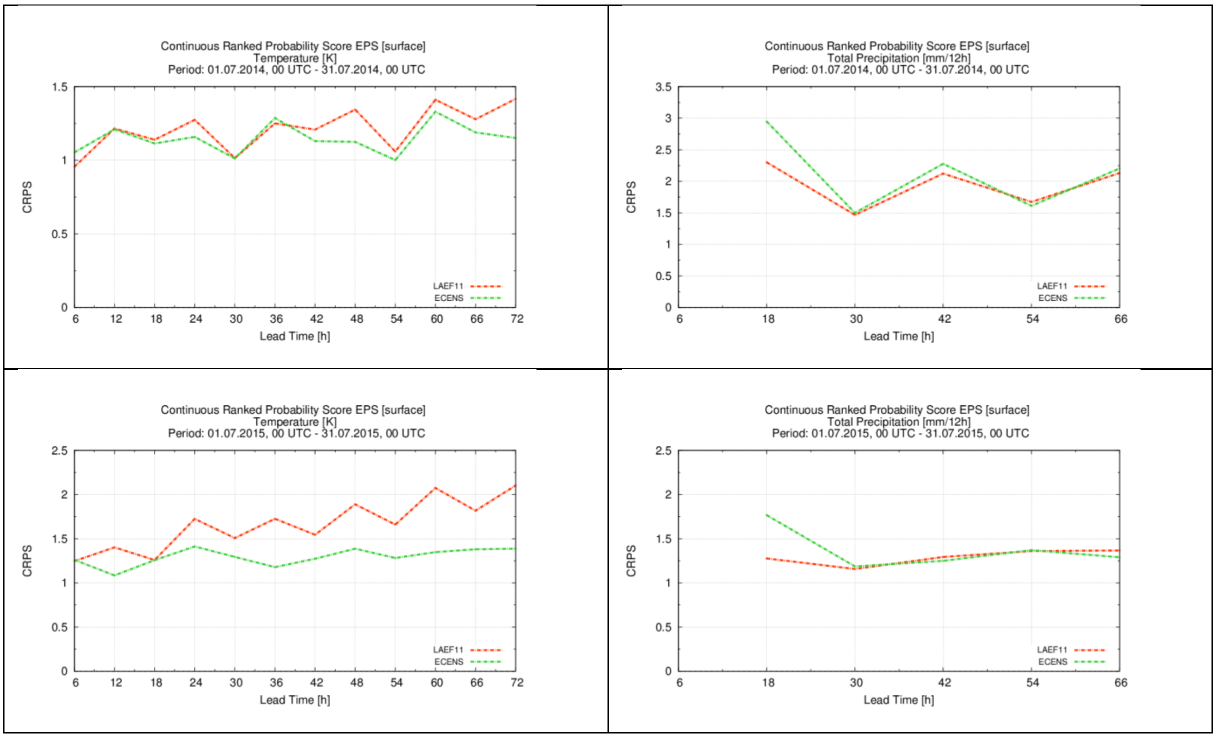

Figure 23: Continuous ranked probability score for temperature (left) and 12h precipitation (right) for ALADIN-LAEF and ECMWF-EPS. The upper panels show results from the verification period in July 2014, hence month with weather conditions close to average. The lower panels are valid for July 2015, an extremely hot and dry month.

Some scores like CRPS or Brier Score can be calculated with respect to a reference value, which can be for example the climatology. To assess the added value of the ensemble systems to forecast the uncertainty, the deterministic forecasts of ALARO were used as reference for the calculation of the skill scores for the verification of ALADIN-LAEF and ECMWF-EPS. It was found that both systems can add significant value to the forecasts of temperature and precipitation in both periods under consideration.

To investigate whether the drought period in July 2015 was predictable well in advance the performance of the ECMWF seasonal forecasts with a forecast range of up to 7 months was also validated.

Figure 24 shows the predicted monthly mean temperature anomalies of ensemble mean for July 2015 from seasonal forecasts starting in January and July 2015, hence a seven and a one month forecast. The temperature anomalies show the deviation of the predicted temperature anomaly with respect to the model climate.

Both forecasts show a positive temperature anomaly for July 2015 ranging between +0.5 to +1 degree with respect to the climate mean for forecasts from January (Figure 24). The January forecast is consistent with the forecasts from the seasonal forecasting system of the following months including June 2015. From those forecasts, July 2015 could be expected to be warmer than usual even several months ago, however the ensemble mean didn’t indicate an extremely warm month. This changed with the forecasts initialized on 1st of July 2015, where a positive temperature anomaly between 2.5 and 4 degree was predicted for Austria, even slightly overestimating the observed temperatures. The forecasts of precipitation anomalies for July 2015 were very consistent and indicated less precipitation than on average already in forecasts initialized in January 2015 and in the subsequent months. So from the seasonal forecasts July 2015 could also be expected to be drier than on average.

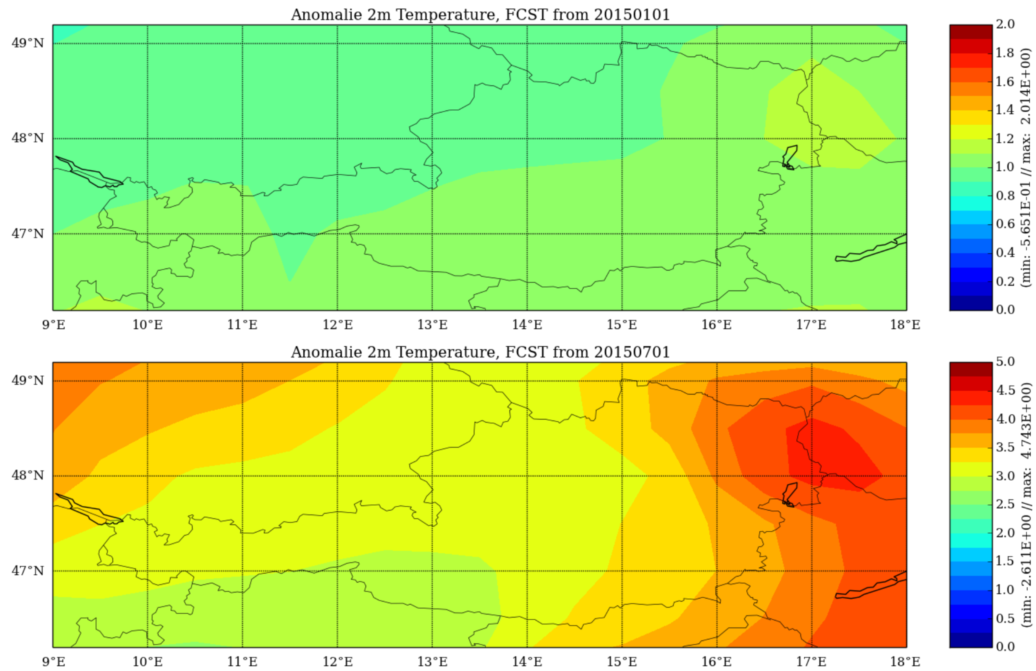

Figure 24: Monthly mean 2m temperature forecasts from ECMWF seasonal forecasts system valid for July 2015. Upper panel shows 2m temperature anomaly of the ensemble mean for forecast initialized on 1st of January 2015, hence a 7 month forecast. Lower panel shows the same field for the forecast initialized on 1st of July 2015.

The seasonal forecasting system consists of a 50 member ensemble hence considering only ensemble mean misses additional information from the forecasting system. In Figure 24 it was shown that the ensemble mean underestimated the positive temperature anomaly for forecasts longer than one month. To investigate whether there was a signal in the long term ensemble forecasts for the drought period, especially the extremely high average temperature, the validation was also done on a probabilistic basis. Therefore all ensemble members were interpolated to the INCA domain and grid and were verified against the INCA analyses. Temperature values were height corrected to the INCA topography by a standard temperature gradient.

One has to keep in mind that in this method the raw model data are used without any post-processing taking the model climate into account. It was found that the heat wave and the correlated drought period in July 2015 was within the predicted probability density function of the ensemble seasonal system in all forecasts starting from January and subsequent months. The real event was mainly covered by the 75% percentile probability forecasts that were calculated in January 2015 and the subsequent months.

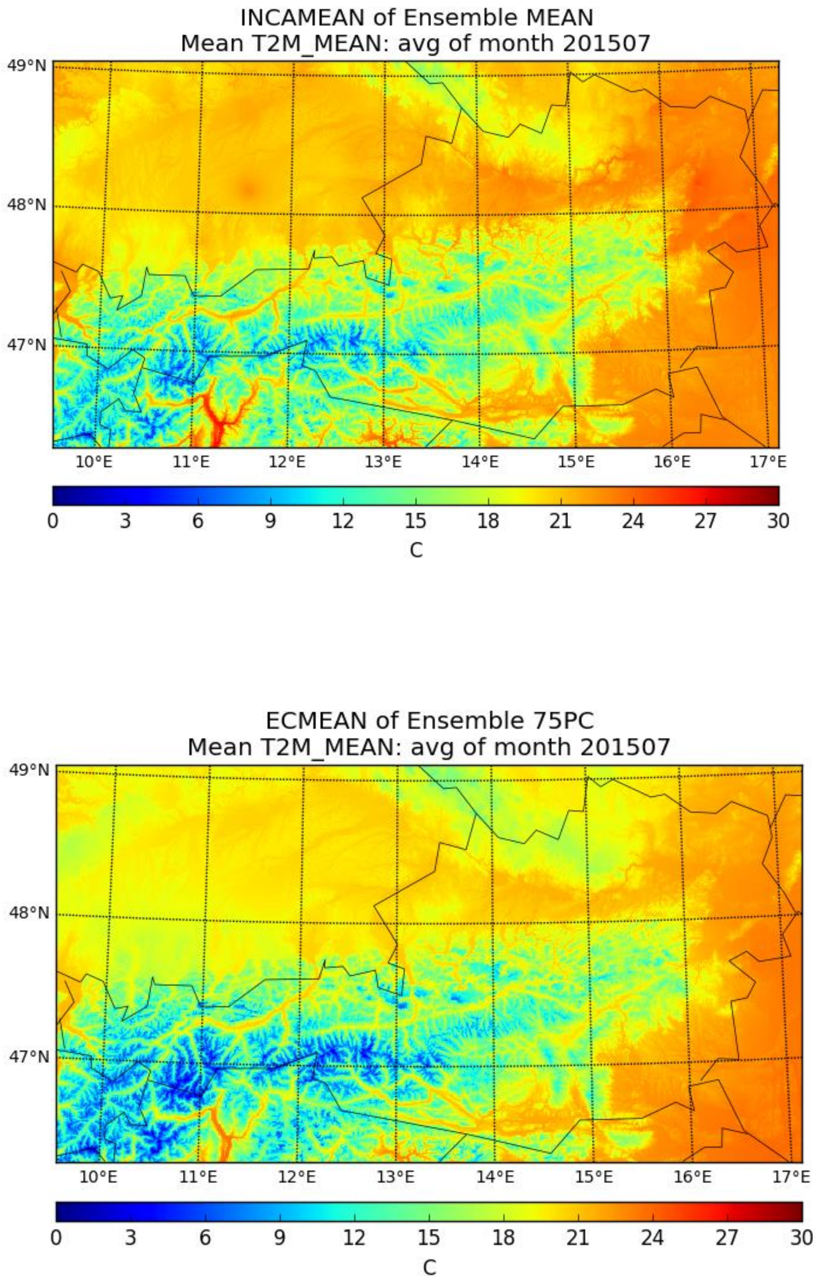

Figure 25: Analyzed mean 2 m temperature from INCA (top) for July 2015 and 75% percentile forecasts from ECMWF seasonal forecasting system initialized at 01/01/2015 (bottom).

An example is shown in Figure 25 which shows the analyzed mean 2m Temperature from INCA and the 75% percentile of the predicted 2m temperature from the ensemble forecasting system. Figure 25 shows that the values of the 75% percentile forecasts are very close to the observed temperatures, with a slight underestimation in Lower Austria. This emphasizes the usefulness of ensemble forecasts in particular for long term predictions. While the ensemble mean only indicated slightly warmer temperatures for July 2015 well in advance, there was already a strong signal in the ensemble system for significantly higher temperatures in the 7 months forecasts. Such information could be very useful for stakeholders, especially those with a high potential loss in drought events, to take precautions to minimize their economic loss.

Summary

Work package 3 within the ADA project dealt with the meteorological input for the drought monitoring and forecasting system. To provide forecasts and analysis of drought relevant meteorological parameter ZAMG has access to a variety of state of the art NWP model with different horizontal resolutions and targeted to different forecasting ranges. The INCA system, running operational at ZAMG is the nowcasting and analyses tool that is used to provide weather forecasts in the nowcasting range up to 6h ahead. Since it uses the operational NWP model ALARO as input seamless forecast for the time range of several hours up to 3 days are available. Forecasts up to 10 days ahead can be retrieved from ECMWF IFS one of the world leading global forecasting systems.

For those three systems probabilistic forecast can be provided by the ensemble system counterparts to quantify the uncertainties in the forecasts. The limited area ensemble system ALADIN-LAEF is used to assess the uncertainty in the ALARO forecasts. To generate reliable probabilistic forecasts a unique method is used to estimate uncertainties in the initial and lateral boundary conditions as well as in the model formulations. For the ensemble INCA system ALADIN-LAEF forecasts are used to predict uncertainties in the nowcasting range. ECMWF also runs a global ensemble system to quantify the uncertainties in the medium-range forecasts. For all available models a special post-processing chain was implemented to provide the drought relevant parameter from the standard model output on a common 1x1km grid in a common format to the project partners.

A special focus was on the quantification of the forecast uncertainty of the drought specific parameter. For En-INCA the added value compared to ALADIN-LAEF in the nowcasting range and to some extend beyond this range was shown. The performance of ALADIN-LAEF and ECMWF-EPS is a specific drought period in July 2015 was evaluated and compared to the performance in “normal” weather situations. While the forecast quality in the extreme hot temperatures of July 2015 was degraded in both systems, precipitation forecast were improved compared to the reference month. The degradation for 2 m temperature was stronger in ALADIN-LAEF than in ECMWF-EPS. To improve the forecast quality of ALADIN-LAEF especially for near surface parameter a new method to estimate the uncertainties in the forecasts was implemented and carefully tested. In the operational version of ALADIN-LAEF the model surface fields are only perturbed in the initial conditions but not during the forecast itself. To account for uncertainties in the surface fields during the forecast a Stochastic Perturbed Physics Tendencies (SPPT) was implemented in ALADIN-LAEF surface forecasts. The method was tested in several case studies to investigate the functionality and the impact of this scheme on the probabilistic forecasts. An evaluation over a one month period was carried out to find an optimum setup for ALADIN-LAEF forecasts. It was shown that the use of SPPT leads to probabilistic forecast with better statistical reliability for 2m temperature forecasts while other parameter under study were hardly affected. Due to the positive impact of SPPT on ALADIN-LAEF forecast quality an incorporation of SPPT in the next operational version of ALADIN-LAEF is planned.

In the course of the project the feasibility of using long term weather forecasts in the range of several months in the drought forecasting tool was discussed. ZAMG has access to the operational seasonal forecasting system of ECMWF-EPS and a special interface for seasonal forecasts was implemented which is necessary since the output frequency of the seasonal forecast system is lower than for the short and medium range forecasting systems. To investigate to what extend drought period can be predicted several months ahead the forecast quality of the seasonal forecasting system was evaluated for July 2015. It was shown that from the first forecast that covers the period of July 2015 up to forecasts initialized in June 2015 a small to moderate positive temperature anomaly in the mean 2m temperature was predicted accompanied with a negative anomaly in precipitation. Only in the forecasts initialized on the 1st of July 2015 a strong temperature anomaly of more than 3K, and thus close to the observed anomaly of approximately 3K, was indicated. However by making better use of the information provided by the ensemble seasonal forecasts it was shown that even in the 7 month forecasts from January 2015 there was a strong signal for a possible extreme hot July 2015. The predicted temperatures of the 75% percentile match the analyzed mean temperature from INCA very well. Using such probabilistic information in the seasonal forecasts could be very beneficial for stakeholders and allow to be prepared for drought periods well in advance. However the evaluation of one drought period has to be extended to more cases to allow statistically robust conclusion about the usability of seasonal drought forecasts.

5 WP 4 – Geographic Information System (GIS) for monitoring and forecasting crop specific drought and heat stress parameters

5.1 Overview

The major focus of work package 4 within the *AgroDroughtAustria* project was the development of a spatial model denominated *ADA-MFS* (Agro Drought Austria Monitoring and Forecasting System) for monitoring and forecasting crop specific drought and heat stress parameters. The model covers automated spatial data manipulation, processing, visualization and storage and is mainly implemented through the software package *ADIS* (Agricultural Drought Information System) as the core component.

The newly developed *ADA-MFS* (Agro Drought Austria Monitoring and Forecasting System) is introduced as a prototype tool for monitoring and forecasting crop specific drought and heat stress parameters for Austria. *ADA-MFS* has been developed within the ACRP project *AgroDroughtAustria* (ADA) with the aim to develop an operational drought monitoring and forecast system, useable for Austrian agricultural conditions and stakeholders. Land use data, information about the soil, vegetation characteristics and meteorological data are used as inputs for *ADIS* (Agricultural Drought Information System) – the core component of *ADA-MFS*. *ADIS* is applied to monitor and forecast reference evapotranspiration, soil water balance, relative soil saturation, drought intensity and various crop specific drought and heat stress indicators. Forecasts are based on historical and forecast meteorological data and are calculated for a short-term period of 10 days and a medium-term period of any number of days – presently as well 10 days. The main results are updated every 3 days and can be published as maps with a spatial resolution of 500 meters for the whole territory of Austria on an appropriate web application.

ADIS is based on the already existing models *SpatialGRAM* (Schaumberger, 2011) and *SOILCLIM* (Hlavinka et al., 2011) for crop specific drought monitoring and forecasting and was developed within the framework of the project using the integrated development environment Eclipse[1] and the object-oriented programming language Java[2]. *ADIS* is designed to work on a Windows Server with Oracle's Java Runtime Environment (JRE) installed and functional. *ADIS* is integrated in the operable *ADA-MFS*, which additionally is composed of a *FTP* (file transfer protocol) component for the download of the meteorological input data and a web based visualisation tool.
ADIS is split up into two major components: the monitoring component that allows the computation of drought and heat stress parameters for a limited time period (1981 till the last past day of the current year) using historical meteorological data and the forecast component for a user defined forecast period using a combination of forecast

[1] Eclipse is an integrated development environment developed by *The Eclipse Foundation* and primarily used is for developing Java applications.
[2] Java is a general-purpose computer programming language that is concurrent, class-based, object-oriented and specifically designed to have as few implementation dependencies as possible.

and historical meteorological data. While the monitoring component of the program is run only once for the historical years 1981 till 2015, the forecast calculations are run on a regular time basis – basically every third day due to a mean forecast computation cycle of approximately two days. In the following chapters the model will be discussed in more detail with the main focus on the program's scope, the system's design, architecture and development, the major components and the overall methodology.

5.2 System development and structure

The goal of the development is the creation of an automated system capable of stable and uninterrupted file creation, file handling and file display via the web with minimum human interaction. The development of the new monitoring and forecasting tool *ADIS* as the main component of *ADA-MFS* includes the integration of parts of *SpatialGRAM*'s and *SOILCLIM*'s source code, of new models and algorithms for crop drought stress detection and of spatial now- and forecast weather data input routines.

ADIS is designed to:

- import large volume digital meteorological, land use, soil and elevation data
- compute soil water balance values for all locations of the study area assigned to ADA specific crops
- assess drought and heat stress related parameters based on the soil water balance results
- compute crop yield reduction values
- perform all computational operations in monitoring and forecast mode
- export computation results for selected parameters in various numerical and graphical file formats
- allow the execution of all necessary computation tasks within a reasonable time frame in a fast and efficient way, carefully utilising available computer resources

The spatial drought monitoring and forecasting computations are based on the calculation of various crop specific biophysical parameters. The most essential parameters are exported as spatial data files and can be outlined as follows:

- Reference evapotranspiration *ET0* [mm]
- Crop coefficient *Kc*, crop interception *interc* [mm], crop evapotranspiration ET_C [mm] and actual evapotranspiration ET_A [mm]
- Soil water content *swc* [mm]
- Relative soil saturation *rss* [%] (expressed in absolute values as well as in classified values)
- Drought intensity *DI* (expressed in absolute values as well as in classified values)
- Heat stress indicator *HSI* [°C], drought stress indicator *DSI* [%] or the combined heat and drought stress indicator *CSI* [°C%]
- Crop yield reduction *YR* [%] (expressed in absolute values as well as in classified values)

The generation of *ADA-MFS* required several different working steps including the coding of *ADIS*. The development was accompanied by additional tasks such as the one-time preparation of meteorological, elevation and land use input data, the development and coding of a *FTP* download tool and of a web page prototype to visualise the results.

The first major working step of *ADIS* programming was the development and coding of adequate I/O interfaces to allow high performance data access and export. Based on the excellent performance and the relative small size of *netCDF* data files, the *netCDF* file format was chosen as main format for the creation, access, and sharing of the data. *netCDF* is described in more detail in the following chapters.

Due to the existence of the models *SpatialGRAM* and *SOILCLIM* and their programmatic implementations, significant time was spent in a second major working step to analyse the methodologies of the two models and to select suitable algorithms for the new software. Appropriate algorithms were, for the most part, transferred unaltered and to a small part adapted to the project specifications. Furthermore new project specific methodologies and algorithms were also developed and implemented.

In the next step a new extensive program logic was coded including the existing and newly developed algorithms. All program features have been implemented as static or instanceable classes in accordance with the object-oriented programming paradigm. All classes with their class methods and the number and types of class variables and, last but not least, the program structure itself have been optimized with regard to a balanced ratio of computer memory consumption and processing speed. Several testing classes have been included to check the program's classes for functionality and correctness. Furthermore various methods have been implemented to export intermediate and final results of crucial calculation steps in *ASCII* text file format for evaluation and graphical visualisation purposes.

Besides *ADIS*, a separate application has been developed and coded to allow the download of all necessary meteorological monitoring and forecast files from a download server of the Austrian Central Institute for Meteorology and Geodynamics *ZAMG* (Zentralanstalt für Meteorologie und Geodynamik). The meteorological files use the *netCDF* file format, are created on a daily basis and can be downloaded at any time. And last but not least a web page prototype was written to allow the illustration of the computation results. The web page is based on the open source platform *MapServer*[3], which allows the building of spatially enabled internet applications.

[3] MapServer is an Open Source platform for publishing spatial data and interactive mapping applications to the web originally developed at the University of Minnesota (USA).

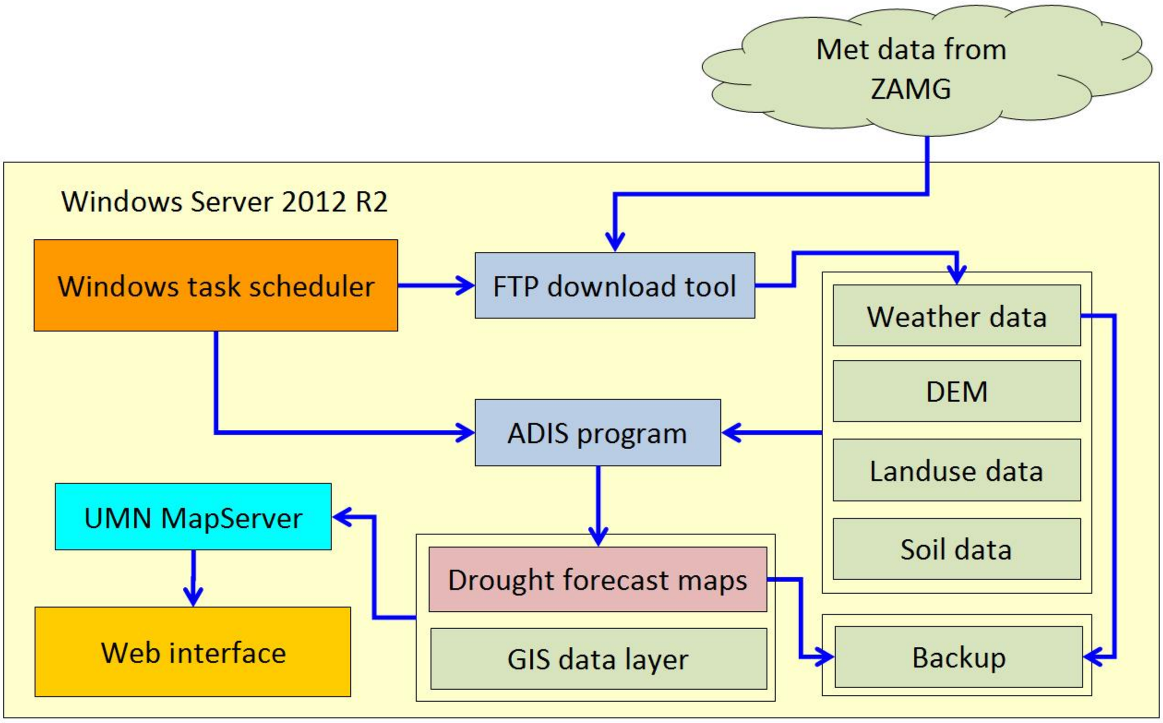

Figure 26: *ADA-MFS* system web architecture.

All components of *ADA-MFS* are located on a Windows server. *ADIS* and the *FTP* download tool are triggered and controlled by the Windows task scheduler. The web architecture is depicted in Figure 26.

<u>ADIS system overview</u>

ADIS is designed as a modular system controlled by a central module which at the same time defines the graphical user interface *GUI*. The user can adjust a limited number of parameters through the *GUI* before any of the four main computation processes is started. All parameter modifications are stored in *ASCII* text files and included at program start. The computations are performed on a daily basis generating a large number of *netCDF* export files requiring a few Tera bytes of disk space. Conceptually *ADIS* is designed to keep the number of I/O operations as low as possible to improve overall performance.

The structural design of *ADIS* implements horizontal and vertical partitions. The horizontal partitions include four main computation processes:

1. the computation of the reference evapotranspiration of historical data (termed ***Historical ET0***) and of forecast data – the computation of the reference evapotranspiration is based on the *FAO* Penman-Monteith method (Allen et al.,1998)
2. the computation of the historical water balance development including heat & drought indicator development and crop yield reduction development but excluding drought intensity development (termed ***Historical WB***)
3. the computation of the historical drought intensity development (termed ***Historical DI***)

4. the computation of the ongoing and predicted development of the crop yield reduction parameters and of all drought parameters of the actual year (termed ***ADA Forecast***)

Each of the four main computation processes can be selected in the program's *GUI* (see Figure 27) and is executed within individual computer sessions. A simultaneous execution of the four tasks is not possible due to hardware restrictions and internal data relationships.

It is not possible, for example, to compute historical or actual drought intensity values prior to the computation of *ET0* and historical soil water balance values. Thus, the following simple calculation sequence is obligatory: initially the *historical ET0* computations have to be executed for all historical years taken into consideration followed by the calculation of *Historical WB*. Only then it is possible to execute *Historical DI* or *ADA Forecast*. *Historical DI* and *ADA Forecast* do not depend on each other and can be arbitrarily executed.

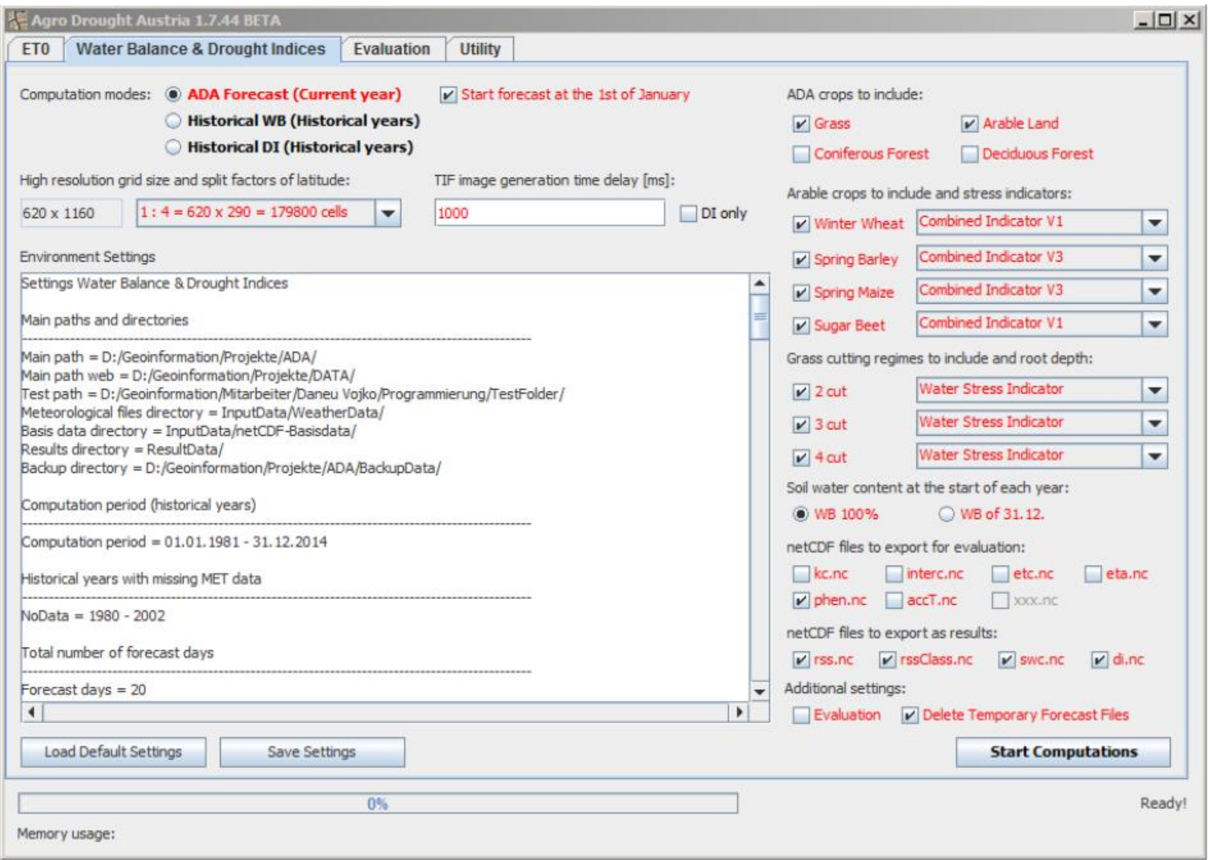

Figure 27: *ADIS* graphical user interface – “Water Balance & Drought Indices” tab selected

All four processes strictly follow a top down control and work distribution without any user interaction. The main modules of the processes are executed in individual threads allowing the visualization of the calculation progress with a progress bar.

The system architecture of *ADIS* is depicted in Figure 28. Starting point of the computation sequence is the one-time calculation of *historical ET0* for all historical years taken into consideration. The process is based on the combination of two modules (Java classes). The first module (“*Control: ET0”*) controls data access to the meteorological input data and the chronological sequence of the computations. This applies to the computation of *ET0* for historical days (for the historical years 1981 till 2015) as well as for the historical days of the current year and any day of the two *ADA* forecast periods described later on. The second module (*“Calc: ET0”*) holds the actual calculation logic. Core part of the module is a double loop that loops through each cell of the region of interest in latitude and longitude direction. *ET0* computation algorithms, which are collected in other Java helper classes, are invoked for each cell addressed in the double loop. This conceptual approach can be found in various other processes within the system architecture. The results of the *historical ET0* computations are exported and stored in *netCDF* file format.

The next essential computation step following *Historical ET0* comprises the execution of the *Historical WB* process. This process starts with the execution of the water balance calculations, which are driven by three modules. The first module is responsible for the temporal sequence of the computations (“*Control: WB, RSS, SI”*) looping through all historical years taken into consideration. At the beginning of each historical year, a second module (“*Calc: Phen”*) executes the calculation of the phenological stage entry dates of each of the considered crops across the whole year allowing afterwards the execution of the subsequent module (“*Calc: WB, RSS, SI”*), which first of all carries out the calculation of the soil water balance for each cell of the area of interest carrying an *ADA* crop type. The module furthermore allows the calculation of relative soil saturation values as well as the calculation of heat & drought indicator values.

The main results and optionally also intermediate computation results are exported and stored in *netCDF* file format. The *Historical WB* process furthermore allows the computation of crop yield reduction values based on heat and drought stress indicators. The module controlling the temporal sequence of the calculations (“*Control: YR”*) loops through each day of the historical year and accumulates the stress indicators (“*Calc: SIS”*) calculated and exported by the preceding modules. For a selected number of days of the historical year, which can be chosen by the user, crop yield reduction values are calculated (“*Calc: YR”*), exported and stored in *netCDF* file format. Two subsequent final modules (“*Control: Results”* and “*Control: Clean”*) conclude the computation process. They are responsible for the distribution and final manipulation of the *netCDF* result files as well as the discharge of temporary files and result files, which are no longer required.

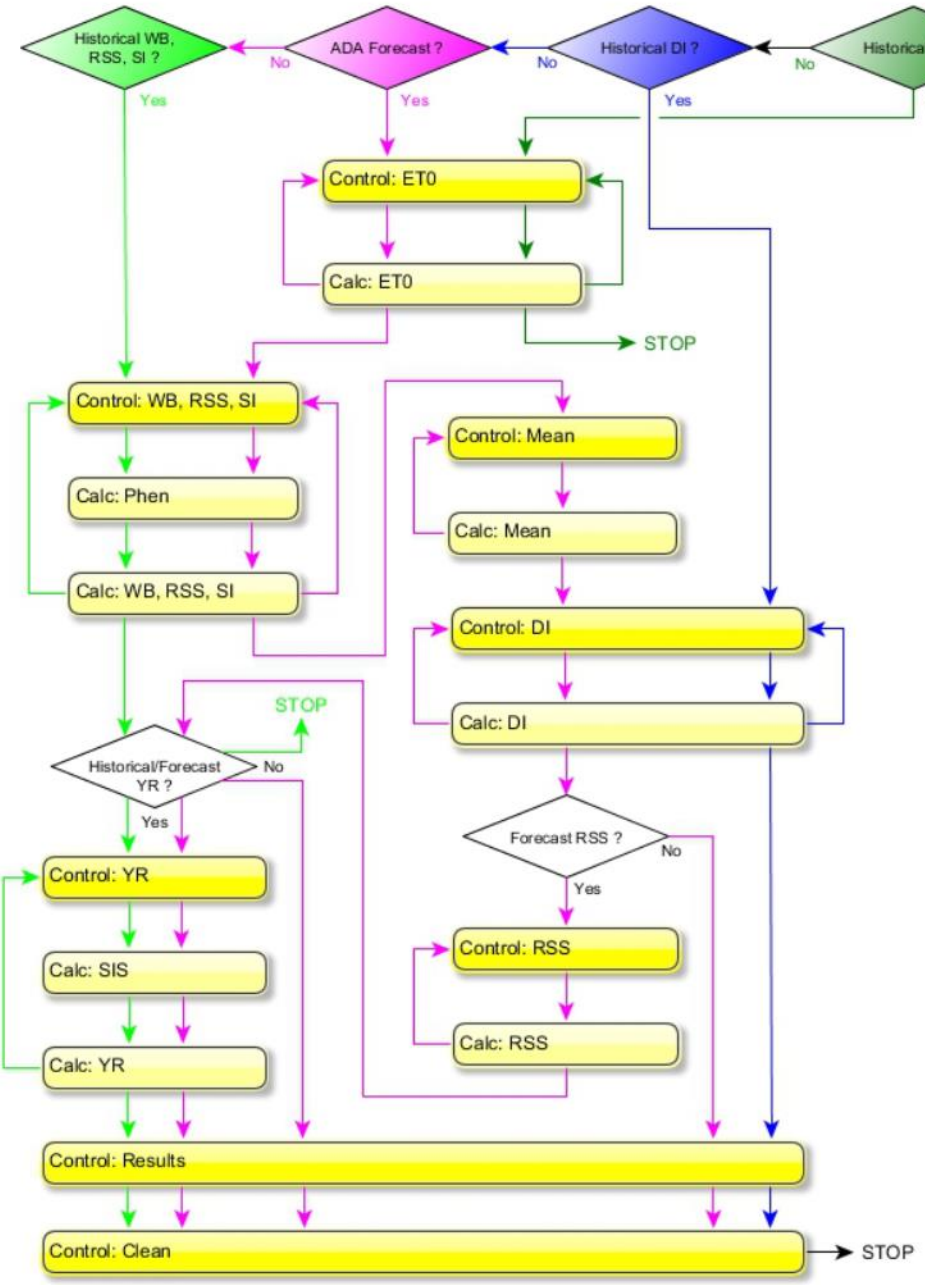

Figure 28: System architecture of *ADIS*. Control and calculation modules are depicted with rounded rectangles in yellow colour shades, decision switches with white or coloured diamond shaped nodes. The four main process flows (*Historical ET0*, *Historical WB*, *Historical DI* and *ADA Forecast*) are distinguished through the use of edges with different colouring.

Once *Historical ET0* and *Historical WB* computations are completed, the historical drought intensity computation process (*Historical DI*) or the forecast process (*ADA Forecast*) can be started. The historical drought intensity values are computed with two modules ("*Control: DI"* and "*Calc: DI"*). The drought intensity is quantified with the help of soil water content values, which are manipulated using a percentile method by NIST (NIST/SEMATECH, 2012). *Historical DI* is concluded in analogy to *Historical WB* using the two final clean up modules.

The most comprehensive process (*ADA Forecast*) allows the forecast of all those parameters, which are also calculated in the historical computations. The forecast refers to the actual (current) year, which can be split up into three stages: the (historical) days before the present (current) day denoted as stage 1, the days of the short-term forecast period which include the current day as first forecast day denoted as stage 2 and the days of the medium-term forecast period denoted as stage 3. The number of days of stage 2 is fixed to 10 days, whereas the number of days of stage 3 can be chosen by the user.

ADA Forecast starts with the computation of all missing *ET0* files for each day of stage1 and 2. Subsequently the water balance calculations as well as the relative soil saturation and stress indicator calculations are carried out for stage 1 in analogy to the *Historical WB* process. The forecast computations of stage 2 are carried out with a combination of forecast and statistically manipulated meteorological input data and stage 3 uses solely statistically manipulated meteorological input data. Stage 1 is based on observed data. The statistical evaluation of meteorological input data of the historical years require two intermediate computation steps ("*Control: Mean"* and "*Calc: Mean"*) to average statistical results. The averaged data is then used to feed the drought intensity calculations, which are run in analogy to the *Historical DI* process. The *ADA Forecast* process furthermore provides the optional classification of predicted relative soil saturation values and the optional forecast of crop yield reduction values. The classification process (Control: RSS and Calc: RSS) uses a classification scheme defined by the user. The forecast of the crop yield reduction is computed in analogy to the *Historical WB* process, again using forecast and statistically manipulated meteorological input data instead of observed data. The forecast process is terminated with the two final clean up modules.

Methodology of *ADIS* data input

The model of *ADIS* works with daily time steps and uses various input parameters. The input information is supplied via binary files in *netCDF* file format. The *netCDF* file format is described later on in more detail. Each input file covers the complete territory of Austria using a grid resolution of 500 or 1000 meters. The *ADIS* input classes implement a method that converts the spatial resolution of 1000 meters to the final resolution of 500 meters. The model requires the following parameters:

- Wind speed at 10 meters [m/s]
- Mean air temperature at 2 meters for 18-6 UTC and for 6-18 UTC [°C]
- Minimum, mean and maximum air temperature at 2 meters [°C]
- Minimum, mean and maximum relative humidity at 2 meters [%]
- Global radiation [MJ/m² day]
- Precipitation sum for 18-6 UTC, for 6-18 UTC and for 0-24 UTC [mm]
- Elevation above sea level [m]
- Field capacity and available field capacity [Vol.%]
- Land cover information confined to a small selection of plant species denominated as *ADA* crops

The meteorological data is compiled by the *ZAMG* using the *INCA* analysis and now-casting system which provides improved numerical analysis in the now-casting and short forecast range up to 48 h (Haiden et al., 2011). The meteorological data is supplied for each day of the historical years from 2003 till the present day (observed data) and modelled for a forecast period of 10 additional days. A resolution of 1000 meters is used. To extend the data basis and due to the lack of *INCA* data for the years 1981 till 2002, weather data has been spatially interpolated by the Agricultural Research and Education Centre Raumberg-Gumpenstein (AREC) using GIS algorithms developed by Schaumberger (2011). Results have been converted from *ArcGIS*[4] format into the *netCDF* file format and stored in the input data base system.

The digital elevation model of the region of interest with a spatial resolution of 1000 meters was also supplied by *AREC*. The computation of soil water balance furthermore requires the knowledge of the water storage capacity of the soil. For this purpose the Federal Agency for Water Management (BAW) has derived field capacity and available field capacity information from the digital soil map of the Federal Research and Training Center for Forests, Natural Hazards and Landscape (BFW) (Murer, 2009, Murer et al., 2004). The water storage capacity information has been supplied by *BAW* with a resolution of 500 meters and for two different soil layers – an upper layer with a thickness of 40 cm and a lower layer with a thickness of 60 cm.

And finally land cover information of the region of interest is needed to identify those areas, which are cultivated or populated with *ADA* specific plants. Only for those plants the monitoring and forecasting of drought and heat stress parameters is carried out. The following plants have been initially selected for the *ADA* computations: grassland, winter wheat, spring barley, maize and sugar beet. The model furthermore has been designed to incorporate coniferous forest and broad-leaved forest as additional plants. All necessary settings have also been worked out for the two forest types and all computations can be carried out without any exception. Nevertheless, due to the complexity of forest modelling in this context and due to questionable results it was decided to keep the focus solely on grassland and the four *ADA* corn types.

As the underlying data for the identification of *ADA* crops, the land use distribution of *CLC2006 Corine Land Cover* data (Commission of the European Communities, 1995) has been used by *AREC*. *Corine* is a pan-European land cover / land use map and one of its databases is an inventory of land cover in 44 classes. In a first step the 44 *Corine* land use classes have been aggregated to 13 classes using a land use classification scheme from the MENDELU University in Brno. In a further step an additional partial aggregation to the seven *ADA* crops has been carried out by *AREC*. The aggregation was partial due to the fact that no distinction of the four *ADA* corn types (winter wheat, spring barley, maize and sugar beet) exists in the *Corine* data base. The four *ADA* corn types are represented in the Corine data base with just one class named *arable land*. In order to nevertheless be able to consider the *ADA* corn types, the following approach was worked out: all *ADA* computations are carried out repeatedly for four different crop scenarios.
The first crop scenario just takes into consideration winter wheat as the only corn type. Subsequently all relevant attributes of winter wheat are allocated to the areas of the Austrian territory defined as *Corine arable land*. The other areas (grassland, coniferous forest and broad-leaved forest) remain unchanged. The resulting land use distribution is used for the subsequent *ADA* computations. After termination of the first calculation

[4] ArcGIS is a geographic information system (GIS) for working with maps and geographic information developed by *Esri* (Environmental Systems Research Institute) in Redlands, California (USA).

cycle and export of the results, the next crop scenario is initiated. Winter wheat is replaced by spring barley and a new calculation cycle is started. This procedure is repeated for maize and sugar beet. Figure 29 shows the *ADA* crop distribution for the Austrian territory. The land use layer is available in *netCDF* format at a resolution of 500 meters.

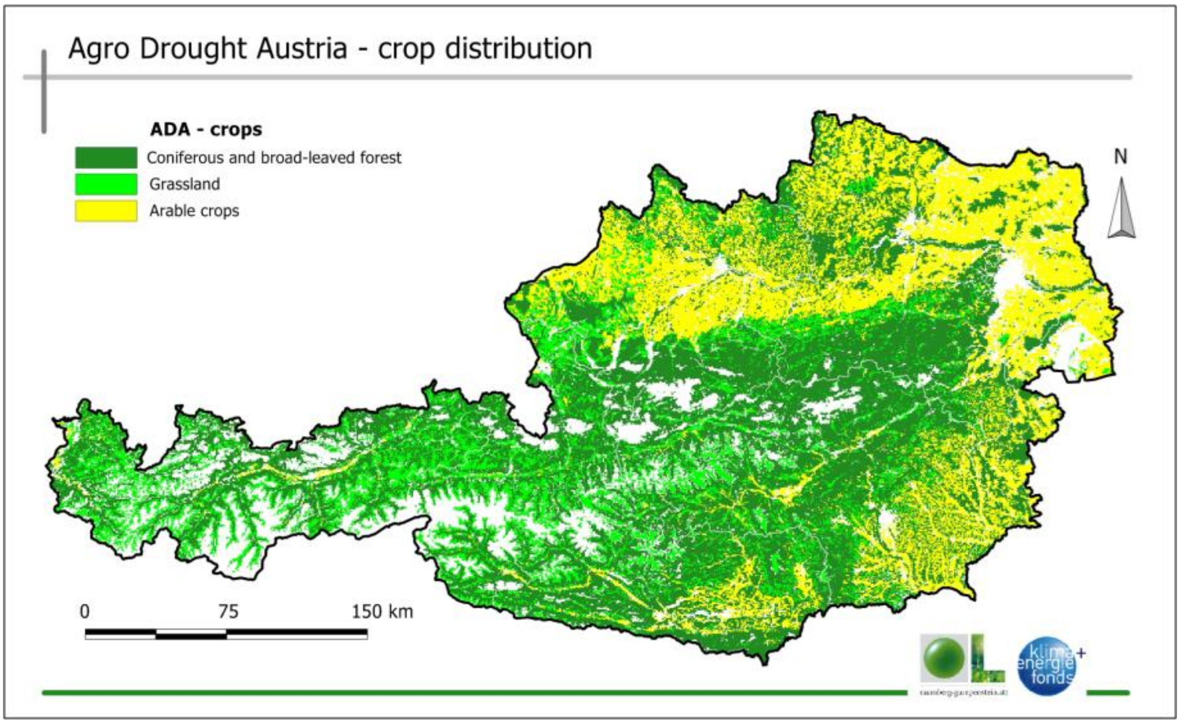

Figure 29: *ADA* crop distribution

Due to the large amount of scientific data involved in the computations it is vital to develop data I/O interfaces, which allow high performance data access and export. *netCDF* (Network Common Data Format) is a set of software libraries and self-describing, machine-independent data formats that support the creation, access, and sharing of array-oriented scientific data. *netCDF* was developed at the University Corporation for Atmospheric Research *UCAR* (www.unidata.ucar.edu) within the *Unidata* program and is still actively supported by *UCAR*.

On the basis of the specific structure of a *netCDF* file and with the need of high I/O performance and low main memory consumption, three *Java* input classes have been written to import *netCDF* files partially or as a whole into *ADIS*. Each import class reads a distinct section of a single-parameter *netCDF* file allowing an efficient allocation of information identical from file to file to corresponding *Java* variables, arrays or lists within *ADIS*. An additional class was written to allow the import of multiple-parameter *netCDF* files. The export of parameter data into a *netCDF* file on the other hand is controlled by one single class. Based on the *netCDF* input classes, one more class finally controls the input procedure allowing an increase of data resolution to predefined scale values.

The *netCDF* parameter reading input classes as well as the *netCDF* output class allow the manipulation of parameter data with different data types (short/integer, float and double). Furthermore an adequate scale factor is used to optionally transform the parameter data into the integer format – thus reducing the size of the *netCDF* files significantly.

Methodology of *ADIS* reference evapotranspiration *ET0* monitoring

According to ALLEN et al. (1998) evaporation is the process whereby liquid water is converted to water vapour and removed from the evaporating surface. Energy is required to change the state of the molecules of water from liquid to vapour. Direct solar radiation and, to a lesser extent, the ambient temperature of the air provide this energy. As evaporation proceeds, the surrounding air becomes gradually saturated and the process will slow down and might stop if the wet air is not transferred to the atmosphere. The replacement of the saturated air with drier air depends greatly on wind speed. Hence, solar radiation, air temperature, air humidity and wind speed are climatological parameters to consider when assessing the evaporation process.

Where the evaporating surface is the soil surface, the degree of shading of the crop canopy and the amount of water available at the evaporating surface are other factors that affect the evapotranspiration process. Frequent rains, irrigation and water transported upwards in a soil from a shallow water table wet the soil surface. Where the soil is able to supply water fast enough to satisfy the evaporation demand, the evaporation from the soil is determined only by the meteorological conditions. However, where the interval between rains and irrigation becomes large and the ability of the soil to conduct moisture to pear the surface is small, the water content in the topsoil drops and the soil surface dries out. Under these circumstances the limited availability of water exerts a controlling influence on soil evaporation. In the absence of any supply of water to the soil surface, evaporation decreases rapidly and may cease almost completely within a few days.

As a first step of the drought monitoring and forecasting computations the evapotranspiration from the reference surface, the so-called reference evapotranspiration *ET0*, is calculated. According to ALLEN et al. (1998) the reference surface is a hypothetical grass reference crop with an assumed crop height of 0.12 meters, a fixed surface resistance of 70 Siemens/meter and an albedo of 0.23. The reference surface closely resembles an extensive surface of green, well-watered grass of uniform height, actively growing and completely shading the ground. The fixed surface resistance of 70 Siemens/meter implies a moderately dry soil surface resulting from about a weekly irrigation frequency.

ET0 of historical years as well as *ET0* of the current year including the first *ADA* forecast period are calculated for each cell of the region of interest (the federal territory of Austria) and for each day. Figure 30 shows an example of the spatial distribution of the reference evapotranspiration on 15.06.2015. *ET0* can be computed solely from meteorological data. As a result of an expert consultation held in May 1990, the *FAO* Penman-Monteith method is now recommended as the sole standard method for the definition and computation of the reference evapotranspiration. The *FAO* Penman-Monteith method requires radiation, air temperature, air humidity and wind speed data and is implemented without any modification in *ADIS*.

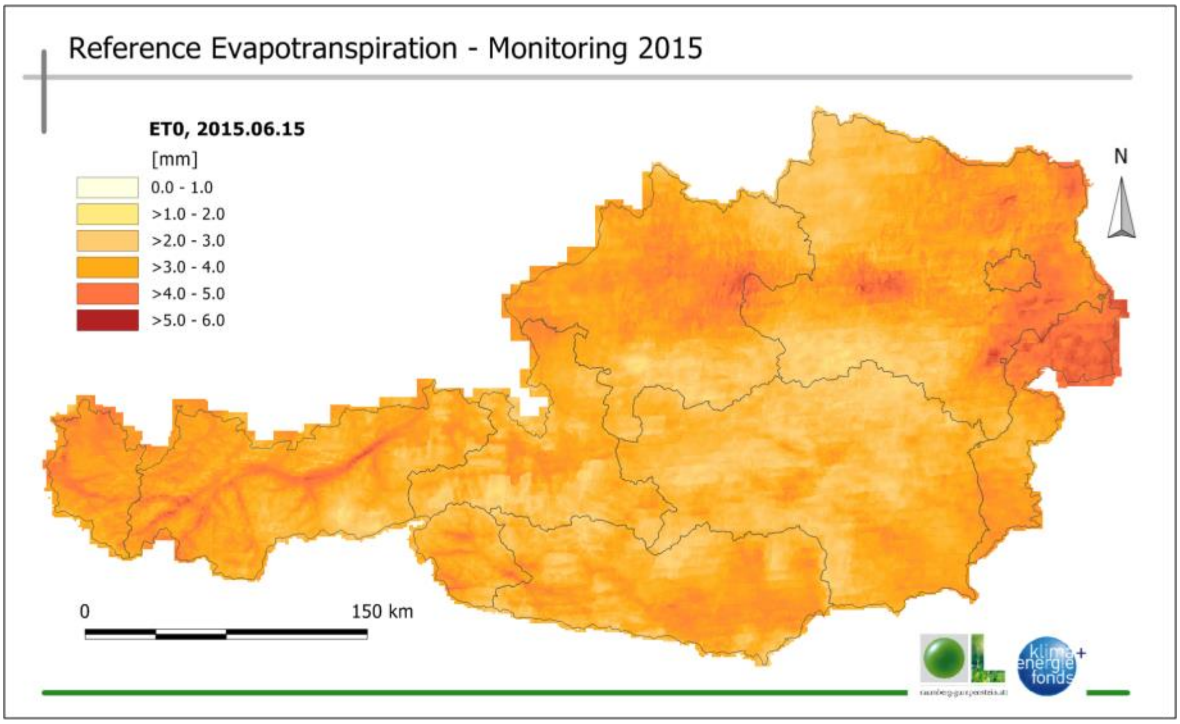

Figure 30: Spatial distribution of the reference evapotranspiration on 15.06.2015.

Methodology of *ADIS* soil water balance and yield reduction monitoring

The *ADIS* modules (“*Control: WB, RSS, SI”* and “*Calc: Phen”* as well *as “Calc: WB, RSS, SI”*) for the computation of the soil water balance as an expression of the mass or volume of water in the soil is based on the concepts and models summarized in the *FAO* Irrigation and Drainage paper No. 56 (Allen et al., 1998 and 2005). The *FAO* models have been adapted to the *ADA* framework combining *SpatialGRAM*'s and *SOILCLIM*'s approaches. In accordance with Allen et al. (1998) soil water balance computations include the estimates of the single crop coefficient *Kc*, of the crop interception preventing a fraction of the precipitation from reaching the soil, of the crop evapotranspiration ET_C and af the actual evapotranspiration ET_A. The soil water balance eventually is quantified by the calculation of the soil water content *swc* described by equations 1-3:

$$swc_{fc} = 1000 \cdot fc \cdot zr \, , \tag{1}$$

$$swc = swc_{fc} - dr \, , \tag{2}$$

$$wilt = (fc - afc) \cdot 1000 \cdot zr \, , \tag{3}$$

where swc_{fc} is the soil water content at field capacity (mm), *fc* is the field capacity (Vol.%), *zr* is the rooting depth (m), *dr* is the root zone depletion (mm), *wilt* is the permanent wilting point (mm) and *afc* is the available field capacity (Vol.%).

With no rain, day for day the *swc* is reduced due to the water use of the plants till it reaches the water content at permanent wilting point. From that point on no more water can be extracted by the plants and the water content at permanent wilting point is kept in the soil for extended periods. Mathematically, the soil water content value therefore always has to be equal or higher than the wilting point value.

The soil water balance computations are carried out for two distinct soil layers (top and sub layer), which are weighted differently and adapted to the main root spaces of the crop types taken into consideration. The crop evapotranspiration of the top soil is weighted with 60 % and the sub soil with 40 % of the total crop evapotranspiration for each *ADA* crop type. The weighting concept implies, that the upper layer is responsible for the major part of crop evapotranspiration (cf. Baeumer, 1978, 28). The thickness of the upper layer of each cell covered with one of the four *ADA* corn types or one of the two *ADA* forest types is set to 40 cm and the thickness of the lower layer to 60 cm. These values can be changed by the user. The thickness values of the upper and lower layers of grassland are set to a fixed value of 20 cm each respectively.

The estimates of the soil water balance and of the crop yield reduction requires an accurate determination of the duration of the crop's phenological stages. The growing phase starts with the beginning of the growing season in the spring. This starting date is thus of decisive importance for the length of the vegetation period and the assessment of the period's phenological stages.

In the prevailing academic literature, a temperature criterion is often used to define the growing season. The criterion, denominated as *Simple Thermal Definition STD* requires a daily mean temperature higher than a threshold value on a defined number of consecutive days. Within the *ADA* framework the start of the growing season has been defined as the first day of 5 consecutive days with daily mean temperatures above 5°C for each *ADA* crop apart from maize. The start of the growing season for maize has been defined as the first day of 5 consecutive days with daily mean temperatures above 10°C. Figure 31 graphically shows the calculation scheme of the start of the growing season for a sample time series. A detailed description of the computation method can be found in Schaumberger (2011, 87ff).

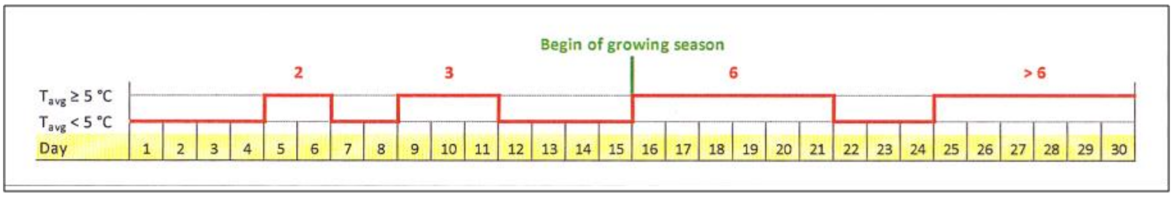

Figure 31: Schematic representation of the beginning of the growing season by *STD.*

Multiple harvests within one vegetation period are a characteristic feature of cultivated grassland. Climatic favourable locations as much as an intensive farming usually allow four harvests (cuts) within one vegetation period, in exceptional cases even more. Cultivated grassland in less-favoured mountain locations mainly allow two or three cuts (Buchgraber et al., 2011).

Grassland harvest dates depend on many factors such as objective measurable criteria (like site and farming conditions) but also individual management options and preferences of the farmer. Because of that the computation of the harvest date basically remains an approximation with an inevitable range of error. Spatial modelling furthermore results in additional constraints leading to the introduction of explanatory variables, which can be supplied as continuous surfaces. The calculation of area-covering harvest date information therefore calls for further simplification and demands even greater concessions on the spread of estimated values against the real value.

Crops are generally due for harvesting when a corresponding phenological stage entry date has been reached. The annual variability of the entry dates depends on the weather and in particular on the temperature development (Ansquer et al., 2009).

To correlate harvest dates of cultivated grassland with temperature sums, long-term observations of temperature profiles and real harvest dates have been analysed. For this purpose, temperature data of monitoring stations spread across the entire country has been supplied by *ZAMG* for the period 1990 till 2009. For the same time period, harvest date information of numerous trials throughout the country has been supplied by *AREC*. The harvest date information includes observations of two cut systems, three cut systems and four cut systems.

The results of the correlations and the medians of all stations for a selected cut regime are depicted in Figure 32. Nine harvest dates can be identified, which represent the statistical central values of each crop growth for each year and station used in the modelling process. The three trend lines of Figure 32 do not show any functional relationship between the days of the year and the temperature sum values but solely show the different gradient's courses of the harvest date related temperature sums. The lower the cut frequency, the higher are the temperature sum level differences related to the harvest dates. As a consequence for the modelling process, the annual variability of the harvest dates predicted by temperature sums rises with increasing trend line slope. Eventually the reasons for this are the longer time durations of the single growth events. Temperature sums calculated in this manner and the corresponding harvest dates depicted in Figure 32 provide the basis for the harvest model of grassland implemented in *ADIS*.

However, harvest dates depend not only on temperature conditions but on many other factors, which cannot be considered in a spatial implementation. As a result it is not possible to estimate harvest dates of grassland with sufficient accuracy based on temperature sums alone. The model used in *ADIS* furthermore does not consider water availability, which according to Smit et al. (2008) has a crucial influence on the productivity of grassland. Nevertheless temperature is particularly suited to describe time shifts of agricultural management as a response to phenological events (Sparks et al., 2005). Therefore the temperature sum approach provides the basis for spatial modelling of harvest events within the scope of *ADA*.

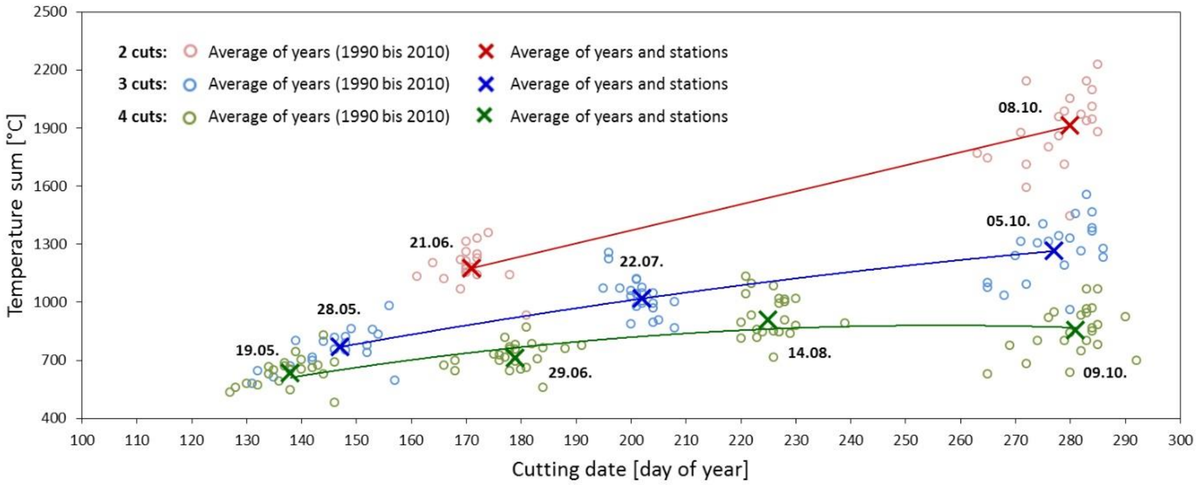

Figure 32: Relationship between temperature sums related to different growth events and harvest dates for different cut regimes and based on long-term average values.

To improve accuracy of the temperature sum approach for grassland and to prevent extreme deviations, relative changes of the annual temperature sums are used to calculate the deviations from the mean values instead of directly using the functional relation between temperature sum and harvest date. This ensures that shifts of harvest dates react less sensitive to temperature sum variations. Figure 33 shows a simplified scheme of the correlation of annual temperature sum anomalies with the resulting range of variation of harvest dates based on long-term grassland trials.

The right column of Figure 33 shows the temperature accumulation for an arbitrary growth of a specific cut regime of grassland. The median of the temperature sum at the harvest date (cutting date) results from all trials within the period of 1990 till 2009 and provides the basis value of 100 %. For each temperature sum, which is related to a mean harvest date of the current year, the deviation from the basis value is calculated and stored.

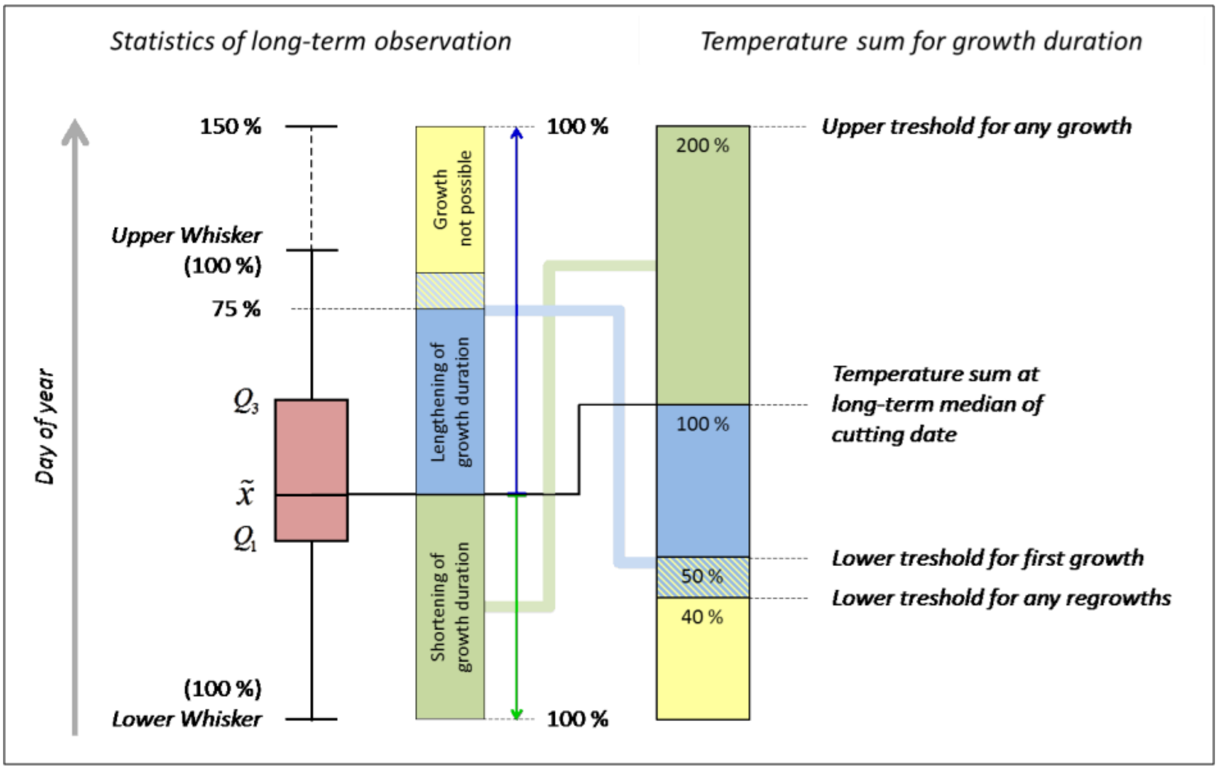

Figure 33: Determination of harvest dates from temperature sums.

The upper threshold value of the deviation is fixed at 200 % (doubling of the temperature sum). All values beyond this limit are left out of consideration due to the assumption, that in those cases a cutting regime of higher frequency (and shorter growth period) is more appropriate and closer to reality. The lower threshold value of the first growth is fixed at 50 %. All values below this limit indicate a location that is not suited to the chosen cutting regime. This restriction prevents the designation of a specific cutting regime to an unsuited altitude given the strong correlation between temperature and altitude. Due to the fact that all growths following the first growth show a higher variability of harvest dates, the lower threshold value is reduced to 40 %.

The left part of Figure 33 shows the statistical parameters of the growth related harvest dates based on long-term observations. The box plot diagram depicts median, first and third quartiles as well as lower and upper whiskers with the interquartile range of 1.5. Those specific values are the basis for the translation of the of the temperature sum deviations. A deviation of more than 100 % results in a shortening of growth duration for the current year, since the ratio of the temperature sums is mapped to the interval between the median of the harvest day and the lower whisker. Above-average temperatures, having for example a deviation of 120 % of the long-term temperature sum, thus lead to an earlier harvest date.

If the temperature sum on the day of the long-term median is not reached, then a lengthening of the growth duration has to be assumed resulting in a later harvest date. That happens quite often in mountainous areas due to the decrease of the temperature sum with altitude. The lower threshold values of the first growth (50 %) and of the following growths (40 %) prevent implausible deviations from the minimum requirements of the temperature. The relative temperature sums are mapped to a larger range of harvest dates due to the extension of the interval between the median of the harvest day and the upper whisker by 50 %. Thus the maximum positive deviation of the harvest date for the first growth amounts to 75 % of the interval between the median of the harvest day and the upper whisker and 90 % for the following growths. Below-average temperatures, having for example a deviation of 80 % of the long-term temperature sum, thus lead to a later harvest date.

The definition of the threshold values (200 % and 50 % respectively 40 %) as well as the mapping procedure to an extended range (150 %) for positive deviations of the harvest dates were introduced due to extensive trials of the years of investigation.

For each cell of the region of interest the mean daily temperatures are accumulated day by day till the long-term median of the harvest dates is reached. In accordance with the methodology described above, the temperature sum is mapped to the value range of the long-term harvest date observations. The deviations of a particular year from the long-term central harvest date are stored in result maps and made available for further investigations. A detailed description of the generation of maps of cutting frequencies can be found in Schaumberger (2011, 205ff).

The cut date median values as well as the upper and lower whisker values for all cutting regimes (two, three and four cut systems) as used for the *ADA* computations are summed up in Table 9.

Table 9: Crop cut date medians as well as upper and lower whiskers for grassland expressed as day of year.

	First cut	Second cut	Third cut	Fourth cut
Crop cut date medians				
2 cut regime	168	274		
3 cut regime	148	206	271	
4 cut regime	139	181	227	277
Upper whisker				
2 cut regime	200	307		
3 cut regime	177	260	301	
4 cut regime	155	225	269	305
Lower whisker				
2 cut regime	141	250		
3 cut regime	125	161	229	
4 cut regime	122	154	193	239

A simplified model is used to describe the harvest frequency and harvest dates of winter wheat, spring barley, maize and sugar beet. Harvest frequency of all four corn types is set to one per year and harvest dates are correlated with temperature sums, fixed dates or fixed time periods. A detailed summary of all specifications in this context including the specifications for grassland can be found in Table 11 and Table 12.

The assessment of harvest dates of the *ADA* corn types and of grassland is partially based on the calculation of temperature sum values *TS*. A degree-day algorithm is used by *ADIS* to accumulate temperature values from day to day starting with the 1st of January and ending with the 31st of December of each year taken into consideration.

The algorithm first calculates the temperature value *DD(t)* as outlined in formulas 4a and 4b:

$$DD(t) = 0 \qquad (t \le Tb), \qquad (4a)$$
$$DD(t) = t - Tb \qquad (t > Tb), \qquad (4b)$$

where *DD(t)* is the degree-day temperature value of a single day (°C), *t* is the mean daily temperature (°C) and *Tb* is a crop specific basis temperature (°C). The single degree-day temperature values *DD(t)* are summed up from day to day resulting in the temperature sum *TS* (°C). The values of the basis temperatures as used in the *ADIS* computations are summed up in Table 10:

Table 10: Basis temperature values of the *ADA* crops.

Grassland	0°C
Winter wheat, spring barley, sugar beet	5°C
Maize	8°C

The crop evapotranspiration ET_C differs from the reference evapotranspiration *ET0* as the ground cover, canopy properties and aerodynamic resistance are taken into account. In the crop coefficient approach, ET_C is calculated by multiplying *ET0* with the crop coefficient *Kc*. The crop development is defined in terms of phenological development stages with varying *Kc* factors as a function of temperature sum (i.e. cumulative daily mean temperature), fixed dates and fixed time periods. The effects of characteristics that distinguish field crops from grass are integrated into the *Kc* calculations.

In compliance with the *FAO* and *SOILCLIM* methodologies, 6 phenological stages are implemented in the program's description of the crop coefficient curves of winter wheat, spring barley and sugar beet:

1. Stage *out (interim):* stage with no plant growth during the winter season
2. Stage *ini:* stage that starts with the sowing event and lasts till plant emergence
3. Stage *dev:* plant development stage till achievement of maximum plant size with linear *Kc* value increase
4. Stage *mid:* stage till achievement of plant maturity
5. Stage *late:* stage between plant maturity and harvest with linear *Kc* value decrease
6. Stage *end:* stage of soil tillage after harvest

Since sugar beet cannot be forced into the predefined scheme of six phenological stages, a simplified model with three stages (*out*, *ini* and *dev*) is used to match the *Kc* curve as closely as possible to realistic conditions. Due to the multiple harvest feature of cultivated grassland, an adapted crop coefficient scheme is applied in compliance with the corresponding cut regime. In this case, too, less different stages are needed to describe the *Kc* course namely *out*, *ini*, *dev* and *end*. Due to multiple harvests of grass, the mid stage is replaced by multiple *dev* stages. All these considerations are also illustrated in Figure 34.

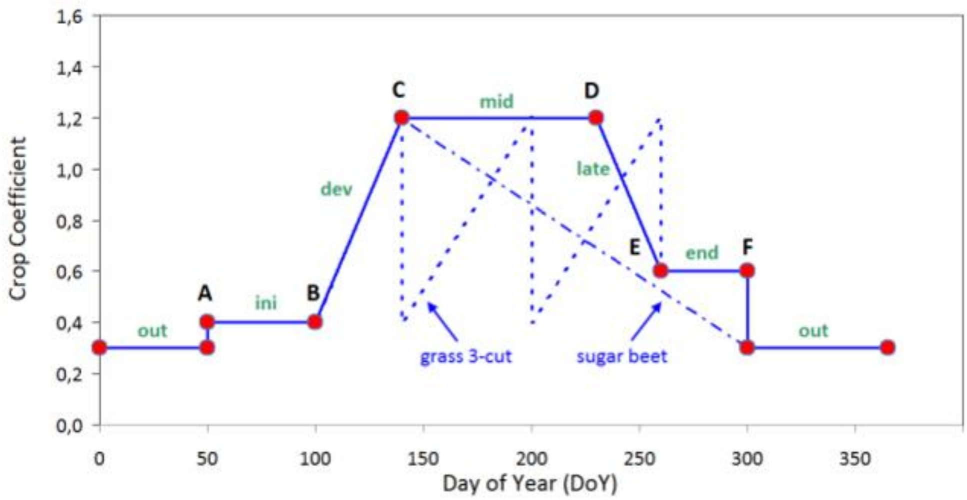

Figure 34: *Kc* courses of different *ADA* crop types. The blue continuous line represents the *Kc* courses of winter wheat, spring barley and sugar beet, the blue dashed lines the *Kc* courses of grass (3 cut regime) and sugar beet. The 2 and 4 cut regimes of grass have *Kc* courses in accordance with the number of cuts. The graph focuses on the illustration of the phenological stages – the values of the crop coefficients are arbitrary.

The phenological stage entry events for the individual crop types as implemented in *ADIS* are outlined in Table 11 and Table 12.

Table 11: Phenological stage entry events of grassland for different cut regimes.

	ini	dev1	dev2	dev3	dev4	end	out
2 cut regime	01.03	SGS	1170°C			1900°C	31.10
3 cut regime	01.03	SGS	770°C	1020°C		1260°C	31.10
4 cut regime	01.03	SGS	630°C	710°C	910°C	850°C	31.10

The entry events of the *ini* and *out* stages are defined with calendar dates, the entry events of the first development stage *dev1* with the start of growing season and the entry events of *dev2*, *dev3*, *dev4* and *end* with temperature sums.

Table 12: Phenological stage entry events of the four *ADA* corn types.

	ini	dev	mid	late	end	out
Winter wheat	01.03	SGS	350°C	692°C	+14	30.11
Spring barley	01.03	SGS	502°C	568°C	+14	30.11
Maize	01.04	SGS-M	249°C	1238	+14	30.11
Sugar beet	01.03	300°C	2400°C			31.12

The entry events of the *ini* and *out* stages are defined with calendar dates, the entry events of the development stage *dev* with the start of growing season of winter wheat and spring barley (SGS) and maize (SGS-M) as well as with a temperature sum for sugar beet. The entry events of *mid* and *late* are defined with temperature sums and the entry events of *end* are defined with a period of 14 consecutive days.

ET0 as well as ET_C depict the amount of evaporation at standardized conditions – assuming fully saturated soil layers. In reality ET_C is reduced significantly with the lack of soil water due to drought conditions. In accordance with Allen et al. (1998, 161) an additional water stress coefficient *Ks* is introduced to correct ET_C and compute the actual evapotranspiration ET_A according to formula 5:

$$ET_A = Ks \cdot ET_C \qquad (5)$$

With the knowledge of ET_A the root zone depletion *dr* can be calculated and thereby also the soil water content *swc*, as outlined at the beginning of this chapter. The soil water content is then expressed as proportion of water soil profile saturation in %, denominated as relative soil saturation *rss* (Trnka et al., 2014). *rss* is calculated using formula 6, classified, exported in *netCDF* file format and presented as final result of the soil water balance computations.

$$rss = (swc - wilt) / (swc_{fc} - wilt), \qquad (6)$$

where *rss* is the relative soil saturation (%), *swc* is the actual soil water content (mm), swc_{fc} is the soil water content at field capacity (mm) and *wilt* is the permanent wilting point (mm). Although not directly related to the soil water balance, an additional parameter is computed within the soil water balance module "*Calc: WB, RSS, SI"*. It is the *ADA* crop stress indicator parameter *SI*, which is introduced and developed within the *ADA* project. The amount of yield loss due to crop stress depends on growth stage, severity of the stress, and the number of days the crop is stressed. A set of calibrated indicators and methods on crop specific drought and heat vulnerability and impacts based on field experiment data and crop model application have been developed within the *ADA* project.

Three different crop stress indicators *SI* have been taken into further consideration and implemented in *ADIS*:

1. Aa drought stress indicator *DSI* showing the percentage ratio of the current root zone depletion (mm) to the soil water content at available field capacity (mm) for an upper soil layer of 20 cm thickness,
2. Aa heat stress indicator *HSI* as a function of the maximum daily temperature and a predefined temperature threshold value,
3. Aa combined stress indicator *CSI* as a function of the drought stress indicator and the maximum daily temperature.

The assessment of the stress indicators is incorporated in the water balance computation process to avoid double calculation of necessary parameters like the root zone depletion or soil water content values, thus increasing the overall performance of *ADIS*. With the export of the *SI* results as *netCDF* files, the water balance computations are completed.

To estimate crop yield losses due to drought and heat stress, simple interrelations have been worked out. A viable approach has been found through formula 7, which shows the impact of the crop stress indicator factor on crop yield reduction as a linear function:

$$YR = B \cdot sis + A, \qquad (7)$$

where *YR* is the relative crop yield reduction as percentage of the maximum possible crop yield (%), *sis* is the crop specific stress indicator sum and *A* and *B* are crop specific coefficients. The stress indicator sums are computed in analogy to the computation of temperature sums for each day of the accumulation period but without any restricting constraint. The accumulation periods differ from crop to crop and are outlined in Table 13:

Table 13: Start dates and end events of the stress indicator sum accumulation.

	Accumulation start date	Accumulation end event
Winter wheat	01.03.	Start of stage *end*
Spring barley	01.03.	Start of stage *end*
Maize	01.05.	Start of stage *end*
Sugar beet	01.05.	Start of stage *out* (31.12.)
Grassland – 2 cut regime	01.05.	Start of stage *end* (second harvest)
Grassland – 3 cut regime	01.05.	Start of stage *dev3* (second harvest)
Grassland – 4 cut regime	01.05.	Start of stage *dev4* (third harvest)

The crop yield reduction values are finally classified using the following classification scheme: 0-5%, 5-30%, 30-60% and >60%. The classified results are exported in *netCDF* file format and can be presented to the stake holders as final results.

Methodology of *ADIS* drought intensity monitoring

Another product of *ADIS* are maps of the intensity of dryness referred to as drought intensity maps (Trnka et al., 2014). Drought intensity can be expressed as a measure of deviation from the statistically derived „normal“ state. For each grid cell the current soil water content at a given day is compared to the soil water content distribution of the historical years from 1981 till 2015 for the same day +/- 10 days. The drought intensity value expresses the probability of repetition of soil moisture in the given day. The drought intensity computations rely on a percentile-based approach, using a percentile method by NIST (NIST/SEMATECH, 2012).

Computing the percentile value of the cell’s *swc* for a given day in relation to the group of *swc* observations for the same day of all years taken into consideration reveal its percental deviation from the “normal” *swc* state. The higher the *swc* deviation from the entire observation set (the smaller the percentile value), the higher is the drought magnitude of the cell for the particular day. To suppress statistical outliers, the *swc* values of 10 days before and 10 days after the particular day are included in the percentile computations. The default number of 10 days can be altered by the user. The percentile values are classified using a user defined drought intensity class table. By default Table 14 is used (Trnka et al., 2014):

Table 14: Drought intensity classification in relation to percentile values.

Percentile	Drought intensity class
0 – 1	Extreme drought
> 1 – 2	Exceptional drought
> 2 – 5	Significant drought
> 5 – 10	Moderate drought
> 10 – 20	Starting drought
> 20 – 30	Decreased soil moisture content
> 30	No drought

Drought intensity class results are exported in *netCDF* file format and can be presented to the stake holders as another final result.

Methodology of *ADIS* drought forecast

Predicting future dry events in a region is essential for finding sustainable solutions to water management and risk assessment of drought occurrences. A drought early warning system with severity and spatial extent in a timely manner provides invaluable information to decision-makers and stakeholders. The drought prediction approach used in *ADIS* is based on weighted meteorological historical and forecast data for a short-term forecast period of 10 days, on historical meteorological data for medium-term forecast of any number of days and on an averaging process.

The basic approach of the *ADIS* forecast model consists in a repeated calculation of soil water content time series for each historical year and a subsequent arithmetic averaging of the results as shown in Figure 35. The fundamental difference to the *swc* monitoring option as described before is the differing meteorological input data used in the *swc* forecast computations.

The following example describes an *ADA* forecast for an arbitrary day (03.04.) in 2015: The forecast computation process starts with the *swc* computation of all past days of the current year (stage 1: 01.01.2015 till 02.04.2015) using measured meteorological data. The subsequent swc computation of all days of the short-term forecast period (stage 2: 03.04.2015 till 12.04.2015) are based on forecast meteorological data delivered by *ZAMG*. The *swc* values of the medium-term period (stage 3: 13.04.2015 till 22.04.2015) are then calculated using meteorological input data of the first historical year (1981). To suppress a discontinuous time series pattern of the *swc* between the short- and medium-term period a weighting process including historical meteorological data of the first historical year is applied to the short-term meteorological forecast values. A weighting algorithm is used that emphasizes the forecast data at the beginning of the short-term forecast period and the historical data at the end of the short-term period. The *ADIS* forecast computation process is then repeated for all remaining historical years (1982 till 2014) resulting in 34 different *swc* time series which are arithmetically averaged.

The resulting averaged *swc* values are finally expressed as relative soil saturation values, classified ("*Control: RSSCLASS*" and "*Calc: RSSCLASS*") and exported in *netCDF* file format. The averaged *swc* values are furthermore also used to calculate crop yield reduction and drought intensity forecast values. The results of 6 selected days of the two forecast periods are converted into a graphical format and published via an appropriate web application.

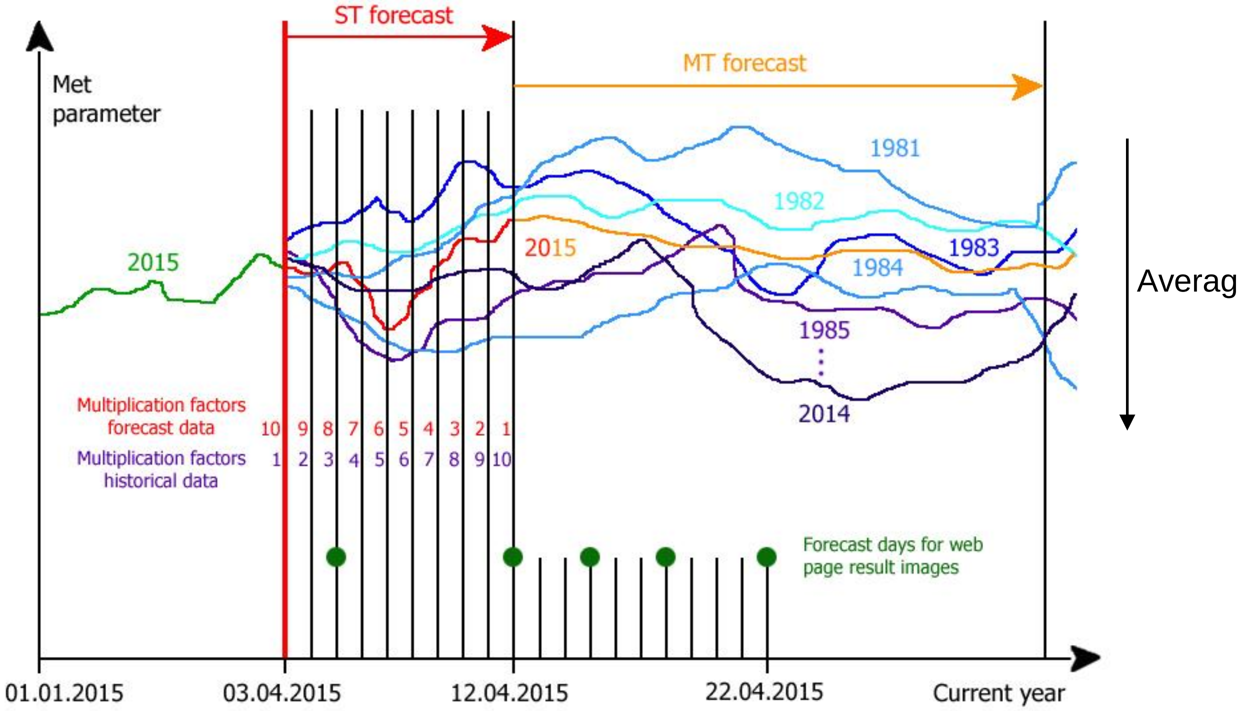

Figure 35: *ADIS* forecast model. Example of an *ADA* forecast computed on 03.04.2015. Green line: *swc* values computed with observed meteorological data from 01.01.2015 till 02.04.2015. Blue line (1981): *swc* values of the *ST*-forecast period (03.04.2015 till 12.04.2015) are computed with inversely weighted (see displayed multiplication factors) and averaged forecast and historical meteorological data from 03.04. till 12.04. The *swc* values of the *MT*-forecast period (13.04.2015 till 22.04.2015)) are computed with historical meteorological data from 13.04.2015 till 22.04.2015. The *swc* course of the other historical years (blue lines 1982 till 2014) are computed analogously. All blue *swc* lines are then averaged resulting in the final red and orange *swc* forecast course. The *swc* forecast results of 5 days (green dots) are picked out from the 20 days period, exported as *netCDF* file and published on a web page.

5.3 The ADA Web-Interface

The results of the Agro Drought Austria Monitoring and Forecasting System *ADA-MFS* are maps showing the relative soil saturation, drought intensity and crop yield reduction situation over the Austrian territory in a grid resolution of 500 meters for rooting zone layers of 0-40 cm (grassland) and 0-100 cm (winter wheat, spring barley, maize and sugar beet). All examples displayed from Figure 36 to Figure 41 are for a selected date (13.07.2015) and calculated with historical (measured) meteorological data. The maps are visualised in the web page prototype.

Crop related relative soil water saturation by July 13 2015:

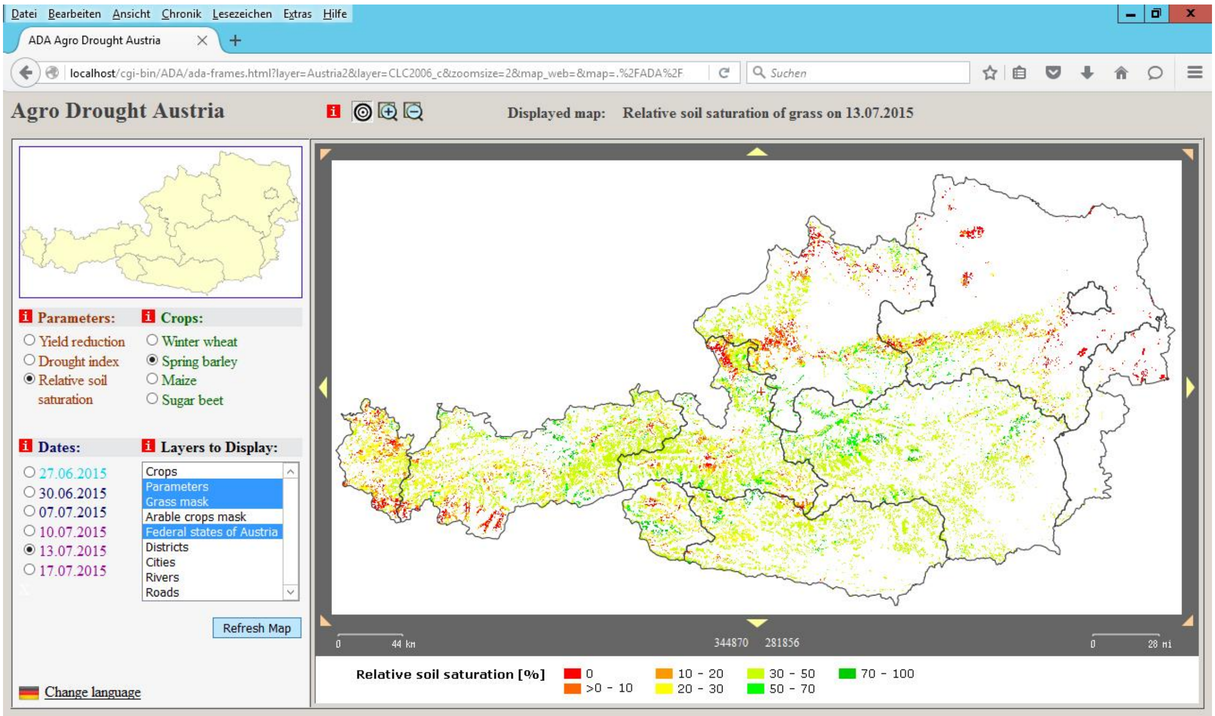

Figure 36: Relative soil saturation distribution of grassland for the Austrian territory on 13.07.2015.

The following Figure 37 consists of 4 screenshots a) to d).

a)

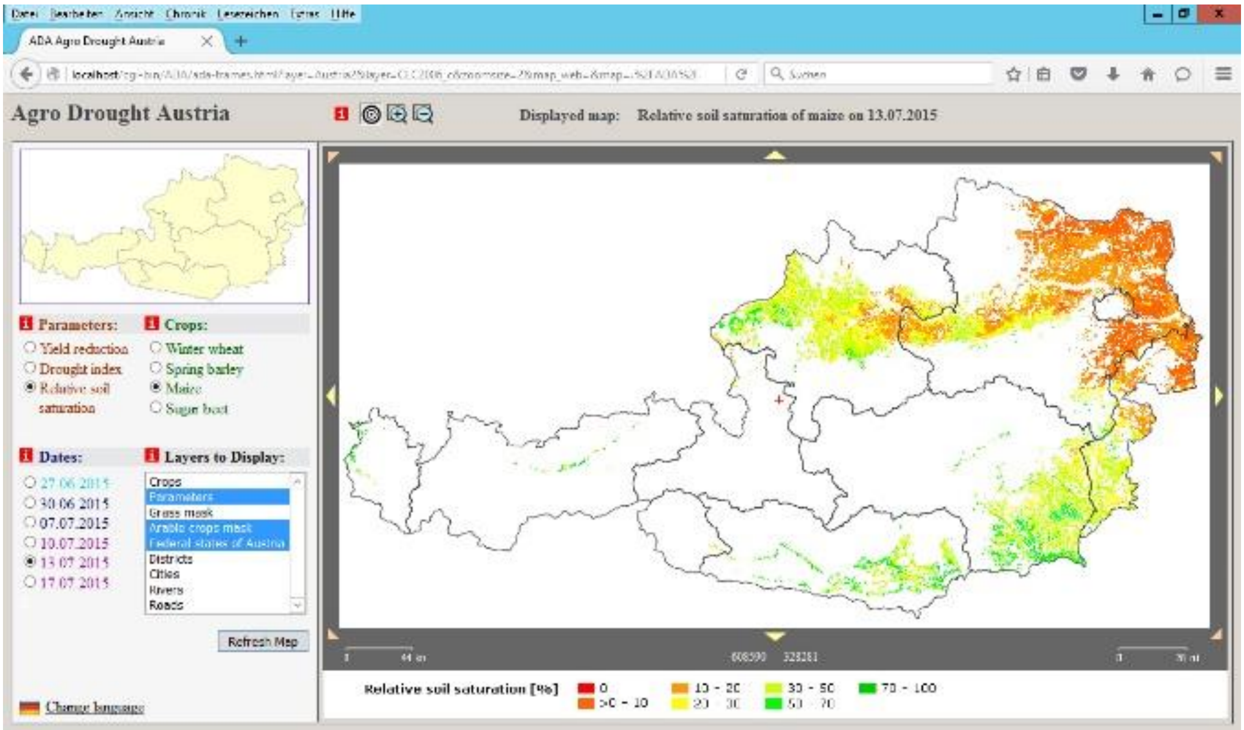

b)

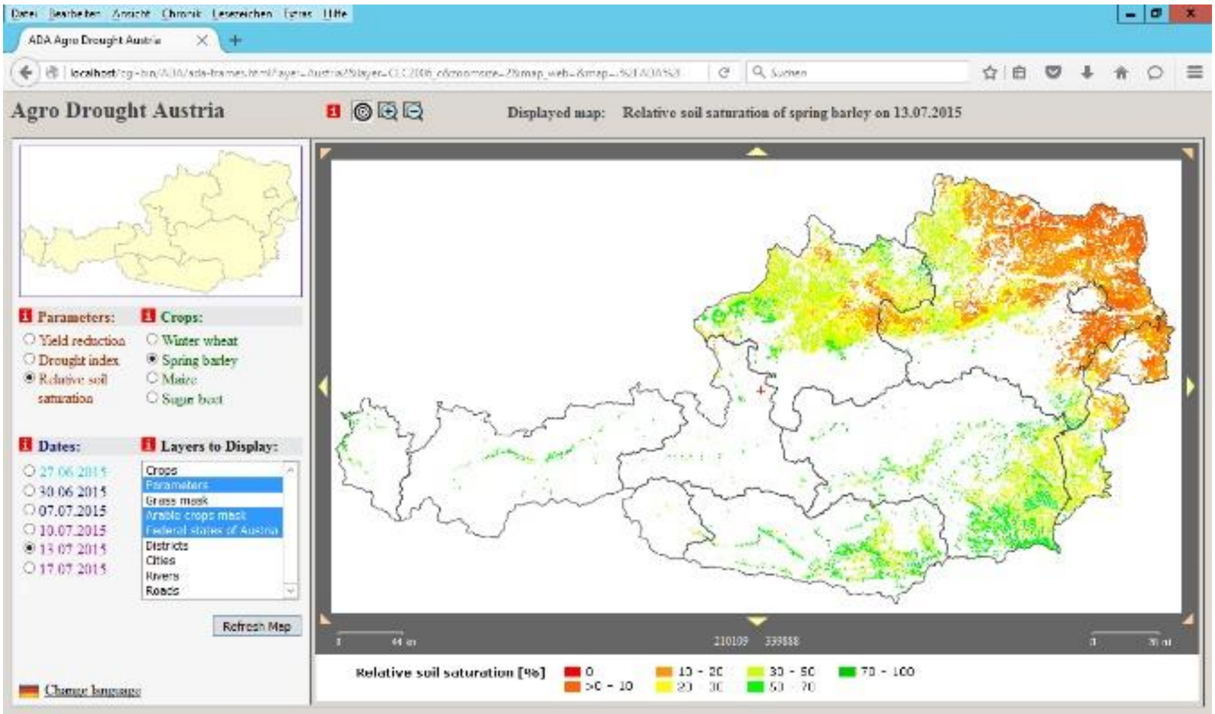
Agro Drought Austria
Displayed map: Relative soil saturation of spring barley on 13.07.2015
Parameters:
Yield reduction
Drought index
Relative soil saturation
Crops:
Winter wheat
Spring barley
Maize
Sugar beet
Dates:
27.06.2015
30.06.2015
07.07.2015
10.07.2015
13.07.2015
17.07.2015
Layers to Display:
Crops
Parameters
Grass mask
Arable crops mask
Federal states of Austria
Districts
Cities
Rivers
Roads
Refresh Map
Change language
Relative soil saturation [%]

c)

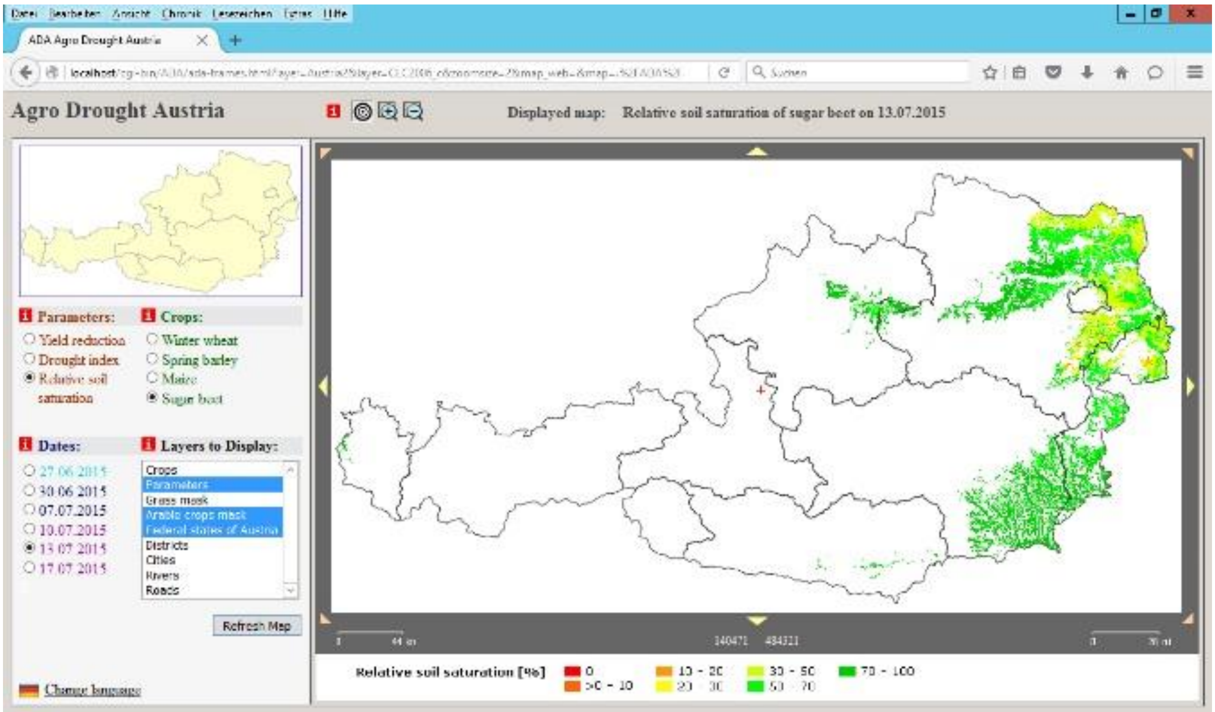
Agro Drought Austria
Displayed map: Relative soil saturation of sugar beet on 13.07.2015
Parameters:
Yield reduction
Drought index
Relative soil saturation
Crops:
Winter wheat
Spring barley
Maize
Sugar beet
Dates:
27.06.2015
30.06.2015
07.07.2015
10.07.2015
13.07.2015
17.07.2015
Layers to Display:
Crops
Parameters
Grass mask
Arable crops mask
Federal states of Austria
Districts
Cities
Rivers
Roads
Refresh Map
Change language
Relative soil saturation [%]

d)

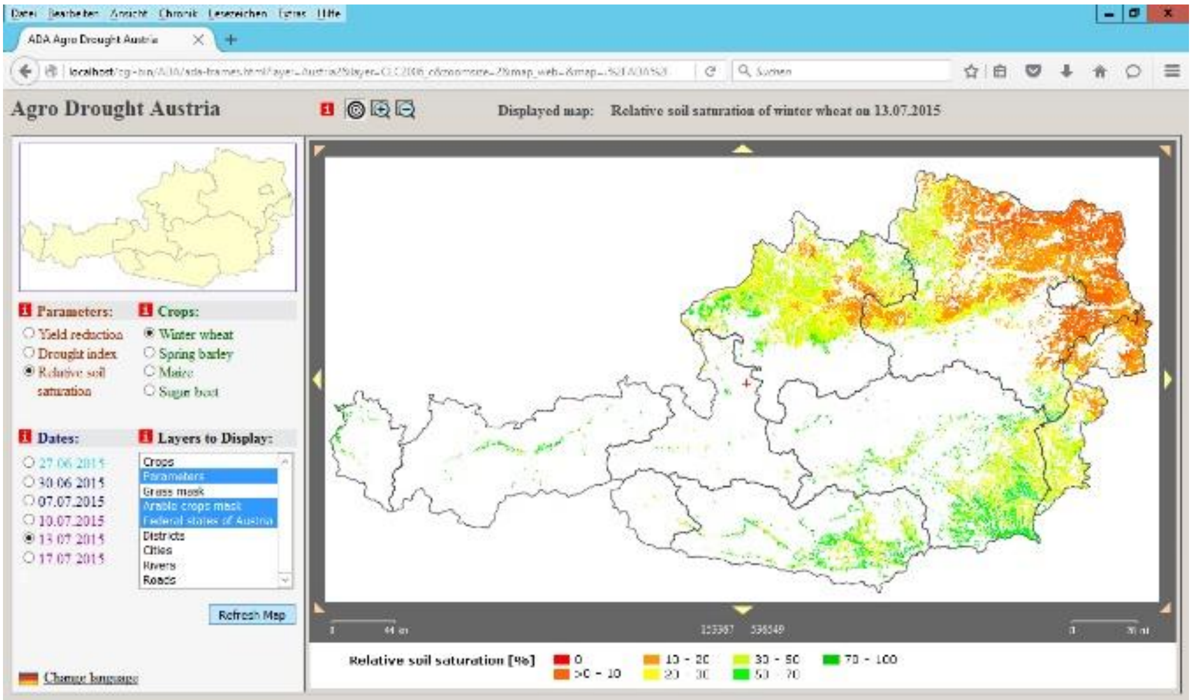

Figure 37a-d: Relative soil saturation distribution of maize (a), spring barley (b), sugar beet (c) and winter wheat (d) for the Austrian territory on 13.07.2015.

Crop related drought index by July 13 2015:

a)

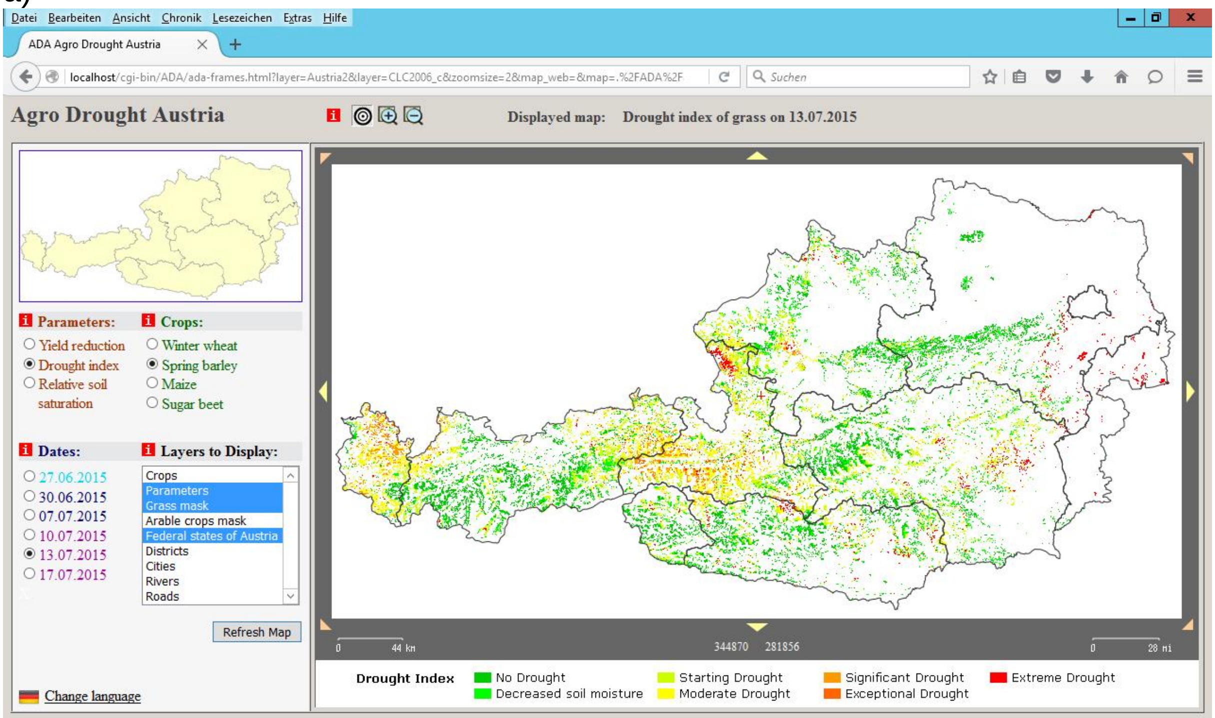

Figure 38: Drought intensity distribution of grassland for the Austrian territory on 13.07.2015.

The following Figure 39 consists of 4 screenshots a) to d).

a)

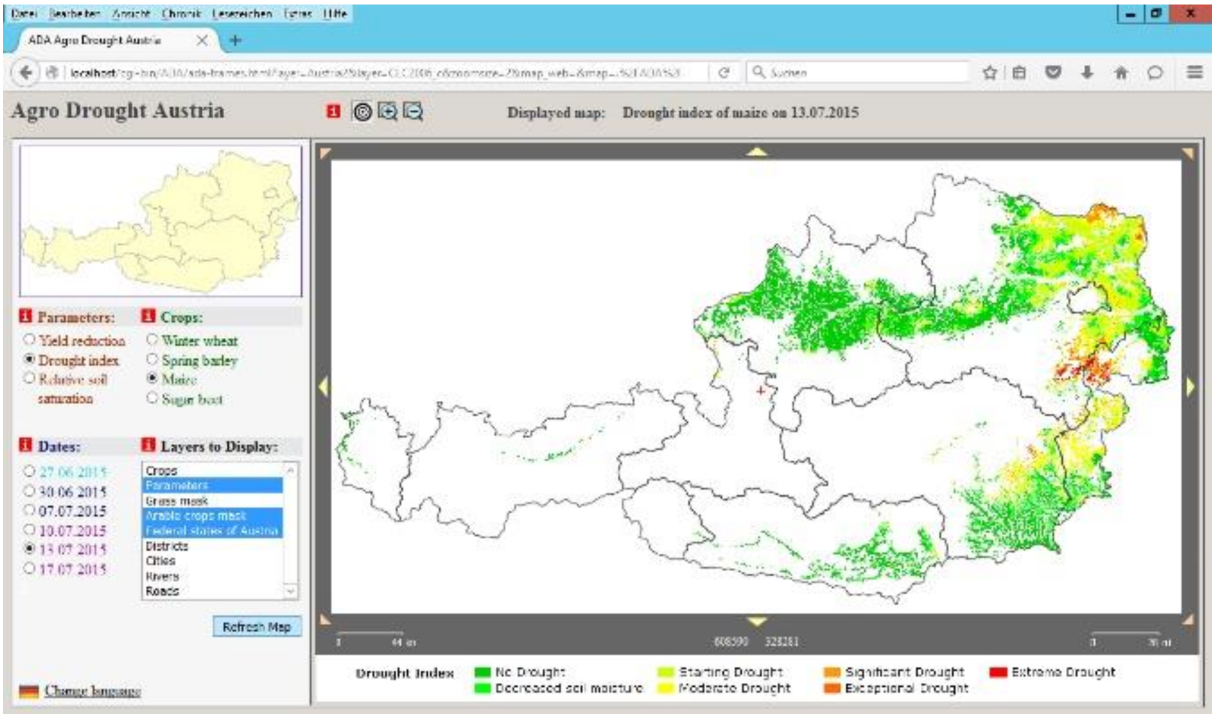

b)

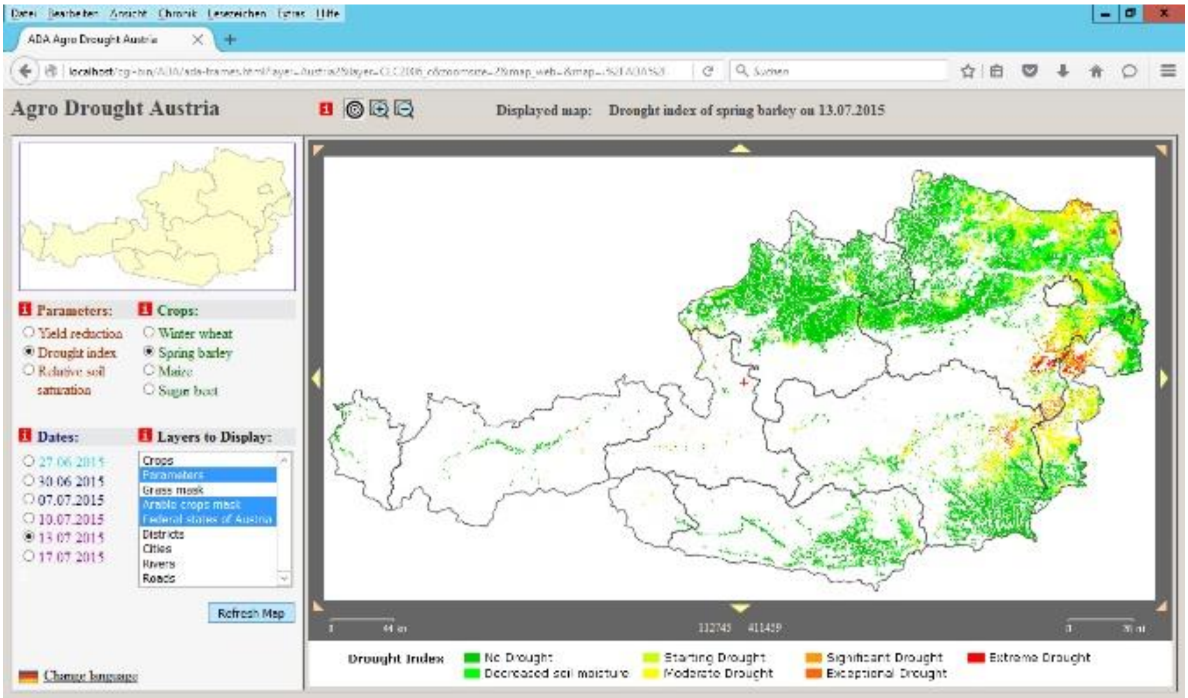

c)

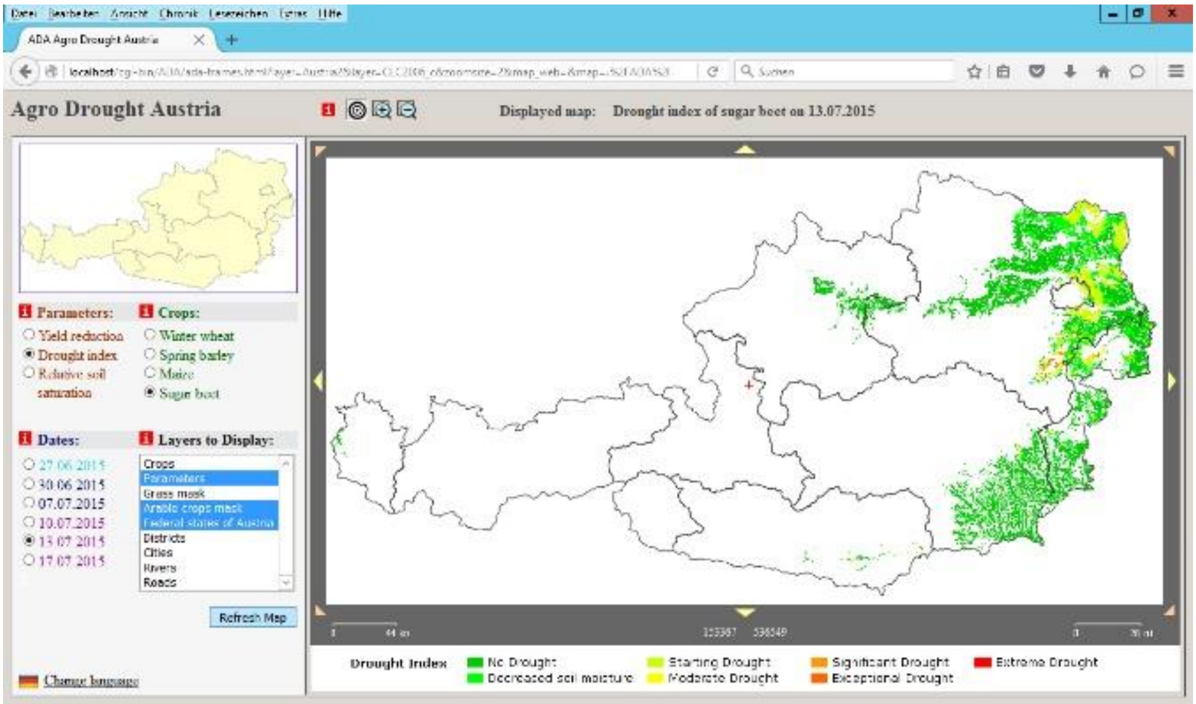

d)

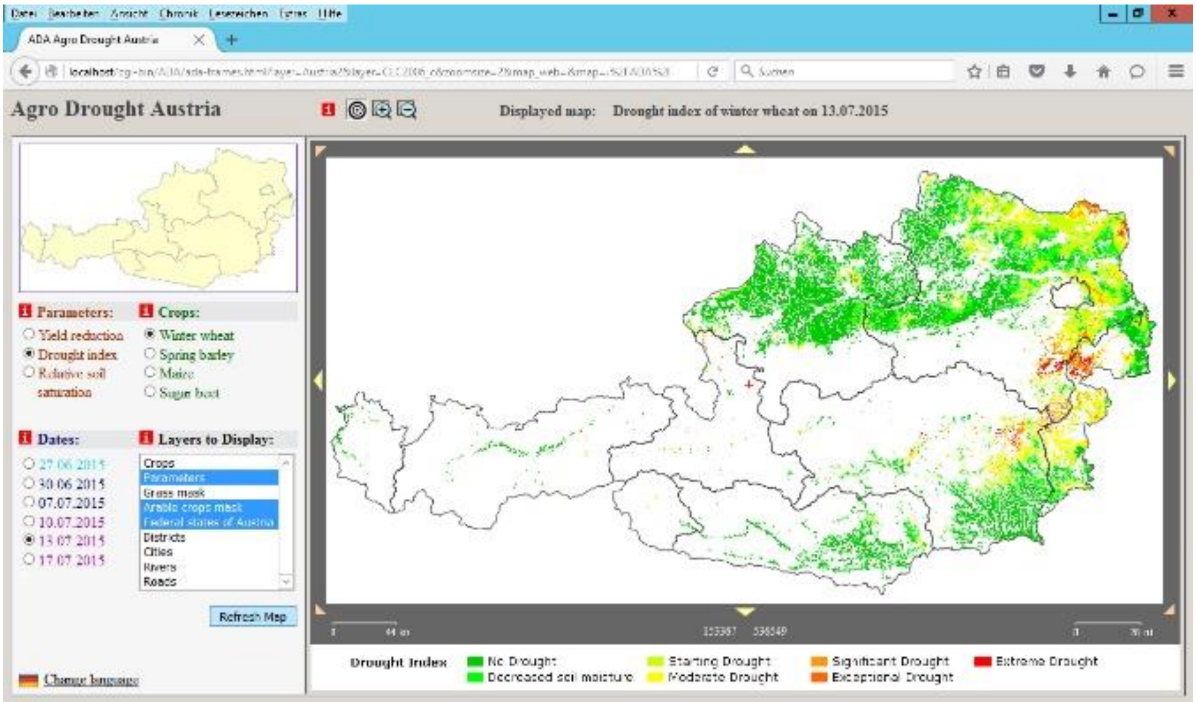

Figure 39a-d: Drought intensity distribution of maize (a), spring barley (b), sugar beet (c) and winter wheat (d) for the Austrian territory on 13.07.2015.

Crop related yield reduction by July 13 2015:

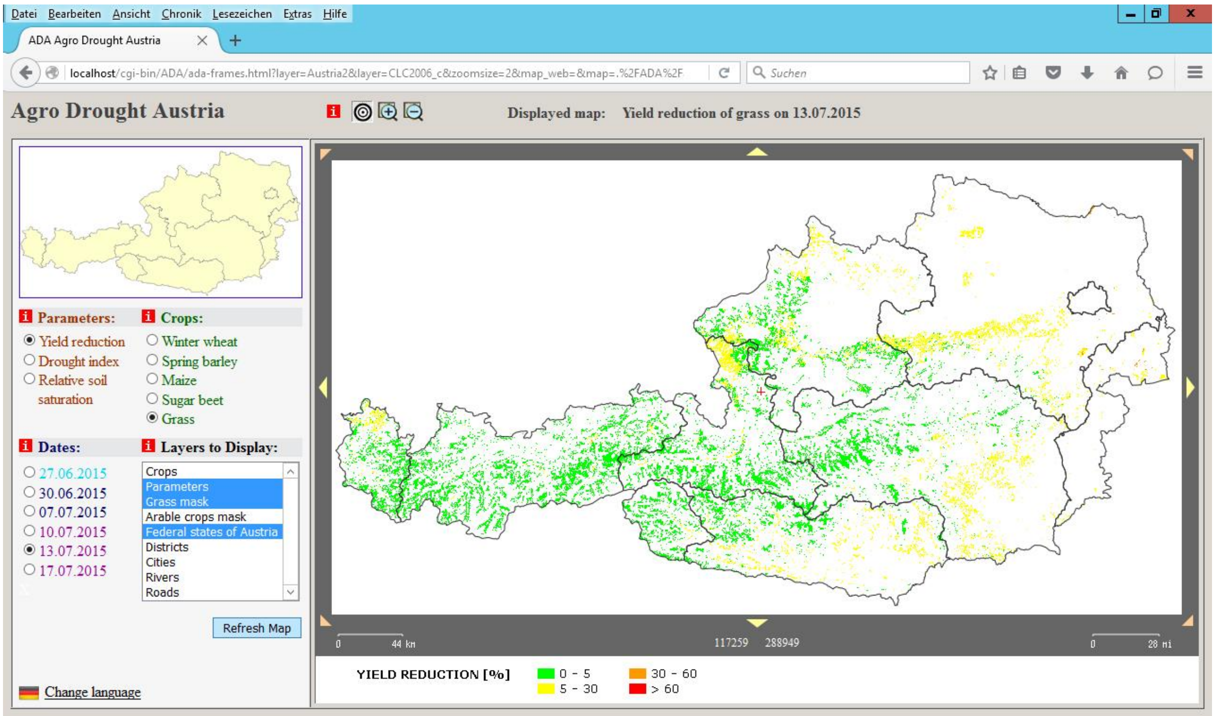

Figure 40: Crop yield reduction distribution of grassland for the Austrian territory on 13.07.2015.

The following Figure 41 consists of 4 screenshots a) to d).

a)

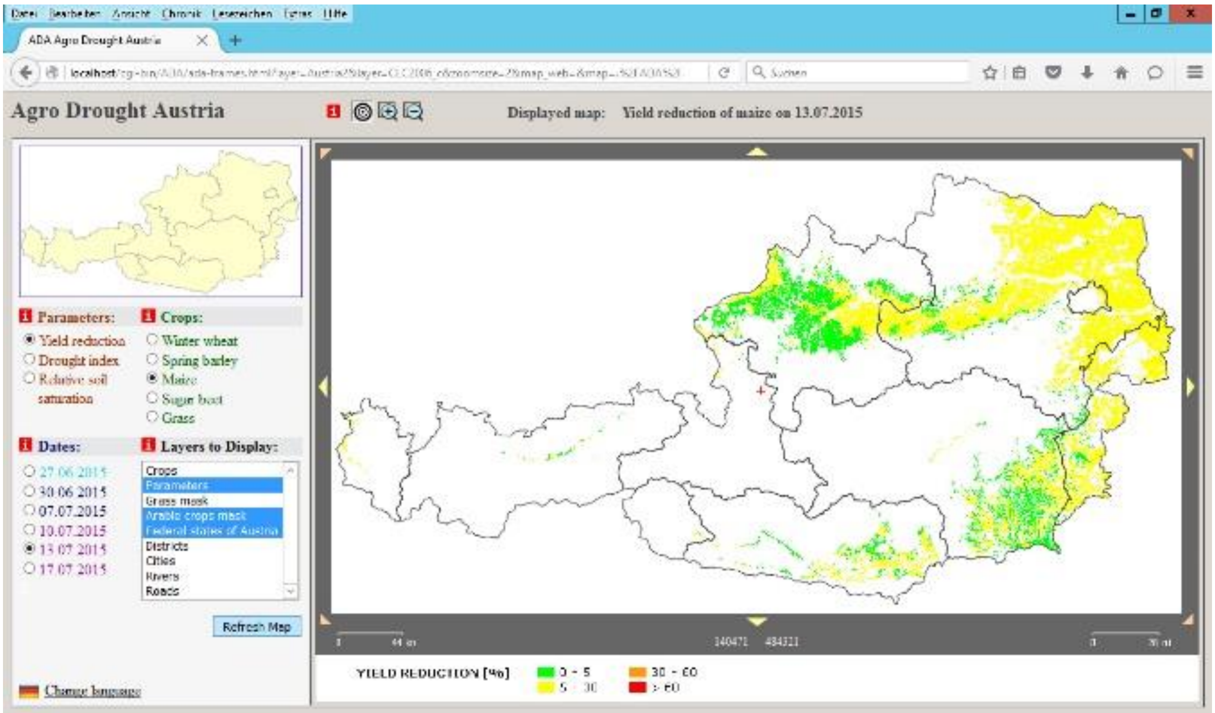

b)

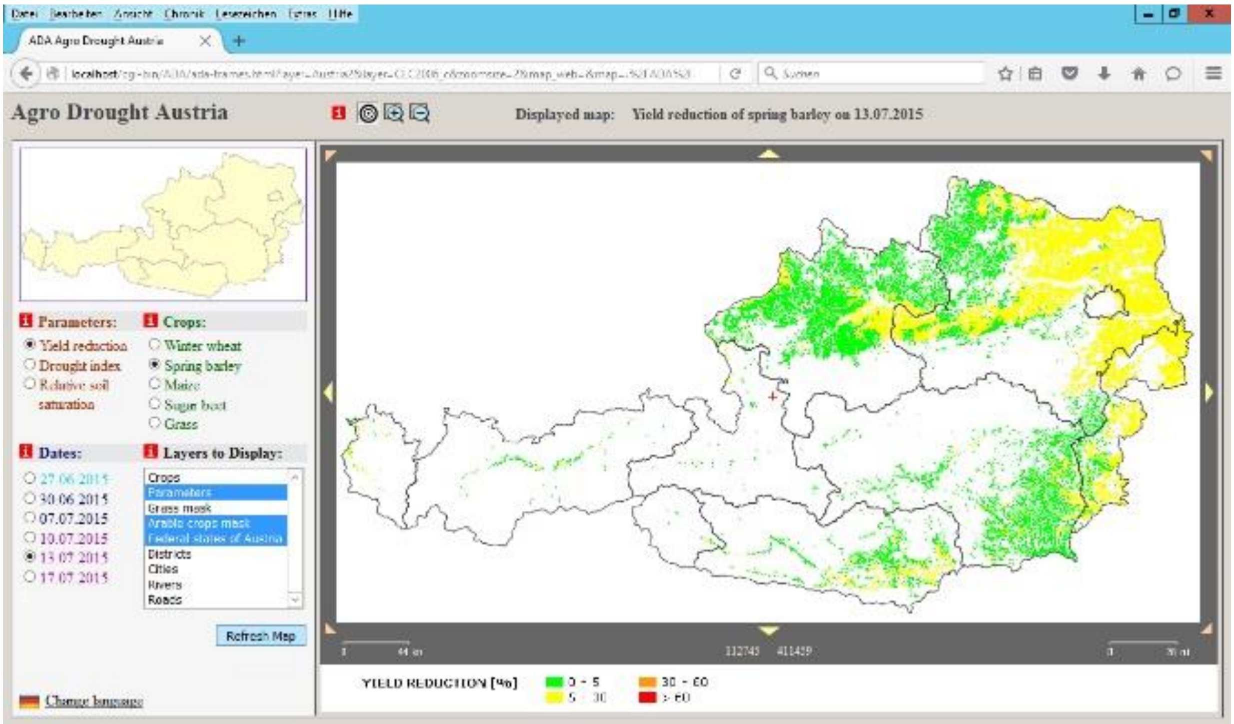

Agro Drought Austria
Displayed map: Yield reduction of spring barley on 13.07.2015
Parameters:
Yield reduction
Drought index
Relative soil saturation
Crops:
Winter wheat
Spring barley
Maize
Sugar beet
Grass
Dates:
27.06.2015
30.06.2015
07.07.2015
10.07.2015
13.07.2015
17.07.2015
Layers to Display:
Crops
Parameters
Grass mask
Arable crops mask
Federal states of Austria
Districts
Cities
Rivers
Roads
Refresh Map
Change language
YIELD REDUCTION [%]
0 - 5
5 - 30
30 - 60
> 60

c)

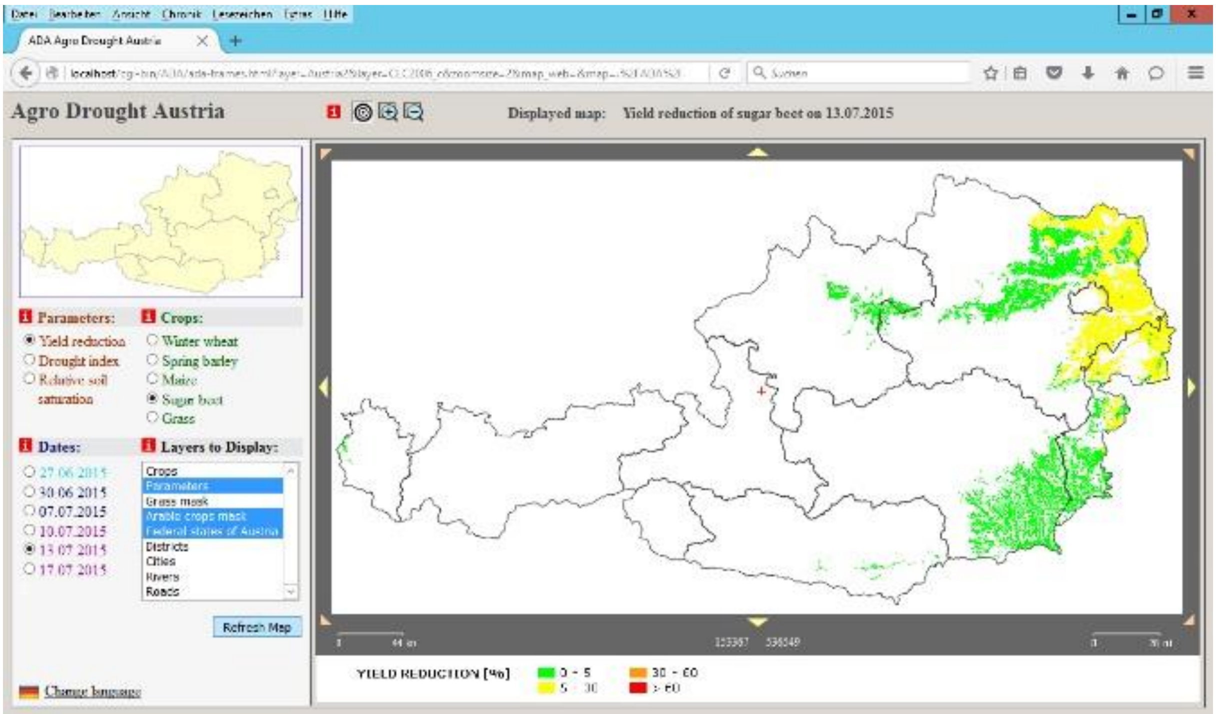

Agro Drought Austria
Displayed map: Yield reduction of sugar beet on 13.07.2015
Parameters:
Yield reduction
Drought index
Relative soil saturation
Crops:
Winter wheat
Spring barley
Maize
Sugar beet
Grass
Dates:
27.06.2015
30.06.2015
07.07.2015
10.07.2015
13.07.2015
17.07.2015
Layers to Display:
Crops
Parameters
Grass mask
Arable crops mask
Federal states of Austria
Districts
Cities
Rivers
Roads
Refresh Map
Change language
YIELD REDUCTION [%]
0 - 5
5 - 30
30 - 60
> 60

d)

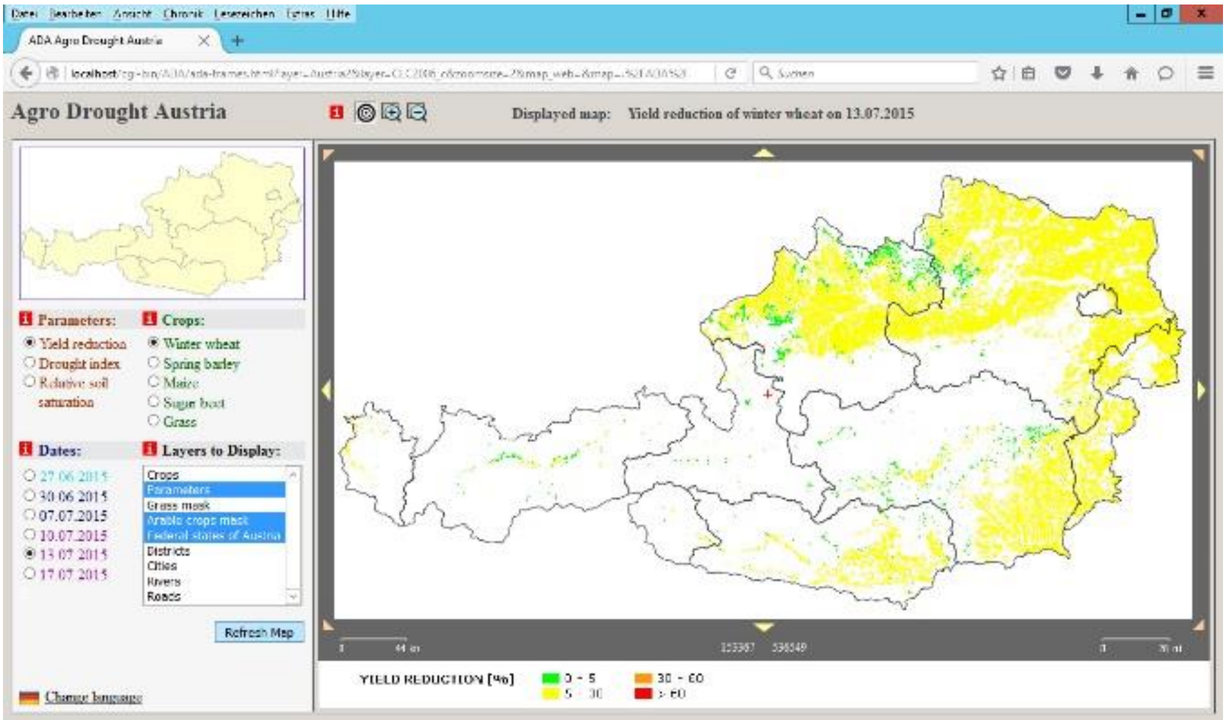

Figure 41a-d: Crop yield reduction distribution of maize (a), spring barley (b), sugar beet (c) and winter wheat (d) for the Austrian territory on 13.07.2015.

6 WP 5 – ADA System test

Stakeholders, including farmers were involved to discuss the functionality and user acceptance of the presented results via a web portal during the presentation of the system in October 2015 in Deutsch-Wagram. User feedbacks were already used to improve certain features of the web portal (see Figure 36).

The operable drought monitoring system “AgroDroughtAustria” was spatially validated and tested over several sites in Austrian crop production regions. For that purpose a questionnaire was distributed and interviews were carried out to gather independent yield data from farmers from the extreme year 2015 and compared with ADA GIS outputs. Figure 36 to Figure 41 show the results from farm yields from Lower Austria, Burgenland and Styria for the 4 crops.

The results show in same cases (i.e. for maize) distinct deviations from farmer reports. These cases could however explained by major small scale deviations in the underlying ADA data base from reality, such as soil conditions or the not considered groundwater impact. Smaller deviations are still common due to natural variations in reality which cannot be resolved by the ADA system, such as crop management options, soil cultivation or crop cultivar effects on stress sensitivity. Such deviations should be addressed by applying the pre-defined uncertainty ranges of yield impacts as shown in Figure 42. However, this validation and recalibration activity will be continued in the frame of another project beyond the ADA project, and is recommended as an important activity for a permanent improvement of a crop drought monitoring systems to meet the stakeholder needs and acceptance.

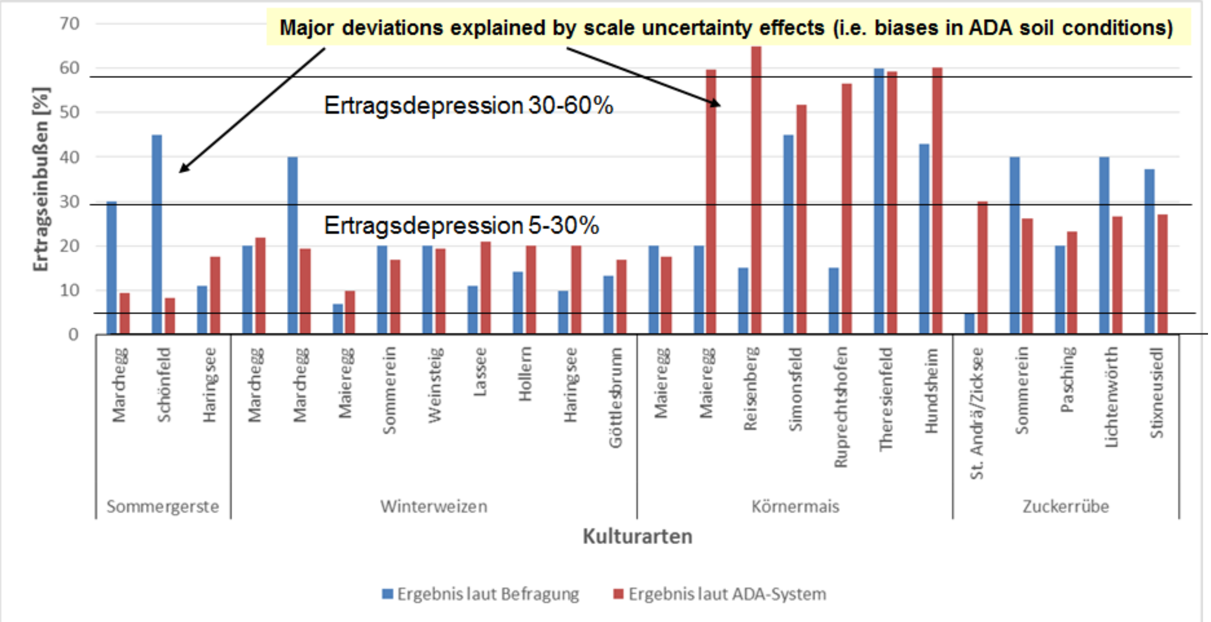

Figure 42: ADA system validation on yield depletion by drought and heat stress in 2015 by farmer inventory in eastern Austria.

7 Conclusions and recommendations

For the aim to develop an operational drought and heat monitoring system for 4 main crops and permanent grassland (meadow) we applied a straightforward approach of identifying, based on the collected and available data sets for Austria, most effective methods and algorithms with acceptable overall performance identifying drought status, crop risk and crop yield impacts. However, there is still potential to improve and regionalize the applied methods in future research with extended data bases including feedbacks from farmers on location specific drought and heat impacts on crops.

For example, besides the general relation of yield to environmental/climatic stresses, we also studied the role of cover cropping and tillage as two management measures with particular relevance for agricultural water management. Cover cropping is frequently considered as incompatible with water limited sites as it is supposed to deplete soil water storage. Our data demonstrate that in most environments (years x sites) in Eastern Austria cover cropping is feasible and does not result in significant yield differences. Maize seems to be most sensitive to potential depletion effects: although in most cases no significant yield differences are detected, there are more cases of adverse yield effects than favorable ones. This is not the case in sugar beet and spring barley (winter wheat is not considered here due to the unbalanced data owing to rare cover cropping before winter crops).

However, overall management operations can only partially mitigate environmental stresses due to adverse climatic factors. Still under more extreme climatic conditions under climate change it can be expected that management decisions might have stronger – either adverse (e.g. water depletion by cover crops) or favorable (e.g. water saving by reduced tillage) – impacts, which opens also a wide field for further research.

Work package 3 within the ADA project dealt with the meteorological input for the drought monitoring and forecasting system. To provide forecasts and analysis of drought relevant meteorological parameter ZAMG has access to a variety of state of the art NWP model with different horizontal resolutions and targeted to different forecasting ranges. The INCA system, running operational at ZAMG is the nowcasting and analyses tool that is used to provide weather forecasts in the nowcasting range up to 6h ahead. Since it uses the operational NWP model ALARO as input seamless forecast for the time range of several hours up to 3 days are available. Forecasts up to 10 days ahead can be retrieved from ECMWF IFS one of the world leading global forecasting systems. For those three systems probabilistic forecast can be provided by the ensemble system counterparts to quantify the uncertainties in the forecasts. The limited area ensemble system ALADIN-LAEF is used to assess the uncertainty in the ALARO forecasts. To generate reliable probabilistic forecasts a unique method is used to estimate uncertainties in the initial and lateral boundary conditions as well as in the model formulations. For the ensemble INCA system ALADIN-LAEF forecasts are used to predict uncertainties in the nowcasting range. ECMWF also runs a global ensemble system to quantify the uncertainties in the medium-range forecasts. For all available models a special post-processing chain was implemented to provide the drought relevant parameter from the standard model output on a common 1x1km grid in a common format to the project partners.

A special focus was on the quantification of the forecast uncertainty of the drought specific parameter. To improve the forecast quality of ALADIN-LAEF especially for near surface parameter a new method to estimate the uncertainties in the forecasts was implemented and carefully tested. In the operational version of ALADIN-LAEF the model surface fields are only perturbed in the initial conditions but not during the forecast itself. To account for uncertainties in the surface fields during the forecast a Stochastic Perturbed Physics Tendencies (SPPT) was implemented in ALADIN-LAEF surface forecasts. Due to the positive impact of SPPT on ALADIN-LAEF forecast quality an incorporation of SPPT in the next operational version of ALADIN-LAEF is planned.

In the course of the project the feasibility of using long term weather forecasts in the range of several months in the drought forecasting tool was discussed. ZAMG has access to the operational seasonal forecasting system of ECMWF-EPS and a special interface for seasonal forecasts was implemented which is necessary since the output frequency of the seasonal forecast system is lower than for the short and medium range forecasting systems. To investigate to what extend drought period can be predicted several months ahead the forecast quality of the seasonal forecasting system was evaluated for July 2015. Using probabilistic information in the seasonal forecasts could be very beneficial for stakeholders and allow to be prepared for drought periods well in advance. However the evaluation of one drought period has to be extended to more cases to allow statistically robust conclusion about the usability of seasonal drought forecasts.

The Agro Drought Austria Monitoring and Forecasting System enables via internet menu driven presentation of maps on specific dates showing the relative soil saturation, drought intensity and crop yield reduction situation over the Austrian territory in a grid resolution of 500 meters for rooting zone layers of 0-40 cm (grassland) and 0-100 cm (winter wheat, spring barley, maize and sugar beet). This tool, including methods and results achieved are of high interest for insurance companies, extension services and agricultural ministry of Austria, and for all stakeholders including farmers in the sector.

However, based on the promising project results and on the further research challenges identified, a follow up project was started (COMBIRISK) in order to extend the ADA system for a range of further weather based cropping risks including an extension of the relevant data base. In parallel, the consortium is addressing together with international partners the possibility of an operational implementation of the system, which will be permanently open for stakeholders and being improved under scientific supervision and stakeholder participation.

<u>Recommendations gathered from the ADA project and for research regarding further improvements of the ADA drought monitoring system can be summarized as follows:</u>

● ADA system structure is suitable for spatial mapping/forecast of additional weather related risk indicators beside drought and heat (i.e. other crop risks from adverse weather conditions) and has potential for an operational multiple agricultural risk monitoring and forecasting tool.

● Performance potentials could be increased by including remote sensing products.

● International cooperation for drought/heat monitoring system is strongly recommended to increase the efficiency and robustness of system performance

● Operational implementation requests permanent scientific and technical maintain (and therefore financial resources) and institutional cooperation and agreements (weather and forecast data, feedback system - validation etc.)

● Extending and improving data bases (soil characteristics, crop risks, damage, yields etc.) for further calibration and validation are recommended for permanent improvements of performance and reduction of regional biases and uncertainties.

● Stakeholder/user feedbacks to increase user acceptance and fit to user needs is indispensable.

8 Literature

Allen, G. R.; Pereira, S. L.; Raes, D. and Smith, M. (1998): Crop Evapotranspiration – Guidelines for Computing Crop Water Requirements. FAO Irrigation and drainage paper 56. Rome, Italy: Food and Agriculture Organization of the United Nations. ISBN 92-5-104219-5.

Allen, G. R.; Walter, A. I.; Elliot, L. R. and Howell, A. T. (2005): ASCE standardized reference evapotranspiration equation. American Society of Civil Engineers, 216.

Andersson, E., J.-N. Thepaut, 2008: ECMWF's 4D-Var data assimilation system – the genesis and 10 years in operations, ECMWF Newsletter, 115, 8-12.

Ansquer, P.; Al Haj Khaled, R.; Cruz, P.; Theau, J.-P.; Therond, O. and Duru, M. (2009): Characterizing and predicting plant phenology in species-rich grasslands. Grass and Forage Science 64 (1), 57-70.

APCC (2013). Österreichischer Sachstandsbericht Klimawandel 2014 (AAR14). Austrian Panel on Climate Change (APCC), Verlag der Österreichischen Akademie der Wissenschaften, Wien, Österreich, 1096 Seiten. ISBN 978-3-7001-7699-2

Baeumer, K. (1978): Allgemeiner Pflanzenbau. 2. Auflage, Verlag Eugen Ulmer, Stuttgart, 264 S.

Buchgraber, K.; Schaumberger, A. and Pötsch, E.M. (2011): Grassland Farming in Austria - status quo and future prospective. 16th Symposium of the European Grassland Federation "Grassland Farming and Land Management Systems in Mountainous Regions", Gumpenstein, Austria, Grassland Science in Europe, 16, August 29-31, 2011, 13-24.

Barkmeijer, J., R. Buizza, and T. N. Palmer, 1999: 3D-Var Hessian singular vectors and their potential use in the ECMWF ensemble prediction system. *Quart. J. Roy. Meteor. Soc.*, 125, 2333–2351

Barry, R. G., 1992: *Mountain Weather and Climate.* Routledge, London.

Barnabás, B., Jäger, K., Fehér, A. (2008). The effect of drought and heat stress on reproductive processes in cereals. Plant, Cell and Environment 31, 11-38.

Bloch, D., Hoffmann, C. M., Märländer, B. (2006). Impact of water supply on photosynthesis, water use and carbon isotope discrimination of sugar beet genotypes. European Journal of Agronomy 24, 218-225.

Bodner, G., Nakhforoosh, A., Kaul, H. P. (2015). Management of crop water under drought: a review. Agronomy for Sustainable Development 35, 401-442.

Buizza, R., and T. Palmer, 1995: The singular vector structure of the atmospheric general circulation. *J. Atmos. Sci.,* 52, 1434-1456

Buizza, R., M. Miller, and T. N. Palmer, 1999: Stochastic representation of model uncertainties in the ECMWF Ensemble Prediction System. *Quart. J. Roy. Meteor. Soc.,* 125, 2887–2908

Ciais, P., Reichstein, M., Viovy, N., Granier, A., Ogée, J., Allard, V., Chevallier, F. (2005). Europe-wide reduction in primary productivity caused by the heat and drought in 2003. Nature 437, 529-533.

Commission of the European Communities (1995): CORINE Land Cover. {http://www.eea.europa.eu/publications/COR0-landcover}. Retrieved 12.02.2016.

Eitzinger, J; Trnka, M; Semeradova, D; Thaler, S; Svobodova, E; Hlavinka, P; Siska, B; Takac, J; Malatinska, L; Novakova, M; Dubrovsky, M; Zalud, Z. (2013). Regional climate change impacts on agricultural crop production in Central and Eastern Europe - hotspots, regional differences and common trends. J AGR SCI. 2013; 151(6): 787-812.

European Environment Agency (2013): Global and European temperature (CSI 012/CLIM 001/CLIM 003). {http://www.eea.europa.eu/data-and-maps/indicators/global-and-european-temperature/ds_resolveuid/6f7963c558e848778854afba1c6066dc} Retrieved 11.02.2016.

Gerard, L., J.M. Piriou, R. Brozkova, J.-F. Geleyn, and D. Banciu, 2009: Cloud and precipitation parameterization in a meso-gamma scale operational weather prediction model. *Mon. Wea. Rev.*, 137, 3960–3977, doi: 10.1175/2009MWR2750.1

Haiden, T., and G. Pistotnik, 2009: Intensity-dependent parameterization of elevation effects in precipitation analysis. *Adv. Geosci.,* 20, 33-38.

Haiden, T.; Kann, A.; Wittmann, C.; Pistotnik, G.; Bica, B. and Gruber, C. (2011): The Integrated Nowcasting through Comprehensive Analysis (INCA) System and Its Validation over the Eastern Alpine Region. Weather and Forecasting, 26/2, pp. 166-183. doi: 10.1175/2010WAF2222451.1.

Herrero, M. P., Johnson, R. R. (1981). Drought stress and its effects on maize reproductive systems. Crop Science 21, 105-110.

Kann A., T. Schellander-Gorgas, and C. Wittmann, 2015: Enhanced short-range forecasting of sub-inversion cloudiness in complex terrain, *Atmos. Sci. Lett*., 16, 1-9. doi: 10.1002/asl2.511.

Lobell, D. B., Field, C. B. (2007). Global scale climate–crop yield relationships and the impacts of recent warming. Environmental Research Letters 2, 014002.

Molteni, F., T. Stockdale, M. Alonso Balmaseda, G. Balsamo, R Buizza, L. Ferranti, L. Magnusson, K. Mogensen, T.N. Palmer, F. Vitart, 2011: The new ECMWF seasonal forecast system (System 4), *Technical Memorandum, Technical Memorandum*, 656, [Available online at: http://www.ecmwf.int/publications]

Murer, E. (2009): Überprüfung und Verbesserung der Pedotransferfunktion zur Ermittlung der Wasserspeicherfähigkeit im Boden, Abschlussbericht, Bundesamt für Wasserwirtschaft, Institut für Kulturtechnik und Bodenwasserhaushalt, Petzenkirchen, 54 S.

Murer, E.; Wagenhofer, J.; Aigner, F. und Pfeffer, M. (2004): Die nutzbare Feldkapazität der mineralischen Böden der landwirtschaftlichen Nutzfläche Österreichs. In Bundesamt für Wasserwirtschaft (eds.): Schriftreihe BAW, 20, Bundesamt für Wasserwirtschaft, Institut für Kulturtechnik und Bodenwasserhaushalt, Petzenkirchen, 72-78.

NIST/SEMATECH (2012): e-Handbook of Statistical Methods, {http://www.itl.nist.gov/div898/handbook/}. Retrieved 12.02.2016.

Olesen, J. E., Bindi, M. (2002). Consequences of climate change for European agricultural productivity, land use and policy. European Journal of Agronomy 16, 239-262.

Palmer, W. C. (1965). Meteorological Drought, Res. Pap. 45, 58 pp., U. S. Dep. of Commer., Wash., D.C. Palmer, T., R. Buizza, F. Doblas-Reyes, T. Jung, M. Leutbecher, G.J. Shutts, M. Steinheimer, A. Weisheimer, 2009: Stochastic parametrization and model uncertainty. Technical Memorandum, Technical Memorandum, 598 , 42 pp.[Available online at: http://www.ecmwf.int/publications]

Palmer, W.C. (1968). Keeping track of crop moisture conditions, nationwide: The new Crop Moisture Index. *Weatherwise* 21, 156–161.

Reidsma, P., Ewert, F., Lansink, A. O., Leemans, R. (2010). Adaptation to climate change and climate variability in European agriculture: the importance of farm level responses. European Journal of Agronomy 32, 91-102.

Richardson K. *et al.*, 2009. Synthesis Report from Climate Change Global Risks, Challenges and Decisions, Copenhagen 10-12 March, 2009, University of Copenhagen, p. 38

Schaumberger, A. (2011): Räumliche Modelle zur Vegetations- und Ertragsdynamik im Wirtschaftsgrünland. Dissertation, Technische Universität Graz, Institut für Geoinformatik, 264 S.

Sherman, C. A., 1978: A mass-consistent model for wind field over complex terrain. *J. Appl. Meteor*., 17, 312-319.

Semenov, M. A., Shewry, P. R. (2011). Modelling predicts that heat stress, not drought, will increase vulnerability of wheat in Europe. Nature Scientific Reports, 1.

Smit, H.J.; Metzger, M.J. und Ewert, F. (2008): Spatial distribution of grassland productivity and land use in Europe. Agricultural Systems 98 (3), 208-219.

Sparks, T.H.; Croxton, P.J.; Collinson, N. und Taylor, P.W. (2005): Examples of phenological change, past and present, in UK farming. Annals of Applied Biology 146 (4), 531-537.

Sperry, J. S., Adler, F. R., Campbell, G. S., Comstock, J. P. (1998). Limitation of plant water use by rhizosphere and xylem conductance: results from a model. Plant, Cell and Environment 21, 347-359.

Strauss, F., Formayer, H., & Schmid, E. (2013). High resolution climate data for Austria in the period 2008–2040 from a statistical climate change model. International Journal of Climatology, 33(2), 430-443.

Suklitsch, M., A. Kann, and B. Bica, 2015: Towards an integrated probabilistic nowcasting system (En-INCA), Adv. Sci. Res., 12, 51-55, doi:10.5194/asr-12-51-2015.

Thaler, S., Eitzinger, J., Trnka, M., Dubrovsky, M. (2012). Impacts of climate change and alternative adaptation options on winter wheat yield and water productivity in a dry climate in Central Europe. The Journal of Agricultural Science, 150, 537-555.

Toth, Z., and E. Kalnay, 1993: Ensemble forecasting at NCEP: The generation of perturbation. *Bull. Amer. Meteor. Soc*., 74, 2317-2330

Trnka M., Kyselý J., Možný M., Dubrovský M. (2009): Changes in Central European soil moisture availability and circulation patterns in 1881-2005. International Journal of Climatology, 29: 655-672

Trnka, M., Eitzinger, J., Semeradova, D., Hlavinka, P., Balek, J., Dubrovsky, M., Kubu, G., Stepanek, P., Thaler, S., Mozny, M. & Zalud, Z. (2011). Expected changes in agroclimatic conditions in Central Europe. *Climatic Change* **108**, 261-289.

Trnka M.; Hlavinka P.; Semerádová D.; Balek J.; Možný M.; Štěpánek P.; Zahradníček P.; Hayes M.; Eitzinger J. and Žalud Z. (2014): Drought monitor for the Czech Republic - www.intersucho.cz. Rožnovský, J., Litschmann, T., (eds): Mendel a bioklimatologie. Brno, 3.– 5.9.2014, ISBN 978-80-210-6983-1.

UNEP (1992). World Atlas of Desertification.

Van den Putte, A., Govers, G., Diels, J., Gillijns, K., Demuzere, M. (2010). Assessing the effect of soil tillage on crop growth: A meta-regression analysis on European crop yields under conservation agriculture. European Journal of Agronomy 33, 231-241.

Vastarelli, P., Moschella, A., Pacifico, D., Mandolino, G. (2013). Water stress in Beta vulgaris: osmotic adjustment response and gene expression analysis in ssp. vulgaris and maritima. American Journal of Plant Sciences 4, 11-16.

Wang, Y., C. Williamson, D. Garvey, S. Chang, and J. Cogan, 2005: Application of a multigrid method to a mass-consistent diagnostic wind model. *J. Appl. Meteor*., 44, 1078-1089.

Wang, Y., M. Bellus, C. Wittmann, M. Steinheimer, F. Weidle, A. Kann, S. Ivatek-Šahdan, W. Tian, X. Ma, S. Tascu, and E. Bazile, 2011: The Central European limited-area ensemble forecasting system: ALADIN-LAEF. *Q.J.R. Meteorol. Soc.*, 137, 483–502. doi: 10.1002/qj.751

Wang, Y., M. Bellus, J. F. Geleyn, X. Ma, W. Tian, and F. Weidle, 2014: A new method for generating initial perturbations in regional ensemble prediction system: blending. *Mon. Wea. Rev.,* 142, 2043-2059.

Wilhite, D.A., and M. Glantz (1987). Understanding the drought phenomenon. The role of definitions. In: WILHITE, DA & EASTERLING, W.E., eds. Planning for drought. Boulder. Colorado.

Bisher erschienen in der Reihe BOKU-Met Report:

Berichte von 2003 – 2008

1 Eitzinger, J., Kubu, G., Formayer, H., Haas, P., Gerersdorfer, T., Kromp-Kolb, H. (2009): **Auswirkungen einer Klimaänderung auf den Wasserhaushalt des Neusiedlersees** (Endbericht im Auftrag der Burgenländischen Landesregierung vom 15. Juli 2005).

2 Frank, A., Seibert, P. (2009): **Diagnose von Extremereignissen aus großräumigen meteorologischen Feldern** (Endbericht StartClim.4, November 2003).

3 Formayer, H., Matulla, C., Haas, P., Groll, N. (2009): **Statistische Downscalingverfahren zur Ableitung von Extremereignissen in Österreich aus GCM-Feldern** (Endbericht StartClim.5, November 2003).

4 Schwarzl, I., Haas, W. (2009): **Kommunikation an der Schnittstelle Wissenschaft und Bildung** (Endbericht StartClim.11, November 2003).

5 Formayer, H., Haas, P., Matulla, C., Frank, A., Seibert, P. (2009): **Untersuchungen regionaler Klimaänderungsszenarien hinsichtlich Hitze- und Trockenperioden in Österreich** (Endbericht StartClim2004.B, November 2003).

6 Schwarzl, I., Lang, E. (2009): "**Hängen Hitze und Leistungsfähigkeit zusammen?**" Ein Projekt an der Schnittstelle Wissenschaft und Bildung (Endbericht StartClim2004.G, Jänner 2005).

7 Formayer, H., Kromp-Kolb, H. (2009): **Hochwasser und Klimawandel**. Auswirkungen des Klimawandels auf Hochwasserereignisse in Österreich (Endbericht WWF 2006).

8 Gerersdorfer, T., Frank, A., Formayer, H., Haas, P., Moshammer, H. (2009): **Untersuchung zur nächtlichen Abkühlung in einem sich ändernden Klima** (Endbericht StartClim2005.A1b, November 2006).

9 Krüger, B. C., Schicker, I., Formayer, H., Moshammer, H. (2009): **Feinstaub und Klimawandel – Gibt es Zusammenhänge in Nordostösterreich?** (Endbericht StartClim2006.A, Juli 2007).

10 Rössler, M., Laube, W., Weihs, P. (2009): **Avoiding bird collisions with glass surfaces**. Experimental investigations of the efficacy of markings on glass panes under natural light conditions in Flight Tunnel II (Final report, March 2007).

11 Formayer, H., Hofstätter, M., Haas, P. (2009): **Untersuchung der Schneesicherheit und der potenziellen Beschneiungszeiten in Schladming und Ramsau** (Endbericht STRATEGE, Oktober 2007).

12 Kromp-Kolb, H., Formayer, H., Haas, P., Hofstätter, M., Schwarzl, I. (2009): **Beobachtete Veränderung der Hitzeperioden in Oberösterreich und Abschätzung der möglichen zukünftigen Entwicklungen** (Endbericht Band 1 der Forschungsreihe „Auswirkungen des Klimawandels auf Oberösterreich“, Februar 2007).

13 Moshammer, H., Gerersdorfer, T., Hutter, H.-P., Formayer, H., Kromp-Kolb, H., Schwarzl, I. (2009): **Abschätzung der Auswirkungen von Hitze auf die Sterblichkeit in Oberösterreich** (Endbericht Band 3 der Forschungsreihe „Auswirkungen des Klimawandels auf Oberösterreich“, Juli 2007).

14 Formayer, H., Kromp-Kolb, H., Schwarzl, I. (2009): **Auswirkungen des Klimawandels auf Hochwasserereignisse in Oberösterreich** (Endbericht Band 2 der Forschungsreihe „Auswirkungen des Klimawandels auf Oberösterreich“, Mai 2007).

15 Simic, S., Schmalwieser, A.W., Moshammer, H. (2009): **Gesundheitsrisiken für die österreichische Bevölkerung durch die Abnahme des stratosphärischen Ozons** (Endbericht StartClim2007.B, Juni 2008).

16 Formayer, H., Clementschitsch, L., Hofstätter, M., Kromp-Kolb, H. (2009): **Vor Sicht Klima! Klimawandel in Österreich, regional betrachtet** (Endbericht Global 2000, Mai 2008).

Berichte ab 2009

17 Eitzinger, J., Kubu, G. (eds.) (2009): **Impact of Climate Change and Adaptation in Agriculture** (Extended Abstracts of the International Symosium, University of Natural Resources and Applied Life Sciences (BOKU), Vienna, June 22-23 2009).

18 Formayer, H., Kromp-Kolb, H. (2009): **Klimawandel und Tourismus in Oberösterreich.**

19 Fleischhacker V., Formayer H., Seisser O., Wolf-Eberl S., Kromp-Kolb, H. (2009): **Auswirkungen des Klimawandels auf das künftige Reiseverhalten im österreichischen Tourismus.** (Forschungsbericht im Auftrag des Bundesministeriums für Wirtschaft, Familie und Jugend).

20 Seibert, P., Radanovics, R., Krüger, B. C. (2010): **Sources of Air Pollution Relevant for the Austrian Biosphere Reserve Wienerwald.** Final Report for the Project "Sources of Air Pollution Relevant for Austrian Biosphere Reserves: Quantification, Trends, Scenarios", Man and Biosphere Programme (MaB), Austrian Academy of Sciences (ÖAW).

21 Arnold, D., D. Morton, I. Schicker, P. Seibert, M. W. Rotach, K. Horvath, J. Dudhia, T. Satomura, M. Müller, G. Zängl, T. Takemi, S. Serafin, J. Schmidli, S. Schneider (2012): **High Resolution Modelling in Complex Terrain.** Report on the HiRCoT 2012 Workshop, Vienna, 21-23 February 2012.

22 Matthias Schlögl (2013): **Validierung von atmosphärischen Dispersionsmodellen Beurteilung der Qualität von meteorologischen Schadstoffausbreitungsmodellen durch statistische Parameter am Beispiel der Anwendung des Lagrange'schen Teilchensimulationsmodells FLEXPART auf die ^{137}Cs-Emissionen bei den Katastrophenereignissen in Fukushima Dai-ichi.** (Bachelorarbeit).

23 Petra Seibert, Dèlia Arnold, Nikolaus Arnold, Klaus Gufler, Helga Kromp-Kolb, Gabriele Mraz, Steven Sholly, Antonia Wenisch (2013): **Flexrisk – Flexible tools for assessment of nuclear risk in Europe.** Final Report. PRELIMINARY VERSION MAY 2013.

24 Dallhammer E., Formayer H., Jiricka A., Keringer F., Leitner M., McCallum S., Schmied J., Stanzer G., Völler S. (2015): **Strategische Unterstützung bei der Projektplanung zur Berücksichtigung von Klimawandelfolgen**. (Endbericht zum Forschungsprojekt ENVISAGE-CC)

25 Eitzinger, J., Daneu, V., Bodner, G., Kubu, G., Loiskandl, W., Macaigne, P., Thaler, S., Schaumberger, A., Wittmann, C., Weidle, F., Kann, A., Murer, E., Krammer, C., Trnka, M., Hayes M. (2016):
Drought monitoring system for Austrian agriculture – AgroDroughtAustria (Final Scientific Report of project "AgroDroughtAustria" of the Austrian Climate Change Research Program).

Alle Berichte sind unter http://www.boku.ac.at/met/report/ online verfügbar.